

## ABSTRACT

Title of Dissertation:                   INTRINSIC PHYSIOLOGY AND INHIBITORY  
  ANATOMY OF THE AVIAN AUDITORY BRAINSTEM

James Baldassano  
Doctor of Philosophy 2024

Dissertation directed by:            Dr. Katrina MacLeod, Department of Biology

Soundwaves are rapidly modulated, multi-dimensional stimuli. The cochlea decomposes these signals into frequency and intensity information which is conveyed via the auditory nerve into the brain. How does the brain manage to extract these multidimensional signals from auditory nerve activity? How does it sculpt this input so that both the microsecond precision of “where?” and the spectrotemporal modulations of “what?” are encoded with high fidelity? Birds are powerful models for studying early auditory processing because they interact with sounds similarly to mammals but have a simpler neuronal architecture. We describe the intrinsic physiology and anatomy and auditory brainstem neurons involved in spectrotemporal processing.

In birds, the auditory nerve synapses onto two anatomically distinct cochlear nuclei, cochlear nucleus magnocellularis (NM) which encodes frequency/timing information, and the more heterogeneous cochlear nucleus angularis (NA) which encodes

intensity information. NA has been shown to encode the acoustic envelope, likely through a subset of neurons that respond preferentially to modulations in their inputs via an adaptive spike threshold. We first examined the intrinsic basis of this adaptive threshold and found that a dendrotoxin-sensitive low threshold potassium conductance is responsible for it.

In addition to the intrinsic properties of neurons, inhibition sculpts a number of auditory processes. The majority of inhibition in the avian auditory brainstem originates in the superior olivary nucleus (SON), which has multiple response types & projects either to multiple lower order ipsilateral nuclei, including NA & NM, or to the contralateral SON. Retrograde labeling experiments have demonstrated that these projections originate from distinct populations of SON neurons, however it is not clear if there is a relationship between response types and postsynaptic target. We used in vitro electrophysiology and neuronal reconstruction to establish a relationship between response types and targets.

While the function of inhibition is well documented in timing circuits, its role in intensity processing is less clear. We used dynamic clamp to model inhibitory conductances while recording from NA neurons in vitro to determine how inhibition impacts the range of inputs that a NA neuron can encode before its firing rate saturates.

# INTRINSIC PHYSIOLOGY & INHIBITORY ANATOMY OF THE AVIAN AUDITORY BRAINSTEM

by

James Baldassano

Dissertation submitted to the Faculty of the Graduate School of the  
University of Maryland, College Park, in partial fulfillment  
of the requirements for the degree of  
Doctor of Philosophy  
2024

## Advisory Committee:

Dr. Katrina MacLeod, Ph.D. advisor

Dr. Catherine Carr, Ph.D. co-advisor

Dr. Daniel Butts, committee member

Dr. Colenso Speer, committee member

Dr. Robert Dooling, Dean's Representative

© Copyright by  
James Baldassano  
2024

## Acknowledgements

I would like to thank my advisor, Katrina MacLeod, for her boundless support, patience, enthusiasm, and intellectual guidance as I slowly became a scientist. Next, I would like to thank my co-advisor, Catherine Carr, for her endless curiosity and inspirational passion for science. Thank you to my committee members, Daniel Butts & Colenso Speer, and former committee member, Samira Anderson, for their engagement and encouragement throughout the years. Thank you to Bob Dooling for being my Dean's Representative. Thank you to the wonderful professors I have had throughout my time here at University of Maryland, particularly Quentin Gaudry's course on neuroanatomy.

I would like to thank my mother, Diane, for her unwavering support over the last 6 years. Her enthusiasm for good news, empathy for bad news, and pragmatism during worrisome news led me through the emotional roller coaster of life, especially in this last year. Thank you to my siblings, Renée & Alex, who always are supportive and laugh at my stupid jokes. I would like to thank both of my similarly named bands, Miss Monster & Miss Moon (and my former bands Bad Monuments & The Mudlarks), for providing me with the opportunity to play music with wonderful people whilst ignoring the literature on hearing loss. Thank you to NCCCs, for providing a much needed social outlet after the socialness of grad school took a hit from COVID. Thank you to my cohort who made joining graduate school such an enjoyable and fun experience. Thank you NACS for allowing me to meet so many wonderful people (and thank you, wonderful people!). Thank you to the folks from the neurobiology course at MBL for making Summer 2019 unforgettable. Finally, thank you to my friends who have been with me since before graduate school (or that I met during) and who hopefully will be there until well after- in particular Mike Baratta, Richie Bottalico, Mike Rotenberg, and John White.

# Table of contents

## Contents

Chapter 1 Introduction .....	1
Section I- The Auditory Periphery .....	2
Auditory processing is initiated at the periphery.....	3
Section II: How is auditory information extracted from the auditory nerve and relayed in the brain?.....	6
Interaural time difference .....	9
Operating modes- Do neurons care about the timing of their inputs? Or just the amount of input?.....	21
What is driving the differences between differentiators and integrators? Spike threshold adaptation via sodium channel inactivation and potassium channel activation.....	24
Potassium conductances in auditory processing .....	28
Section III: How does inhibition sculpt auditory processing?.....	33
Inhibition in the auditory brainstem of birds- where does it come from?.....	34
Inhibition in avian brainstem timing circuits- mechanisms and impact.....	35
Inhibition in avian brainstem intensity circuits and the encoding of dynamic range.....	36
Physiology & anatomy of superior olivary nucleus.....	38
Inhibition in the mammalian auditory brainstem.....	42
Section IV- Dynamic clamp: Modeling intrinsic ion channels, synaptic conductances, and noise stimuli. ....	43
Modeling in dynamic clamp- what can you do with it? .....	44
Conductance clamp as an alternative for noisy currents.....	45
Chapter 2 Low threshold voltage-gated potassium channels in the cochlear nucleus angularis ..	47
Materials and methods .....	49
Results .....	58
Spiking Patterns in NA Are Shaped by a DTX-Sensitive Potassium Conductance.....	58

The DTX-Sensitive Conductance Improves Temporal Firing Reliability and Information Content in Tonic Firing Neurons .....	63
Kv1 Channel Expression Drives Fluctuation Sensitivity by Contributing to an Adaptive Spike Threshold.....	68
Discussion.....	75
Ionic Basis of Electrophysiological Diversity in NA .....	76
Neurons in the NA Utilize Kv1 Channels to Encode the Temporal Dynamics of Their Inputs .....	77
Spike Threshold Adaptation in NA Neurons May Rely on the Low-Threshold Potassium Conductance .....	79
Functional Analogs of NA Neurons in the Mammalian Cochlear Nucleus .....	80
Summary .....	81
Chapter 3 Electrophysiological properties and anatomy of the avian superior olivary nucleus...	83
Materials and Methods.....	85
Results .....	92
SON contains heterogeneous electrophysiological phenotypes .....	92
SON neurons display varied levels of temporal reliability.....	98
SON tonic phenotypes exist along a spectrum of fluctuation sensitivity .....	99
SON neurons exited nucleus in at least three distinct fiber tracts and correlated with physiological phenotype.....	102
Cells in SON are clustered by their electrophysiological phenotype .....	103
Rostrocaudal distribution of SON phenotypes.....	103
Discussion.....	108
Two tonic firing phenotypes in SON. ....	108
SON neurons encode temporal features of sound .....	110
SON neurons provide inhibition to divergent postsynaptic targets organized by intrinsic spiking properties.....	111
Role of inhibition in the avian auditory brain stem.....	112
Mammalian vs avian inhibitory architecture. ....	114
Chapter 4 : The impact of GABAergic-like conductances on intensity coding and using conductance clamp to measure operating modes.....	116

Introduction .....	116
Materials and methods .....	118
Brain slice preparation.....	118
Whole cell patch-clamp electrophysiology.....	118
Modeling GABAergic-like inputs.....	118
Dynamic range .....	119
Conductance clamp model of noise.....	122
Results .....	123
Modeled GABAergic conductances expand the dynamic range of tonic firing NA neurons .....	123
Conductance clamp firing responses maintain fluctuation sensitivity.....	127
Discussion.....	129
Inhibition in intensity coding .....	129
Conductance and current models – when to use them?.....	131
Conclusions.....	133
References.....	134

## Table of Figures

Figure 1-1 Interaural time difference in the nucleus laminaris .....	12
Figure 1-2 Nucleus angularis encodes envelope information .....	17
Figure 1-3 In vitro response types in the avian cochlear nuclei .....	18
Figure 1-4 Different operating modes exist in NA .....	23
Figure 1-5 Spike threshold is inversely correlated with the rate of membrane depolarization....	27
Figure 1-6 In vitro and in vivo responses of the SON.....	41
Figure 1-7 Different applications of dynamic clamp .....	46
Figure 2-1 Schematic for DTX experiment.....	57
Figure 2-2 Dendrotoxin-I altered the spiking responses in a subset of nucleus angularis (NA) neurons.....	61
Figure 2-3 Dendrotoxin-I (DTX) did not alter firing or intrinsic properties of damped neurons. .....	62
Figure 2-4 Dendrotoxin-I (DTX) reduced the spike timing reliability in a tonic II neuron in nucleus angularis (NA).....	65
Figure 2-5 Dendrotoxin-I (DTX) reduced the spike timing reliability in cell type-specific manner.	66
Figure 2-6 Mutual information (MI) between spike trains by cell type. ....	67
Figure 2-7 Dendrotoxin-I (DTX) reduced the high-pass response selectivity in a subset of nucleus angularis (NA) neurons .....	69
Figure 2-8 Dendrotoxin-I (DTX) diminished fluctuation sensitivity in differentiators.....	72
Figure 2-9 Dendrotoxin-I (DTX) had no impact on fluctuation sensitivity metrics in integrators .....	73
Figure 2-10 Dendrotoxin-I (DTX) altered the dynamics of action potential initiation and threshold variability during periods of high current fluctuation. ....	74
Figure 3-1 Intrinsic physiological phenotypes of SON neurons.....	95
Figure 3-2 Chattering and regular firing phenotypes were quantifiably differentiable by regularity analysis. ....	96
Figure 3-3 Intrinsic membrane properties differ between SON phenotypes .....	97
Figure 3-4 Spike timing reliability depends on cell type. ....	100
Figure 3-5 Temporal fluctuation sensitivity depends on cell type .....	101
Figure 3-6 Morphological analysis of axonal projection patterns. ....	105
Figure 3-7 Distribution of the location of cell bodies within SON differs with physiological type.....	106
Figure 3-8 Axonal projection patterns differed across the rostrocaudal extent of SON. ...	107
Figure 4-1 Schematic of experimental design for GABAergic experiment .....	121
Figure 4-2 Example of the influence of GABAergic-like conductance on F-I functions .....	125

Figure 4-3 GABAergic-like conductances expand the dynamic range of NA neurons by increasing the current required to produce saturation .....	126
Figure 4-4 <i>Integrative properties are captured similarly in conductance clamp &amp; current clamp</i> .....	128

## Chapter 1 Introduction

In this dissertation, I investigated the intrinsic and anatomical properties of specific electrophysiological phenotypes within the avian auditory brainstem using *in vitro* electrophysiology, pharmacology, anatomical reconstructions, and dynamic clamp. The results of these experiments indicated that 1) a dendrotoxin sensitive, low-threshold activated potassium channel (Kv1) shapes the different spiking response profiles of the cochlear nucleus angularis (NA) and contributes how these neurons encode temporally modulated features, 2) neurons of the superior olivary nucleus (SON) have cell-type specific divergent projections, as well as cell-type specific sensitivities to temporal modulated inputs, and 3) dynamic clamp models of GABAergic-like conductances expand the range of input intensities that cochlear neurons can encode.

To provide context for the results, I will review in chapter 1 the literature on auditory coding, particularly from the auditory periphery to the auditory brainstem in mammals and birds, the anatomy of auditory brainstem circuits, and the contribution of both intrinsic and synaptic mechanisms to extracting temporally precise information from auditory nerve inputs.

I will address several key contextual questions in chapter 1. How is sound information first represented when entering the brain via the auditory nerve? How are neurons in the cochlear nucleus, which receives input directly from the auditory nerve, specialized to extract relevant auditory information? How is this extracted information utilized in computations such as interaural time difference (ITD) and interaural level difference (ILD)? What intrinsic and synaptic strategies do these circuits use to encode the multimodal, rapidly modulating auditory landscape with high fidelity?

Comparative neuroethology allows for a deeper understanding of how the nervous system adapts to fulfill particular behavioral needs, while simultaneously revealing conserved or convergent strategies for neural processes (reviewed in (Miller et al., 2018)). A powerful example of this is the auditory periphery of birds and mammals. These systems arose independently, but use remarkably similar strategies, such as synaptic properties and intrinsic neuronal physiology for encoding specific features of sound. However, while birds utilize sound information for the same tasks as mammals, they have a simplified anatomy. Therefore, we utilized the avian system as our model.

We will discuss here the avian auditory periphery and auditory brainstem in comparison with the mammalian system. We will focus on how differential ion channel expression and intrinsic specializations give rise to different phenotypes that encode specific auditory features. Additionally, we will focus on the usage of inhibition in each system, and then finally focus on its potential role in intensity coding.

## Section I- The Auditory Periphery

Sound is a multimodal and rapid stimulus. A primary interest of mine throughout these experiments is how the brain, particularly early processing structures such as the cochlear nucleus, are able to extract specific components of information and do so with high precision. Modern auditory systems in birds and mammals evolved simultaneously from the development of the tympanic middle ear approximately 300-400 million years ago (Clack & Anderson, 2016). This development allowed hearing to evolve into the complex process it is today, particularly for processes such as sound localization and communication. Sound localization is vital for animals

to either detect prey or predators, allowing animals to adapt their behaviors accordingly (Payne, 1971). Vocal communication allows animals to convey complex information, whether it be for mating, or for information processing (Garcia & Favaro, 2017).

Sound waves are multidimensional stimuli, containing both frequency and amplitude information. The expanded role of auditory processing in behavior required the development of neural mechanisms to encode the processing of complex sound information. The rapid nature of auditory signals means that the neural architecture in place must be specialized to preserve temporal features. Understanding how intrinsic properties of neurons contribute to these processes is a core question to this dissertation.

## Auditory processing is initiated at the periphery

In both birds and mammals, auditory information is transduced in the cochlea, which propagates waves of sound information and decomposes the waves into their fundamental frequencies via frequency-selective hair cells. Hair cells have bundles of stereocilia on their apical side that are mechanically displaced by shearing from the tectorial membrane. This deflection opens mechano-electrical transduction (MET) channels which cause an influx of positive ions, depolarizing the cell and subsequently releasing neurotransmitter onto the auditory nerve (D. Corey & Hudspeth, 1983; D. P. Corey & Hudspeth, 1979; Hudspeth, 1983).

Birds tend to have lower hearing ranges than mammals, typically maxing out at ~10 kHz (G. A. Manley, 2017). This range is much more comparable to humans than other model organisms, such as mice and rats, which have significantly higher hearing ranges, reaching up to 38 kHz (Reviewed in(Escabi et al., 2019).

### *The auditory nerve carries all sound information into the brain*

Sound information enters the brain via the auditory nerve, a bundle of fibers from the cochlea. The physiology of auditory nerve fibers (ANFs) is similar between mammals and birds, with birds having lower frequency ranges than common animal models, such as mice and chinchillas (G. A. Manley et al., 1991; Sachs & Abbas, 1974; Saunders et al., 1985). In both birds and mammals, each excitatory hair cell innervates numerous afferent fibers (Fischer et al., 1988; Liberman, 1982; G. A. Manley et al., 1991). In mammals, different subtypes of afferent ANFs have been demonstrated, each characterized by their level of spontaneous activity and sound threshold (Petitpré et al., 2018).

ANFs tend to have narrow V-shaped frequency tuning curves, even at sound pressure levels well above their threshold (Köppl, 1997a; G. A. Manley et al., 1991; Müller et al., 1997). All ANFs demonstrate spontaneous activity (Sachs & Abbas, 1974) with lower frequency ANFs having higher spontaneous rates. A typical spontaneous rate is ~50-100 Hz with Poisson-like inter-spike intervals (Hill et al., 1989; Köppl, 1997a, 1997b). Recordings from the auditory nerve produce responses that have low latency (< 3 ms) and have characteristic response profiles referred to as a “transient-sustained,” where firing briefly spikes but retain an elevated firing rate throughout the sound stimulus (Sachs & Abbas, 1974). The discharge rate of ANFs increases monotonically with sound level, with the discharge rates of birds being higher than those of mammals, as well as larger dynamic range of sound intensities (G. A. Manley et al., 1991).

ANFs have distinct response patterns that are seen when recorded from *in vivo* that are characterized by sustained responses that are highest at the onset of a sound stimulus and decay

over time (Sachs et al., 1974). These fibers produce their action potentials at a particular part of the carrier wave, a phenomenon known as phase-locking.

Phase-locking is critical for accurate frequency discrimination but becomes more difficult with increasing sound frequency, due to the decreased distance between phase repetitions on subsequent cycles. However, despite having lower hearing ranges than mammals, barn owl ANFs are able to strongly phase-lock up to 10 kHz (Köppl, 1997b), which is significantly higher than what is seen in generalist birds like chickens, which can phase lock up to ~5 kHz (Salvi et al., 1992) or chinchillas, which can phase lock up to 7 kHz despite significantly higher hearing ranges (Kale & Heinz, 2010). In general, phase-locking in ANFs exceeds that seen in timing cochlear nuclei of both birds & mammals (Joris et al., 1994; Köppl, 1997b; Salvi et al., 1992; Warchol & Dallos, 1990). ANFs also encode the auditory envelope, meaning their firing rate changes in response to temporal modulations (Moller, 1976). The auditory nerve forms excitatory synapses on neurons of the cochlear nucleus, where neurons are specialized to extract specific features from auditory nerve activity.

## Section II: How is auditory information extracted from the auditory nerve and relayed in the brain?

A fundamental question in auditory neuroscience is how does the brain extract specific features from the auditory nerve and translate it into relevant electrical information? The first relay point of auditory information in the brain is the cochlear nucleus (Boord & Rasmussen, 1963; Feldman & Harrison, 1969). This makes it an ideal candidate for studying the neural computations required to extract sound information. Birds are a powerful model for answering this question because of their comparatively simpler neuronal architecture.

A primary feature of this “simpler architecture” is the presence of two anatomically and functionally distinct cochlear nuclei: nucleus magnocellularis (NM) and nucleus angularis (NA) (C. E. Carr & Boudreau, 1991; Karten, 1967; Parks & Rubel, 1978; T. Takahashi et al., 1984). NM encodes timing information while NA encodes intensity information. These nuclei are the origin of parallel processing pathways, meaning these features ascend in auditory structures independently of each other (Sullivan & Konishi, 1984). NM extracts timing information, which is important for interaural time difference (ITD) processing. However, this means that NA must extract all other information (reviewed in MacLeod & Carr, 2007)

Both NM and NA are excitatory feed-forward, meaning that the only excitatory inputs are from the auditory nerve (Reviewed in Ryugo & Parks, 2003). This lack of local connectivity in NA and NM makes them ideal candidates for studying how the brain extracts auditory information because inferences can be made about the function of neurons based on their voltage responses. This can then allow us to examine how neurons use intrinsic specializations to encode

specific features of ANF activity. The following sections will examine how neurons in NM & NA are equipped to encode specific features of ANF input, while drawing comparisons to mammalian homologs.

### *How does timing information get extracted in the nucleus magnocellularis?*

NM is located medially in the brainstem, about a third of the way from the midline to the edge of the brainstem and is highly specialized for encoding information about the fine structure of the acoustic signal (Konishi et al., 1985). Dendrites of most NM neurons are retracted during development, so inputs from auditory nerve fibers (ANFs) synapse directly onto the soma of these neurons (Parks & Jackson, 1984; Parks & Rubel, 1978). As such, neurons in NM have rapid excitatory postsynaptic potential (EPSP) kinetics and phase lock reliably so they can preserve temporal features in their outputs (Köppl, 1997b; Warchol & Dallos, 1990).

The intrinsic physiology of NM neurons is critical for temporal selectivity. One of the defining features of NM neurons, and timing neurons in general, is the presence of a large low voltage activated potassium conductance (G<sub>lt</sub>), which occurs via Kv1 channels. These channels are open around the resting membrane voltage, leading to a low input resistance (H. Brew & Forsythe, 1995; Rathouz & Trussell, 1998). Kv1 channels are rapid and resulting in a high-pass filtering that selects for well-timed inputs because they will repolarize the membrane if excitatory inputs do not occur rapidly enough, driving the temporal precision necessary for phase-locking (Fukui et al., 2006).

These channels are the primary drivers behind the canonical “single-spike” phenotype associated with NM neurons, where a neuron will produce a single action potential in response to

depolarizing current injection (Fig 1-2). This response is regardless of the size of the current (Rathouz & Trussell, 1998). When dendrotoxin (DTX), a Kv1 antagonist, was applied to NM neurons, they fired multiple action potentials upon depolarizing current injections (Fukui & Ohmori, 2004).

In addition to the prominent Kv1 conductance, there is a high-threshold potassium ( $K^{+}_{HVA}$ ) and a transient type-A potassium conductance. The  $K^{+}_{HVA}$  conductance occurs via Kv3 channels (Rathouz & Trussell, 1998), which are critical for rapid repolarization of the membrane during spike trains and can be blocked by tetraethylammonium (TEA). TEA application widens action potentials, thus slowing down spiking activity. These allow neurons to fire rapid spikes during bouts of excitatory drive. The function and molecular substrates of the A-type currents are less clear.

Rapid sodium channel kinetics also contribute to temporally precise firing. NM neurons have transient inward sodium currents that have amplitudes up to 5 nA. Molecular studies have demonstrated a prominent Nav1.6 conductance in NM. These channels are ideal for encoding rapidly repeating high frequency inputs. When compared to other types of sodium channels, Nav1.6 channels activate earlier during depolarization, have a lesser rate of use-dependent inactivation (particularly at high frequencies), and better promote persistent ( $I_{NaP}$ ) and resurgent ( $I_{NaR}$ ) sodium currents. Both types of currents are critical for rapid spiking (reviewed in Hong & Sanchez, 2018).

### *Timing cells of the mammalian cochlear nucleus*

The functional mammalian homolog of NM is the “bushy cell” of the VCN. Bushy cells are morphologically characterized by their short dendritic arbors and axons that don’t have collaterals. Bushy cells have two subtypes, spherical (SBCs) which receive a few (~4), large

synapses from the auditory nerve, and globular bushy cells (GBCs) which receive ~20 medium sized synapses from the auditory nerve (Ryugo & Sento, 1991). Both subtypes are temporally precise and encode timing information from the auditory nerve via intrinsic properties similar to NM neurons—a low input resistance, largely due to a large low-threshold potassium conductance, and have a classic single spike response as well (Oertel et al., 2008). These features indicate a level of ubiquity amongst neurons that encode timing information.

### Interaural time difference

In order to determine the spatial origin of a sound, animals must use auditory cues. This spatial information is not obtained from a monaural cue, but rather from binaural integration of sound inputs at both ears. An interaural time difference (ITD) is the disparity in time from when sound waves reach one ear versus the other ear. ITDs are critical for sound localization (Ashida & Carr, 2011; Yamada & Kuba, 2022). Since the disparity of sound waves hitting one ear before the other is miniscule, usually within the microsecond range, the architecture for ITD processing must be precise and efficient. The computations for ITDs occur within the brainstem of both birds and mammals, being extracted at a 3<sup>rd</sup> order nucleus in both systems. This early integration encapsulates the computational efficiency of this process. In birds, the computation occurs at nucleus laminaris (NL) while in mammals, the medial superior olive (MSO). Neurons in these coincidence detecting structures are specialized for preserving their temporal inputs, therefore, there are similarities between them and the timing neurons of the cochlear nuclei.

#### *Coincidence detection in the nucleus laminaris*

The synaptic afferents from NM are organized as delay lines, demonstrated in Fig. 1-1. The distances the ipsilateral and contralateral fibers must travel are proportional to when sound

reaches one ear vs when it reaches the other. NM neurons send an axon bilaterally to both NL, with a collateral synapsing onto the dorsal region of the ipsilateral NL and terminating in the ventral region of the contralateral NL (C. Carr & Konishi, 1990).

Neurons in NL are intrinsically specialized to behave as coincidence detectors, thus only producing action potentials when excitatory inputs arrive within a small timeframe (C. Carr & Konishi, 1990; Yang et al., 1999). This efficient anatomy has made the NM-NL circuit an ideal model to study neural computations.

In contrast with NM neurons, NL neurons have dendritic trees that extend both dorsally and ventrally. Higher frequency NL neurons have multiple dendritic branches that are thicker and shorter while lower frequency neurons have fewer dendritic branches that are thinner and longer (Kuba et al., 2005; D. J. Smith & Rubel, 1979). These morphological properties allow for rapid integration of EPSPs in higher frequency NL neurons. Yamada & Kuba (2021) demonstrated that these synapses are clustered in a way that strengthened the attenuation of synaptic responses within a dendritic arbor by promoting sublinear integration. In addition to the delay line, coincidence detection in NL neurons is driven by intrinsic membrane specializations.

Hyperpolarization-activated cyclic nucleotide-gated (HCN) channels, which are responsible for an inward current when neurons are hyperpolarized, are distributed primarily in dendrites and influence conduction through an interaction with Kv1 channels (Yamada et al., 2005; Yamada & Kuba, 2022). Oertel et al (2008) demonstrated that HCN channels in temporally sensitive neurons of the mammalian auditory brainstem colocalized with Kv1 channels, a low threshold potassium channel conductance that is involved with temporal selectivity. The relatively slow kinetics of HCN channels cause the input resistance of neurons to be lowered at rest, thus boosting the impact Kv1 channels have on temporal selectivity (Cao & Oertel, 2017;

Golding & Oertel, 2012; Rothman & Manis, 2003a, 2003c). NL neurons have a large Kv1 conductance, highlighting the potential for interplay between the two conductances. Higher frequency NL neurons have a higher expression of Kv1 channels than lower frequency NL neurons (Yang et al., 1999).

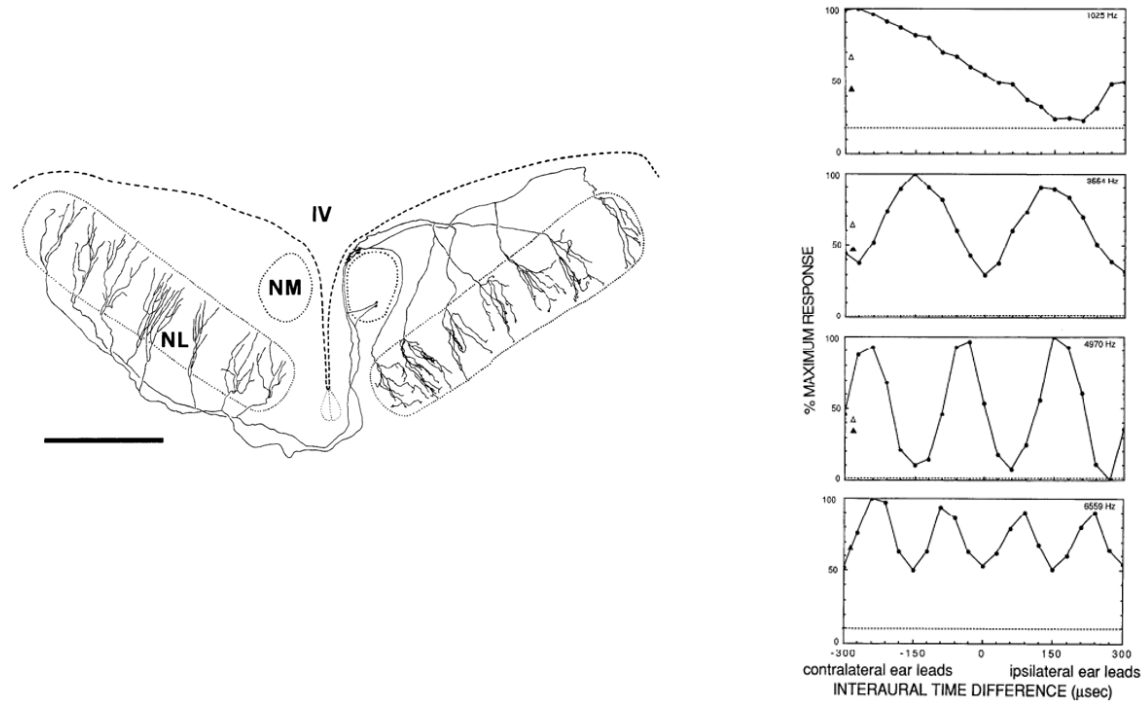


Figure 1-1 Interaural time difference in the nucleus laminaris

Left, anatomy of the NM-NL binaural circuitry. NM sends axons to the ventral dendrites of the contralateral NL and to the dorsal dendrites of the ipsilateral NL. Right, ITD tunings of 4 separate NL neurons with the x axis representing the difference in delay times from sound hitting the ipsilateral vs contralateral ear. Adapted from Carr & Konishi, 1990.

### *Medial superior olive*

In mammals, ITD computation occurs in the medial superior olive (MSO). The MSO integrates excitatory glutamatergic binaural inputs via bushy cells from both cochlear nuclei, but also receives inhibitory inputs from both the medial and lateral nuclei of the trapezoid body (Cant & Hyson, 1992; Franken et al., 2015).

While the exact mechanism by which coincidence detection in mammals takes place is still up for debate (Franken et al., 2015), MSO neurons share a number of intrinsic specializations with the avian NL. They have a bipolar morphology, with dendritic branches to receive binaural inputs (Ollo & Schwartz, 1979; Rautenberg et al., 2009; Scott, 2005; P. H. Smith, 1995). MSO neurons produce temporally precise spikes that rely on excitatory inputs arriving within a small coincidence detection window. This is largely due to their fast membrane time constant and prominent expression of Kv1 & HCN channels, which lowers their input resistance (Brand et al., 2002; Couchman et al., 2010; Fischl et al., 2012; Grothe & Sanes, 1994; Kuwabara & Zook, 1992; Myoga et al., 2014; Pecka et al., 2008; Stange et al., 2013; T. C. Yin & Chan, 1990).

### *How does nucleus angularis encode everything else?*

The sister cochlear nucleus to NM is nucleus angularis (NA). NM is devoted to processing temporal information, meaning that NA must encode all other features of sound, including intensity and envelope information (Soares et al., 2002), as well as localization via interaural level differences (ILD) (Adolphs, 1993; G. Manley et al., 1988; Sato et al., 2010). This

division of labor in the processing of spectral cues underlies our conceptualization of parallel pathways in the ascending auditory circuit.

NA is located bilaterally at the dorsolateral edge of the brainstem. Neurons in NA are tonotopically organized along a dorsolateral-ventromedial axis (Köppl, 2001; Köppl & Carr, 2003; Soares & Carr, 2001). NA receives excitatory inputs from the auditory nerve (Hackett et al., 1982) via many small bouton-like synapses from the auditory nerve (C. E. Carr & Boudreau, 1991; MacLeod & Carr, 2005). These glutamatergic synapses allow for a more graded input that can follow that rapidly modulating amplitude of the auditory signal.

NA was originally thought to strictly encode sound intensity using a “rate-code,” or a firing rate that directly reflected the mean input (Sachs & Sinnott, 1978; Sullivan & Konishi, 1984). However, immunohistochemical experiments in owls show that the dominant AMPA receptor subtypes were GluR3 & GluR4, which have rapid kinetics, and experiments in chicks show rapid desensitization kinetics. These results indicated that they are equipped to encode some sort of temporal features rather than temporally summate inputs (Kubke & Carr, 1998; Levin et al., 1997; MacLeod & Carr, 2005; Raman et al., 1994). These experiments aided in shifting the perception of NA’s role from encoding intensity information with a rate code to envelope coding.

Importantly, while NA neurons are poor at phase-locking (Köppl & Carr, 2003), Steinberg & Pena (2011) used *in vivo* recordings to demonstrate that neurons in NA encoded envelope features more reliably than ANFs, as demonstrated in Fig. 1-2. This means that the ANF-NA synapses, as well as the intrinsic physiology of NA neurons, are selectively filtering inputs in order to encode the temporal modulations in the acoustic envelope.

*In vivo* responses from NA showcase a wide variety of responses. Primary-like responses have an ANF-like post-stimulus time histogram (PSTH), producing a large number of spikes at stimulus onset that gradually adapted to a steady, lower rate. Chop-T units produce spikes with a regular pattern at stimulus onset that produced several distinct peaks in the PSTH (Köppl & Carr, 2003). Köppl & Carr (Köppl & Carr, 2003) describe a rare “Chop-S” neuron type which had a significantly higher latency than other response types. Onset neurons showed only a single prominent, initial peak in their PSTH. Finally, there are type IV neurons, which were characterized by a non-monotonic relationship between sound intensity and firing at their characteristic frequency i.e. they had largely excitatory responses at low sound intensities but became inhibited at higher sound intensities.

NA is equally heterogeneous *in vitro*. There are 4-5 different described response profiles in NA neurons observed upon current injections *in vitro*, including a single-spiking phenotype and several tonic firing phenotypes (Ahn et al., 2014; Baldassano & MacLeod, 2022; Kreeger et al., 2012; Soares et al., 2002), demonstrated in the top row of Fig. 1-3. NM’s response is shown for comparison here.

Single-spiking neurons produce a single action potential at the onset of a current injection. Generally, single spiking neurons are round and have two thick, stubby dendrites. This morphology and response profile is reminiscent of those seen in NM & NL. Single-spiking neurons have a large low-voltage activated potassium conductance as well (Fukui & Ohmori, 2003), indicating that they may have a specialization in encoding temporal properties.

All tonic neurons fire multiple action potentials upon current injection *in vitro* and increase firing rate to increased level of injected current. Tonic 1 neurons fire a burst of action potentials at the onset of a current injection followed by a pause. When given hyperpolarizing

current injections, tonic 1 neurons have a noticeable “sag,” potentially from hyperpolarization activated cyclic nucleotide (HCN) channels. These neurons have radiate dendrites that have several small dendritic branches (Soares et al., 2002). Tonic 3 neurons have no discernable morphological difference from tonic 1 neurons, in that their dendritic branching and soma morphology are similar. However, they have distinct electrophysiological responses. Tonic 3 neurons fire regularly spaced action potentials throughout a current injection with no pause. Additionally, tonic 3 neurons have a much gentler “sag” in their voltage response to hyperpolarizing current injections (Soares et al., 2002). Tonic 2 neurons are morphologically distinct. They have vertically oriented dendrites that extended either perpendicular or within isofrequency “slabs.” They are electrophysiologically characterized by a burst of action potentials after an initial pause. Increasing the amplitude of the current injection causes the spikes to occur earlier in the current injection. Hyperpolarizing current injections give rise to a sag that is in between tonic 1 and tonic 3 neurons (Soares et al., 2002). Finally, damped neurons that produce multiple action potentials that diminish in amplitude throughout a current injection, quickly becoming subthreshold oscillations. More recently, it is suspected that damped neurons are immature phenotypes, as they are not described in hatchlings (D. H. Brown & Hyson, 2019; Soares et al., 2002).

This diversity of responses emerges entirely from intrinsic membrane differences, meaning that NA likely is using heterogeneous membrane properties to encode wide array of features not extracted by timing neurons.

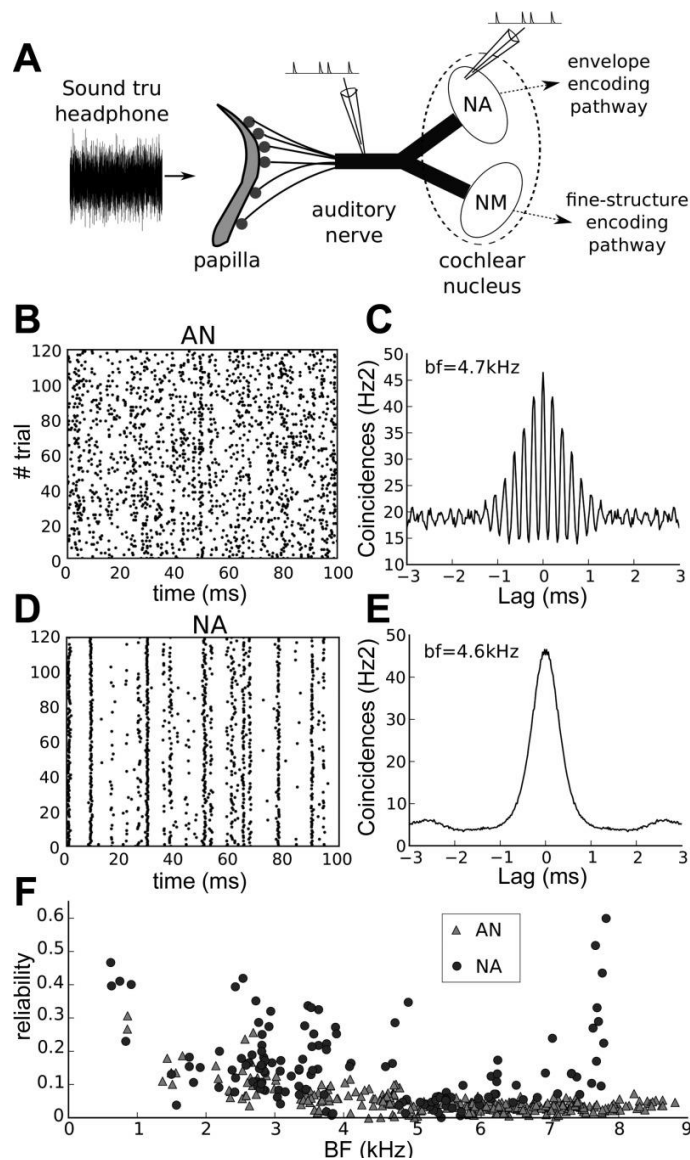


**Figure 1-2 Nucleus angularis encodes envelope information**

Correlation analysis of auditory nerve fibers (ANF) and nucleus angularis (NA) cells. A: schematic of the experimental setup. Broadband noises are presented monaurally through earphones. The first recording site is in the auditory nerve (AN) bundle. The second one is in the envelope coding pathway, the NA. NM, nucleus magnocellularis. B: raster plot of responses to 120 frozen noises of ANF with best frequency (BF) at 4.7 kHz. C: shuffled autocorrelogram (SAC) from the ANF fiber in B. D: raster plot of responses to 120 frozen noises NA cell with BF at 4.6 kHz. The NA response is more reproducible across trials. E: SAC from the NA cell in D. NA does not encode the fine structure (no oscillation). F: population reliability (all input levels are pooled) of the ANF (triangles) and NA (circles) dataset as a function of BF.

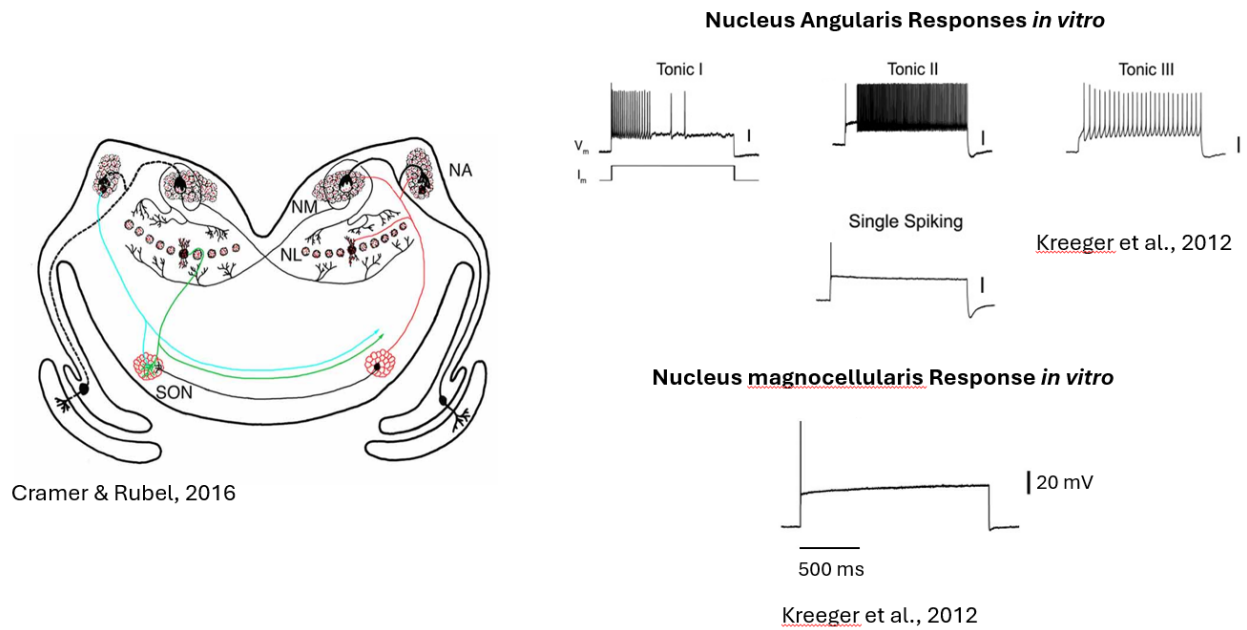


*Figure 1-3 In vitro response types in the avian cochlear nuclei*

Left- A schematic of the avian auditory brainstem, adapted from Cramer & Rubel, 2016

Right- Top row, the described electrophysiological response phenotypes in NA. Bottom row, the canonical single spiking phenotype in NM. Adapted from Kreeger et al., 2012.

### *Intensity coding neurons of the mammalian cochlear nucleus are not direct homologs with NA*

While there is a less clear mammalian functional homolog of NA, stellate cells have been shown to encode intensity information (Rhode, Oertel, et al., 1983). T-stellate cells (named because they project to the “Trapezoid body”) are the excitatory subtype of stellate cells. T-stellate cells encode intensity information from the auditory nerve and do so by receiving multiple small bouton-like synapses from the auditory nerve. They are easily excitable due to their high input resistance. Studies of outward conductances in T-stellate cells showed that there is no low-voltage potassium conductance (P. Manis & Marx, 1991; Oertel et al., 1990). Applying depolarizing current injections elicits a series of regularly spaced action potentials, similar to the tonic 3 variant in NA (P. Manis & Marx, 1991; Oertel et al., 2011; Rhode, Smith, et al., 1983). It is not clear if T-stellate cells contribute to envelope coding in mammalian systems. There does not seem to be a direct homolog to the diversity of responses seen in NA.

### *Measuring temporal features in vitro- Does diversity contribute to better spectro-temporal processing?*

A key component of understanding how the brain encodes spectrotemporal information is understanding how cell types in NA differentially process information. Using square wave currents is the standard practice for characterizing phenotypes in in vitro experiments and can be used to determine many properties of neurons, such as membrane excitability. However, it does not accurately represent the dynamic input neurons will receive in vivo.

Noisy current injections are temporally modulated stimuli that mimic *in vivo* like inputs and were pivotal for demonstrating that neurons are not stochastic, but instead their spiking was dependent on temporal features of their inputs (Mainen & Sejnowski, 1995). They are generated

through a simplified version of the Ornstein-Uhlenbeck process, which produces a Gaussian distributed output (Rauch et al., 2003). White noise with a predetermined standard deviation is run through an exponential filter, causing the rises and decays of the white noise to mimic synaptic conductances and superimposed onto a square current injection of a predetermined mean. Higher standard deviation results in a sharper rate of rise (ROR), mimicking more correlated presynaptic inputs. The ROR is important for preserving stimulus-driven synchrony in neural systems, which can have profound effects on circuits (Ratté et al., 2013).

Experiments using repeated iterations of frozen noise current demonstrated that NA neurons exist along a spectrum of temporal sensitivities. Single spiking neurons are the most reliable, followed by tonic 1 & tonic 2 neurons, and finally tonic 3 neurons (Ahn et al., 2014; Kreeger et al., 2012). Reverse correlations using spike-triggered averages (STAs) demonstrated increasing heterogeneity of neurons sampled resulted in an increase in the information being encoded about the stimulus (Ahn et al., 2014).

This indicates that the range of temporal sensitivities seen across NA neurons is important for encoding spectrotemporal inputs. Since these experiments were accomplished using synaptic blockers, these differences in reliability emerge from intrinsic properties. However, it is not clear what the intrinsic differences between the multiple tonic phenotypes are, nor what is underlying the varied temporal sensitivities. Fukui & Ohmori (2003) demonstrated that applying a Kv1 antagonist, dendrotoxin (DTX), caused single spiking neurons to fire tonically and tonic firing neurons to increase their firing rates, however they did not report on different tonic subtypes. This leads to a key question in chapter 2- What are the intrinsic differences underlying these different cell types?

## Operating modes- Do neurons care about the timing of their inputs? Or just the amount of input?

Neurons are said to function as integrators or coincidence detectors based on how they process inputs. This idea was initially formulated in cortical networks to explain the phenomenon of temporal coding, where neurons respond to the timing of their inputs, rather than the mean level of inputs (König et al., 1996). However, this initial argument posited that cortical neurons behaved as either or, when in reality there exists a functional spectrum of sensitivities to the timing of inputs (Prescott et al., 2008a).

Encoding the varied features of auditory nerve input requires neurons to respond to the temporal features of inputs differently. Frequency information requires rapid kinetics and phase locking capabilities while intensity information requires slow, temporally summation. One end of the spectrum of possible integratory patterns are coincidence detectors, like NL neurons. On the other end is integrators. Integrators, as opposed to coincidence detectors, have long integration time windows that allow for the summation of excitatory inputs (Hodgkin, 1948; Prescott, 2008a; Prescott, 2008b). This long temporal integration window and summation allows integrators to utilize a rate code to reflect the mean level of the input, which in this case can reflect sound intensity (Kalluri & Delgutte, 2003; Pfeiffer, 1966). However, this summation results in a filtering of rapid temporal features.

A subset of NA neurons exists between integrators and coincidence detectors on this functional spectrum. These neurons display tonic firing that can reflect the mean level of input, but also encode temporal components, albeit to a lesser degree than coincidence detectors. These neuron types are referred to as “differentiators,” a phenotype originally described in cortical neurons (Higgs et al., 2006) but have been demonstrated in numerous cortical regions and

auditory brainstem structures. Differentiators tend to have a more sinusoidal input-output function than pure integrators, which have a linear input-output function (Kreeger et al., 2012; Lubejko et al., 2019).

Differentiators may be critical for envelope coding, which requires sensitivity to temporal modulations on a slower time scale than phase locking requires, but enough sensitivity to encode spectrotemporal changes. Since these experiments were done using synaptic blockers, the differences in firing is due to intrinsic properties that are regulating their spiking. Lubejko et al., (2019) demonstrated that these phenotypes emerge from differences in their spike threshold kinetics. However, what is spike threshold adaptation? And what intrinsic properties could lead to differences in how adaptable thresholds are?

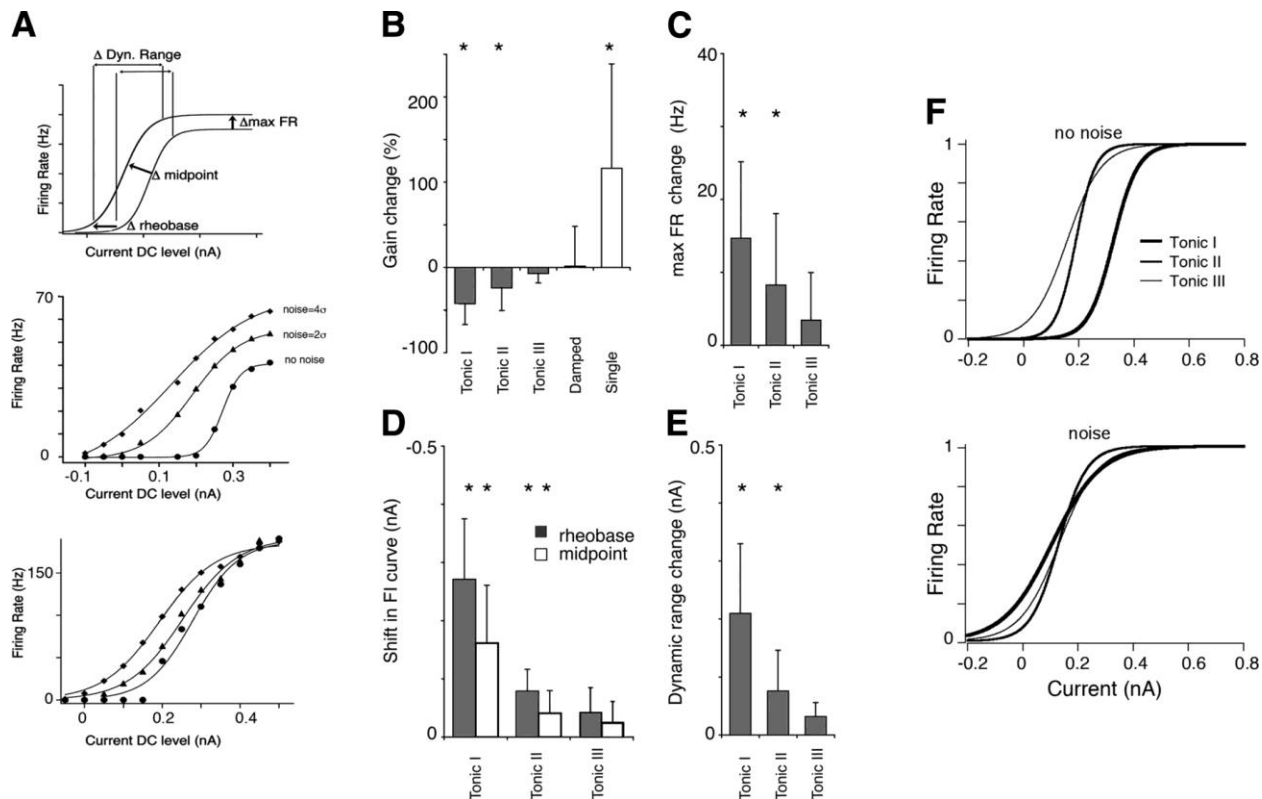


Figure 1-4 Different operating modes exist in NA

Adapted from Kreeger et al., 2012.

Quantification of noise-induced changes in the input-output function for the 3 tonic firing cell types. **A**: schematic of sigmoidal fits and the parameters measured (top), with 2 individual examples of fits shown below (middle, a divergent differentiator; bottom, a convergent differentiator). **B-E**: changes in parameters measured between fits for the no-noise and  $4\sigma$  curves. Values are absolute differences for rheobase, midpoint, maximum firing rate (max FR), and dynamic range for tonic I ( $n = 6$ ), tonic II ( $n = 10$ ), tonic III (5), damped ( $n = 11$ ), and single-spiking neurons ( $n = 9$ ). Negative changes in rheobase and midpoint indicate a leftward shift in the curves with noise and lower thresholds for firing; positive changes in dynamic range indicate a widening of the range. Gain change is expressed as a percentage, where negative values indicate a decrease in the slope with noise (see MATERIALS AND METHODS). Negative gain changes were typical for tonically firing neurons. In contrast, positive gain changes (steeper slopes) were typical for single-spiking neurons. Single-spiking FI curves were fit with a linear estimate to their slopes and compared between noise levels  $2\sigma$  and  $4\sigma$ . Damped neurons showed gain changes, but these either increased or decreased, averaging to zero mean gain change.  $*P < 0.05$  indicates change with significant difference between no-noise and  $4\sigma$  conditions (Student's *t*-test). **F**: FI curves for tonic neurons became more similar with noise. Idealized sigmoidal FI curves generated for each tonically firing neuronal type on the basis of mean parameter values (see Table 2) were dissimilar in the no-noise condition (top) but overlapped when noisy stimuli were used ( $4\sigma$ ; bottom).

## What is driving the differences between differentiators and integrators? Spike threshold adaptation via sodium channel inactivation and potassium channel activation

The “threshold” of a neuron is the voltage at which it has been sufficiently depolarized and the voltage-gated sodium channels open to produce an action potential. It has long been known that the voltage threshold for producing an action potential depends on the membrane’s voltage history (Azouz & Gray, 2000; Calvin, 1974) (Fig.1-5). For example, if a neuron has produced a spike recently, it will have a comparatively elevated spike threshold i.e. a more depolarized threshold. This change in threshold is determined by the kinetics that gate sodium and potassium channels. The strength of these kinetics will determine how rapid a depolarization must be in order to produce a spike.

Sodium channels are composed of 4 individual “gates.” There are 3 activation gates that are voltage dependent and determine the rate of opening of the channel, and there is 1 inactivation gate that is time dependent and closes the channel after a few milliseconds (Hodgkin & Huxley, 1952a, 1952b; Noble & Stein, 1966). These channels remain inactive until the neuron’s voltage becomes more hyperpolarized. During periods of tonic excitation, a neuron will remain depolarized, meaning more sodium channels will enter an inactivated state and are unavailable for recruitment when producing an action potential. In order to produce an action potential in this state, the neuron must rapidly depolarize in order to recruit enough non-inactivated sodium channels. If the depolarization is not rapid enough, it will increase the number of inactivated sodium channels and a spike will not be produced. Generally, the rate of sodium channel inactivation is inversely proportional to how depolarized the threshold is.

Platkiewicz & Brette (2011) determined that sodium channel inactivation is the most metabolically efficient form of threshold adaptation.

Using a computational model of spiking outputs that utilized sodium channel inactivation, Lubejko et al., (2019) demonstrated that the adaptive threshold of differentiators could be explained by sodium channel inactivation. However, experimental confirmation of sodium channel inactivation is difficult, and these results did not rule out potassium channel activation as a driving mechanism.

Contrary to sodium channels, potassium channels consist of 4 activating gates and no inactivating gates (Hodgkin & Huxley, 1952a). These activation gates are voltage dependent but have slower kinetics than sodium channel activation gates. Potassium channels tend to remain open as long as the membrane is depolarized, however they exhibit significantly more heterogeneity than sodium channels.

Kv1 channels impact subthreshold voltage changes and exert a repolarizing force on the membrane. They can contribute to the leak conductance of the neuron, or the channels that are open around rest. Leak channels lower the input resistance of neurons and can make it more difficult for a neuron to produce a spike. Thus, if depolarization does not occur rapidly enough, these channels will repolarize the membrane and prevent a spike from occurring, acting as a high-pass filter. These channels effectively increase the leak conductance and raise the threshold voltage to produce a spike, augmenting the effects of sodium channel inactivation on the adaptive threshold. Kv1 channels also affect the capability of neurons to encode temporal features of inputs due to this increased selectivity towards rapidly rising inputs (Baldassano & MacLeod, 2022; Fontaine et al., 2014; Higgs & Spain, 2011). Experiments in cortical pyramidal neurons showcased that Kv1 channels contributed to dynamic thresholds when application of

DTX nullified the dynamic threshold of the cortical neurons (Higgs & Spain, 2011). Since Kv1 channels have been demonstrated in NA, it is possible that they contribute to the different levels of threshold adaptation between differentiators and integrators, which I investigated in chapter 2.

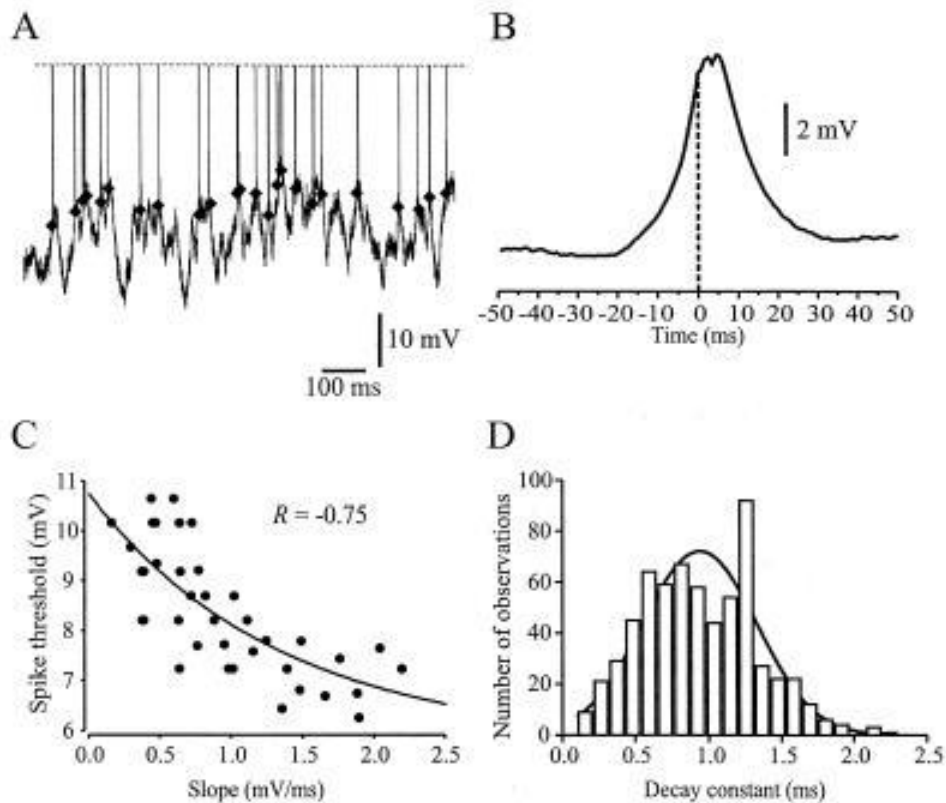


Figure 1-5 Spike threshold is inversely correlated with the rate of membrane depolarization

Adapted from Azous & Gray (2000)

(A) Example of the raw data collected from an intrinsic bursting cell during the response to a drifting grating (0.6 cycles/degree) presented to the dominant eye. (B) Spike-triggered average of the  $V_m$  for all spikes occurring during the presentation of the visual stimulus. The dashed line (time 0) corresponds to the time of action potential generation. The mean rise time (from baseline to peak) for this cell was 12 ms. (C) Scatter plot of  $dV_m/dt$  preceding a spike vs. spike threshold. The data in C were fit by the equation  $y = a + be^{-\tau/c}$ , where  $\tau = dV_m/dt$ . (D) Histogram of the decay constants ( $\tau$ ) obtained from all trials (639/695) that were significantly fit by the equation in C. The mean value is  $0.94 \pm 0.4$  ms.

## Potassium conductances in auditory processing

Voltage-gated potassium channels, Kv channels, are diverse channels that are known to regulate synaptic integration, action potential width, and firing rates (Begum et al., 2016; Gabel & Nisenbaum, 1998; Glazebrook et al., 2002; Ranjan et al., 2019; Storm, 1988). Kv channels are encoded by 40 genes and are organized into 12 different “sub-families,” based on the subunit composition (COETZEE et al., 1999). These channels have a conserved pore structure that allows for selective potassium permeability, but slight elaborations on this pore structure give rise to their variability (Dijkstra, 2003; Doyle et al., 1998; Yellen, 2002). A subset of these channels, namely the Kv1, Kv2, Kv3, Kv4, and Kv7 channels, are particularly important within auditory brainstem processes (Baldassano & MacLeod, 2022; D. H. Brown & Hyson, 2019; Caminos et al., 2007; Fukui & Ohmori, 2003; Johnston, Griffin, Baker, & Forsythe, 2008; Johnston, Griffin, Baker, Skrzypiec, et al., 2008; Johnston et al., 2010; Rathouz & Trussell, 1998; J. Wu & Kaczmarek, 2021).

### *The Kv1 channel: a critical component of auditory temporal processing circuits*

The Kv1 subfamily is arguably the most important potassium channel in auditory processing due to their role in temporal processing (Bal & Oertel, 2001; Baldassano & MacLeod, 2022; H. Brew & Forsythe, 1995; Dodson et al., 2002; Fukui & Ohmori, 2003; Gittelman & Tempel, 2006; Grigg et al., 2000; P. H. Smith et al., 1998; H. Wang et al., 1994). There are several subtypes of Kv1 channels. The predominant subunits in auditory processing are the Kv1.1 and Kv1.2, especially in birds, however Kv1.3 & Kv1.6 subunits have also been demonstrated in the mammalian MNTB (Fu et al., 2021). As mentioned in previous sections, Kv1 channels are low voltage activated, meaning they influence the subthreshold dynamics and

spike initiation kinetics of neurons (Baldassano & MacLeod, 2022; Higgs & Spain, 2011). Since they are typically open around rest, they have similar effects on membrane biophysics as leak channels. These channels are primarily used for lowering temporal jitter by increasing the selectivity of spiking in neurons that encode timing information (Akter et al., 2018; Barnes-Davies et al., 2004; H. Brew & Forsythe, 1995; H. M. Brew et al., 2003; Grigg et al., 2000; Karcz et al., 2011; Klug & Trussell, 2006; P. Manis & Marx, 1991; Oertel et al., 2008; A. D. Reyes et al., 1994; H. Wang et al., 1994).

Kv1 channels are expressed densely in timing nuclei in both mammals and birds (Akter et al., 2018; Bloom et al., 2014; H. M. Brew et al., 2003; Feng et al., 2023; Fukui & Ohmori, 2003; Oertel et al., 2008; Rathouz & Trussell, 1998). The Kv1.1 subunit is the most important of these subunits for temporal processing. Blocking the Kv1.1 subunit causes single spiking neurons to fire tonically in both mammals and birds, while blocking the Kv1.2 & 1.6 subunits merely impacted neuronal jitter (Baldassano & MacLeod, 2022; H. M. Brew et al., 2003; Fukui & Ohmori, 2003). Blocking Kv1.3 subunits did not have a notable impact on spiking activities of the MNTB (Gazula et al., 2010). As explained in previous sections on coincidence detection, Kv1 channels are also critical for ITD processing (Kopp-Scheinflug et al., 2003; Kuba et al., 2002b; Paolini et al., 2001; P. H. Smith et al., 1998; Yamada et al., 2005).

Kv1 channels seem to have different functions in intensity coding neurons of the cochlear nucleus. Bloom et al. (Bloom et al., 2014) demonstrated that Kv1.1 channels are heterogeneously expressed throughout NA, potentially indicating differential expression patterns. Kv1 expression is minimal in the intensity coding T-stellate neurons of the VCN (P. Manis & Marx, 1991; Oertel et al., 2008), however the intensity coding neurons of NA are altered by dendrotoxin (DTX), a potent antagonist of Kv1.1, 1.2, and 1.6 channels (Fukui & Ohmori, 2003). DTX caused single-

spiking NA neurons to fire tonically and caused tonic firing neurons to increase their firing responses, while developmental studies indicate that they become more prominent in tonic neurons in late development (D. H. Brown & Hyson, 2019; Fukui & Ohmori, 2003). We hypothesize a role for these channels in spectrotemporal coding, which we examine more in chapter 2.

### *Other Kv channels in auditory processing*

While Kv1 channels are central to this thesis, their role auditory processing is best understood as one within a larger family of other voltage-activated potassium channels, Kv2-7, which are discussed below.

### *The Kv2 Channel*

Kv2 channels are high voltage activated potassium channels, with activation voltages of  $\sim -15$  mV (Johnston et al., 2010). They are widely expressed in the mammalian brain, along with other electrically active biological systems, such as cardiac myocytes, gastrointestinal smooth muscle, and pancreatic cells (reviewed in Johnson et al., 2019). Irie (2021) used guangxitoxin to demonstrate that these channels are implicated in the firing outputs cartwheel neurons in the dorsal cochlear nucleus, which we discuss later, when encoding high frequency auditory nerve inputs. As mentioned earlier, Kv2 channels have been demonstrated in low frequency encoding NM neurons, making up almost 70% of the total potassium conductance in these neurons (Hong et al., 2018).

### *The Kv3 channel*

Kv3 channels are high voltage activated neurons, similar to Kv2 channels. They activate at high voltages and work to rapidly repolarize the cell membrane during an action potential in order to minimize the action potential width and maximize firing rates (reviewed in Rudy et al., 1999). In mammals, the Kv3.1 & Kv3.3 subunits are crucial for fast spiking at the Calyx of Held, while other knockouts of other subunits were not shown to have much of an effect (Choudhury et al., 2020). In birds, Kv3.1b channels are localized in presynaptic terminals of timing nuclei, and are critical for producing fast, phase-locked spikes (Parameshwaran-Iyer et al., 2003).

#### *The Kv4 channel*

Kv4 channels, also known as Shal type potassium channels, are a diverse set of potassium channels that mediate rapid & transient responses (reviewed in (Nakajo & Kasuya, 2024)). These channels are expressed in a number of systems such as cardiac cells but are also involved in dendritic integration and cell repolarization. Additionally, Kv4 channels are important targets for plasticity (Johnston, 2021). Johnston et al. (Johnston, Griffin, Baker, & Forsythe, 2008) demonstrated an A-type current that is mediated by Kv4 channels in the mouse MNTB. A computational model of this A-current demonstrated that it accelerated the decay of the first few action potentials during high frequency inputs and suggested that blocking it would raise the threshold for smaller inputs. Interestingly, these channels were not observed in the MNTB neurons of rats (Johnston, Griffin, Baker, & Forsythe, 2008).

#### *The Kv7 channel*

Also known as KCNQ channels & “M” channels (D. A. Brown, 1988; D. A. Brown & Adams, 1980), Kv7 channels are low voltage activated channels. There are 5 members of Kv7 channels, Kv7.1-Kv7.5, however only Kv7.2-Kv7.5 are expressed in the nervous system

(Jentsch, 2000; Robbins, 2001). Kv7.2. & 7.3 subunits are the most commonly expressed members, however Kv7.4 is the most expressed in auditory (and vestibular) cells (reviewed in (D. A. Brown & Passmore, 2009; Hansen et al., 2008). Kv7 channels have similar voltage sensitivities as Kv1 channels, however they have significantly slower kinetics, so are not as prominent for coincidence detecting neurons (Kuba et al., 2015).

In the rat auditory brainstem, they are localized at excitatory synapses (Caminos et al., 2007). In birds, Kv7 channels are expressed in the axon initial segment (AIS) of NM neurons, however they become the dominant subtype, instead of Kv1 channels, after removal of the cochlea. This is presumed to be a homeostatic mechanism which increases the excitability of the neurons, thus maintaining functional connections from NM neurons in a Hebbian manner (Kuba et al., 2015).

### Section III: How does inhibition sculpt auditory processing?

In chapter 3 of this dissertation, we examine the intrinsic physiology and anatomy of inhibitory neurons in the superior olivary nucleus (SON). While excitatory information is critical for bringing auditory information into the brain, inhibition sculpts it. Inhibition is required for a number of functions in auditory brainstem processes, such as sharpening phase locking for frequency tuning, boosting gap detection, and improving amplitude modulation coding (Al-Yaari et al., 2019; Dugue et al., 2007; Fukui et al., 2010; Keine et al., 2016; Monsivais et al., 2000; Williamson et al., 2015). The mammalian auditory brainstem accomplishes these tasks with a complex system of inhibitory neurons that includes, local, long range, and feed-forward inhibition (Ferragamo et al., 1998; Ngodup et al., 2020; Oertel, 1983). However, birds do not utilize local inhibition, or connectivity amongst neurons within nuclei, within brainstem structures. Instead, inhibition originates primarily in the superior olivary nucleus (SON) (Bartheld et al., 1989; C. E. Carr et al., 1989; Lachica et al., 1994; Westerberg & Schwarz, 1995). Despite this less complicated architecture, inhibition sculpts auditory inputs in a similar manner to the mammalian system, making it an excellent model to study cell-type specific inhibition (Monsivais et al., 2000; Yamada et al., 2013; Yang et al., 1999).

To determine how the SON may underlie the multiple functions of inhibition in the auditory brainstem, we examined the intrinsic physiological properties of SON neurons. Specifically, we asked 1) is there a correlation between SON response type and axonal projection, 2) do specific SON phenotypes have different capabilities to encode temporally modulated stimuli, and 3) do a subset of SON neurons respond preferentially, i.e. increase their firing rates, to temporal modulations? To provide context for these findings, we will discuss the

effects of inhibition in auditory brainstem functions, the known circuitry of inhibitory neurons, and the in vivo responses in SON.

### Inhibition in the auditory brainstem of birds- where does it come from?

In birds, inhibition in the auditory brainstem originates primarily from one structure, the SON, located bilaterally in the ventrolateral region of the brainstem. In addition to the SON, Carr et al (1989) identified a small population of GABAergic neurons surrounding both NL & NM in barn owls. This was subsequently demonstrated in chickens (Lachica et al., 1994). Yamada et al. (2013) used photoactivated uncaging to activate these neurons and observed phasic inhibition in NL neurons. They proposed that these inputs sharpen ITD processing over a wide range of excitatory input levels, however this function is still largely speculative. Regardless, the lion's share of inhibition in the avian auditory brainstem originates in the SON.

The SON receives excitatory afferents from both NA and NL and is the earliest point of convergence of these parallel circuits (Moiseff & Konishi, 1983). Additionally, it receives inhibitory inputs from the contralateral SON. There is no evidence that inputs from NA and NL synapse onto separate populations of SON neurons (Burger et al., 2005), however that is still speculative and an important question for future experiments.

Neurons in the SON subsequently project back to either the three lower order nuclei (NA, NM, and NL), or to the contralateral SON. Retrograde labeling studies demonstrate that these projections stem from entirely distinct populations of neurons (Burger et al., 2005). Functionally, the effect of inhibition in avian auditory brainstem circuits is most documented in the timing pathway.

## Inhibition in avian brainstem timing circuits- mechanisms and impact

NM neurons phase lock to specific characteristic frequencies of ANF activity to produce precisely timed spikes that are critical for frequency encoding and ITD computation. Therefore, NM neurons must use mechanisms to fine-tune their output across a spectrum of sound intensities and frequencies (Köppl, 1997b; Monsivais et al., 2000). Intrinsic membrane differences and excitatory synaptic dynamics allow for the extraction of different frequency information, however inhibition from the SON sculpts the output. Inhibition in the avian system is primarily GABAergic, however it has been shown in NA, NM, and NL, that glycine is co-localized within the same vesicles as GABA (C. E. Carr et al., 1989; Code & Rubel, 1989; Fischl et al., 2014; Kuo et al., 2009). There are no glycine receptors localized within the synapse of the postsynaptic membrane and glycine only modulates activity during bouts of intense stimulation. There is, however, an abundance of GABA<sub>A</sub> receptors localized to the postsynaptic membrane. Therefore, inhibition is primarily driven by GABA. The inhibitory postsynaptic currents (IPSCs) in NM are shown to be slow and temporally summing (Monsivais et al., 2000).

High intracellular chloride levels shift the reversal potential for chloride to a voltage positive to the resting potential, and therefore current flowing via the ionotropic GABA-receptor channels is depolarizing, leading to a powerful shunting inhibition. The density of GABAergic terminals is highest in lower frequency NM neurons, where it has been shown that inhibition expands dynamic range, or range of sound intensities a neuron can encode before saturating its firing probability (Al-Yaari et al., 2019; Hamlet et al., 2014; Monsivais et al., 2000). Inhibition has been shown to reduce neuronal jitter in NM neurons with characteristic frequencies (CFs) of over 500 Hz, particularly during intense bouts of stimulation (Fukui et al., 2006; Nishino et al., 2008). In addition to the postsynaptic GABA<sub>A</sub> receptors in NM, activation of presynaptic

GABA<sub>B</sub> receptors prevents synaptic depression and causes consistent EPSC amplitudes, driving the temporal precision of phase-locking (Lu et al., 2005).

Inhibition in NL has similar properties to inhibition in NM. It is primarily mediated by depolarizing GABAergic inhibition that causes shunting. Interestingly, the kinetics of IPSCs in NL are more rapid than the IPSCs in NM (Kuo et al., 2009). Early mathematical models of bilateral coincidence detection claimed that the observed relationship of NL firing rate & ITD could be explained by NM's excitatory inputs and that the system did not need inhibitory inputs (Brückner & Hyson, 1998; Colburn et al., 1990). However, Yang et al (1999) stimulated SON efferent fibers while injecting current into NL neurons and showed a significant increase in the amount of current needed to produce spikes when stimulating inhibitory synapses. These results can be interpreted as inhibition tightening the window of excitatory inputs for ITD calculation. Additionally, Takahashi & Konishi (2002) demonstrated the importance of inhibition in ITD calculations of the barn owl by applying GABAergic antagonists to NL and observing a robust drop off in ITD responsiveness in the inferior colliculus. The results from these papers demonstrated that inhibition plays a critical role in assisting timing-coding neurons encode temporal features.

### Inhibition in avian brainstem intensity circuits and the encoding of dynamic range

Intensity processing occurs in parallel with timing circuits in the avian brainstem, beginning with the AN synapsing onto NA. Similar to both NM & NL, NA receives GABAergic input primarily from the SON. However, IPSCs in NA are significantly more varied in their kinetics than IPSCs in timing circuits. Kuo et al (2009) utilized a potassium based intracellular solution in order to classify response phenotypes in current clamp before measuring IPSCs in voltage clamp. They classified neurons as tonic firing or onset (single-spiking) and found that,

although the rise of IPSCs were similar, the decays were significantly more rapid in onset neurons than in tonic firing, which had a wide range of decay values. While it is possible that this range of decay values observed in tonic neurons is from tonic subtype variability, it is not addressed in this study. Additionally, presynaptic GABA<sub>b</sub> autoreceptors modulate activity within NA but suppressing both excitatory and inhibitory activity (Eisenbach et al., 2019).

Less is known about the function of inhibition in NA. NA neurons are physiologically diverse, and likely have different functional roles (especially single spiking neurons), however a primary role is to encode intensity cues from spectrotemporal inputs. As mentioned earlier, NA neurons encode intensity cues by receiving several small bouton-like excitatory synapses from the auditory nerve, allowing them to have a graded level of input that can reflect mean presynaptic levels (Reviewed in MacLeod & Carr, 2007). The range of sound intensities NA neurons can encode, or the difference between the softest sound capable of producing action potentials and the point at which firing rate saturates, is referred to as the neuron's "dynamic range" (Köppl & Carr, 2003).

It is important to maximize the range of sound intensities for several functions, such as distinguishing the proximity of sound sources and determining fitness of a potential threat. In both birds and mammals, individual cochlear neurons tend to have a dynamic range that spans ~25-30dB (Dean et al., 2005; Köppl & Carr, 2003), which is smaller than the dynamic range of ANFs (Köppl, 1997a; Sachs & Abbas, 1974). This is significantly smaller than the total range of sounds that can be encoded, which is ~100-120 dB (Simmons et al., 1971) and it is not likely that neuronal firing rates can accurately reflect this wide range of sound intensities (Colburn et al., 2003). The prevailing theory of intensity coding is that the firing of intensity coding neurons is dependent on the statistics of their inputs, i.e. the auditory context, and that their firing rate is

adaptive to these statistics (Dean et al., 2005, 2008). One of the proposed mechanisms underlying spiking adaptation is inhibition (reviewed in (Benda, 2021). Inhibition via reciprocal circuits can expand the dynamic range of a neuron by increasing inhibitory output as the output of the excitatory neuron increases.

This such loop exists in the avian brainstem via inputs from SON (Al-Yaari et al., 2019; Burger et al., 2005). Al-Yaari et al (2019) demonstrated that inhibition from the SON increases the dynamic range of NM neurons (particularly low best frequency (BF) neurons) by stimulating the auditory nerve and recording from NM cells, then lesioning the SON. The effect on NA neurons has not yet been established, however immunohistochemical studies show inhibitory synapses are distributed throughout NA, both clustered on the cell bodies and within the neuropil (MacLeod & Pandya, 2022). Inhibitory synapses in NA have shown co-release of both GABA and glycine (Kuo et al., 2009). The exact function of each has not been determined. However, it has been shown that each works on different time scales with inhibitory postsynaptic potentials (IPSPs) evoked from glycine operating on more rapid time scales than GABA. However, how do the neurons that are providing these inhibitory inputs actually respond to inputs?

## Physiology & anatomy of superior olivary nucleus

While the function and effects of inhibition in avian auditory processing have been well documented, a primary focus of this dissertation is examining the intrinsic physiology & cell-type specific anatomy of the inhibitory neurons themselves. The avian SON was first described in Boord (1961) in a paper studying efferents in pigeons and caimans. 23 years later, Moisseff & Konishi (1983) published findings from *in vivo* recordings, showing that firing rates in SON neurons were proportional with ipsilateral sound intensity. They reported that these responses

were not sensitive to temporal features of the inputs, just the mean input levels. The firing rate of SON neurons generally increased only with ipsilateral sound presentation, but a subset of cells would respond to both contralateral or ipsilateral sounds, demonstrating that an NA on one side could drive activity in both SON.

While there are more recent experiments recording from SON neurons *in vivo* (Lachica et al., 1994; Tabor et al., 2011), Coleman et al. (2011) was the first to characterize different response types. Here, they describe at least 3 phenotypes- sustained, onset, and suppressed. Sustained neurons fired tonically throughout tone presentations, onset neurons fired at the beginning of a tone presentation, and suppressed neurons have their firing inhibited by tone presentations. While all previous studies showed no temporal responsiveness in SON, Coleman et al (2011) demonstrated that some SON neurons, generally neurons with low CF (below 1 kHz, but up to ~4 kHz occasionally), phase-locked to stimuli with high fidelity, indicating that temporal information is maintained in its outputs. Applying GABA<sub>A</sub> and strychnine, GABA and glycine receptor antagonists respectively, increased firing rates in response to sound stimuli and reduced phase locking in SON neurons. This temporal sensitivity indicates that the inputs to SON maintain some level of temporal information from NL and/or NA and that the binaural inhibition is important for preserving temporal features. However, it is not clear if this range of sensitivities is underlied by different neuron types. We consider the function of this binaural connection in the discussion section of chapter 3.

The most thorough documentation of the SON's output circuitry comes from Burger et al. (2005), where a series of elegant retrograde labeling experiments determined that the SON had divergent output projections: one population that projected ipsilaterally to all three of the lower order nuclei (NM, NL, and NA) and an entirely separate population that projects to the

contralateral SON (SONc). This was determined by injecting different fluorescently labeled retrograde tracers in the SON's targets and measuring co-localization in the ipsilateral SON.

The combination of diverse response types, demonstrated in Fig. 1-6, and divergent projections was the impetus for the set of experiments described here in chapter 2. The avian system is largely devoid of any local inhibition, yet the inhibition present accomplishes the same diverse tasks that the mammalian system does- sharpening of ITD coding, improvement of amplitude modulation coding, better frequency tuning, and improved gap detection. Therefore, we looked at the cell-type specific anatomy of SON cells to determine if specific inhibitory cells are utilized in particular outputs. Additionally, we utilized temporally modulated stimuli *in vitro* in an attempt to bridge the gap between the responses seen *in vivo* and *in vitro*, particularly matching the range of temporal sensitivities seen *in vivo* with the cell types and circuits mapped out *in vitro*.

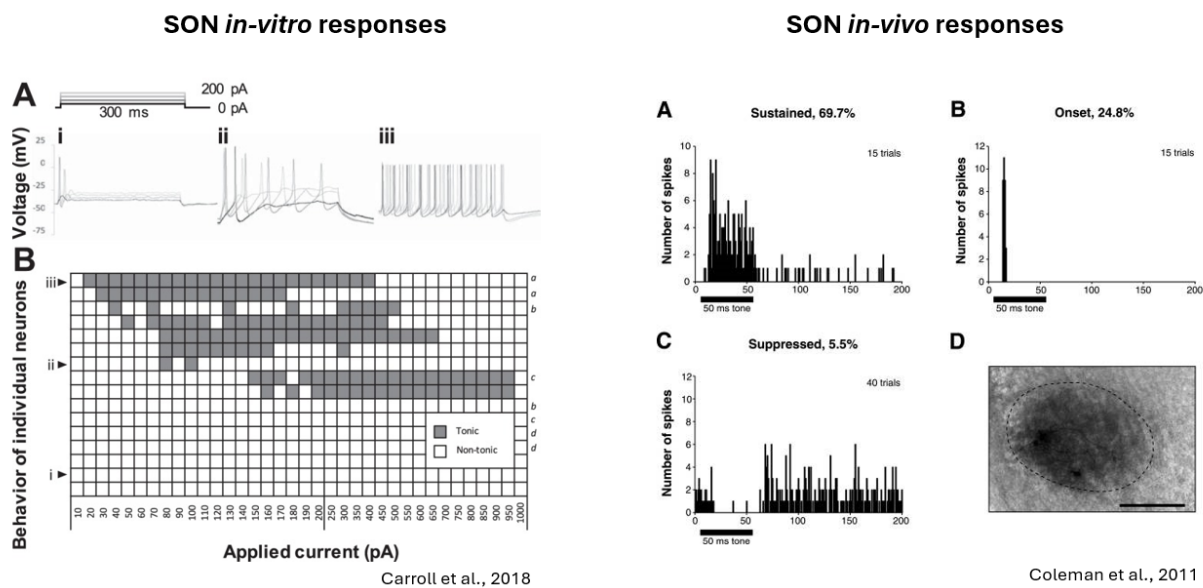


Figure 1-6 *In vitro* and *in vivo* responses of the SON

Left- The SON has two described electrophysiological responses *in vitro*: Single spiking and tonic firing. Adapted from Carroll et al., 2018

Right- There are more at least 3 described *in vivo* responses in the SON: Sustained, onset, and suppressed. Adapted from Coleman et al., 2011.

## Inhibition in the mammalian auditory brainstem

In mammalian brainstem circuits, inhibition is utilized in several ways, both in the sharpening of auditory encoding and potentially in auditory computations like ITD coding. In the mammalian system, a complex web of both local and long-range inhibition is the basis for a number of functions, such as sharpening phase locking for frequency tuning, boosting gap detection capability, and improving amplitude modulation coding (Altschuler et al., 1986; Chanda & Xu-Friedman, 2010; Ferragamo et al., 1998; Kolston et al., 1992; S. Wu & Oertel, 1986; Xie & Manis, 2014).

Inhibitory neurons in the mammalian auditory brainstem are predominantly glycinergic, along with a smaller number of GABAergic projections. In the VCN, the structure considered to be analogous to the avian auditory brainstem, there are two described inhibitory cell types: D-stellate cells and L-stellate cells. D-stellate cells were first described in 1983 (Oertel, 1983). They extend their dendrites across multiple iso-frequency lamina, thus being driven by broadband activity. D-stellate cells, which fire tonically upon current injection, project dorsally toward the DCN, but also project to the contralateral VCN and synapse onto bushy cells (Ngodup et al., 2020). L-stellate cells are also driven by AN activity but are activated by only a small number of isofrequency lamina, thus providing narrowband inhibition to ipsilateral stellate & bushy cells. L-stellate cells, which also fire tonically to depolarizing current injections, are comparatively small with differences in spiking kinetics, such as spike latency (Ngodup et al., 2020).

The DCN is comparatively more complex than the VCN. There are at least 2 inhibitory cell types but nearly 70% of all synapses in the DCN are inhibitory (Rubio & Juiz, 2004). The most abundant inhibitory cell type is known as the “cartwheel” cell type. Cartwheel cells

integrate non-auditory sensory input with auditory inputs before providing lateral inhibition to other cartwheel cells and to pyramidal neurons, the primary excitatory output neuron of the DCN. Each of these different projections has a different function and works on a different timescale for a “context-dependent” form of auditory processing (Mancilla & Manis, 2009). Cartwheel cells have complex firing patterns, producing both complex bursts of activity, as well as simple spikes (Kim & Trussell, 2007; P. B. Manis et al., 1994; Zhang & Oertel, 1993). Tuberculoventral cells receive narrowband inputs from the auditory nerve before providing inhibitory projections to ipsilateral bushy cells in the VCN. While these projections are predominantly glycinergic, GABA has also been described in their synapses (Alibardi, 2000).

As mentioned earlier, inhibition is potentially utilized in binaural computations, like ITD processing, in mammalian auditory systems. Bushy cells have excitatory projections to both the ipsilateral medial nucleus of the trapezoid body (MNTB) & the ipsilateral medial superior olive (MSO). The “bushy cell to MNTB” synapse is a famous connection, the “Calyx of Held,” known for its single large synaptic connection and rapid synaptic kinetics (Reviewed in Baydyuk et al., 2015). Subsequently, the MNTB provides glycinergic inhibition to the contralateral MSO, which integrates the ipsilateral excitation and contralateral inhibition for ITD computation, which are reflected in its firing rate. Despite the stark contrasts in both the brainstem anatomy and function of inhibition, birds use auditory information in a similar manner to mammals, therefore a driving question was how birds utilize inhibition to process sound cues, which we begin to highlight in the next section (reviewed in Burger et al., 2015).

**Section IV- Dynamic clamp: Modeling intrinsic ion channels, synaptic conductances, and noise stimuli.**

In chapter 4 of this dissertation, we utilize a computational simulation of neuronal processes using a technique called dynamic clamp to verify the results of previous experiments as well as begin new experimental directions. The idea of dynamic clamp was first described by Scott (1979) in a Ph.D. thesis entitled “Stimulation simulations of young yet cultured beating hearts,” where two segregated populations of chick ventricular cells were electrical coupled through an electrical circuit. This technique was popular in cardiology and eventually used in neurophysiology in 1993 by Dr. Eve Marder’s lab, as a method for simulating artificial conductances in biological systems (Sharp et al., 1993).

### Modeling in dynamic clamp- what can you do with it?

Dynamic clamp is a technique that is based on conventional current clamp. However, it alters the conductance of a neuron using the measured membrane potential to control the amount of current injected into a neuron using a computer interface that rapidly samples the membrane voltage (Sharp et al., 1993). When simulating a conductance, the dynamic clamp computes the difference between the voltage of the membrane and the reversal potential of a specified conductance. If the sampling and conductance computation are fast enough, the influence of any conductance can be reproduced (reviewed in (Prinz et al., 2004)).

One of the simplest things possible with dynamic clamp is the modeling of voltage independent conductances, such as ligand-gates conductances (Sharp et al., 1993). Subtracting conductances is possible as well. (Sharp et al., 1993) was able to subtract leak conductances that were added from the penetration of the electrode when recording.

More common is the modeling voltage dependent intrinsic conductances. The addition of voltage dependent conductances is a powerful alternative to pharmacology studies, in that the

precision over the channel being modeled in or out, is very high. Additionally, antagonists are not able to be washed out, such as dendrotoxin. This makes washouts and recovery from antagonists not feasible. However, if the kinetics of the conductance has been measured, those values can be used to “rescue” whatever conductance was blocked (Sharp et al., 1993). Adding in conductances also can allow the observation of novel dynamics (Prinz et al., 2004).

A limitation with dynamic clamp comes from the fact that all current is injected into the soma, generally. Therefore, while intrinsic conductances, particularly ones expressed at the soma, can be modeled with high accuracy, mimicked conductances that would occur far from the soma can only be approximated (Prinz et al., 2004). Neurons in NA are generally small, including dendritic branching, (<100 nM) (Soares et al., 2002) and therefore, electrotonically compact. We take advantage of this in chapter 4, when we model GABAergic conductances in NA.

### Conductance clamp as an alternative for noisy currents

A critique of noisy currents as a paradigm is that they are not responsive to changing properties of the cell’s membrane. In current clamp, the fluctuation of current which causes the neuron to produce a spike is unaffected by the spike. Normally, there is a shunting effect. The action potential is then driven to have a shape (height and width) which bears very little relation to the prevailing input level or its recent history. Additionally, as the voltage is pushed away from the reversal potential, the driving force of the excitatory input should be diminished, a process that is absent in current clamp (Prescott et al., 2006). Examples of dynamic clamp are demonstrated in Figure 1-7.

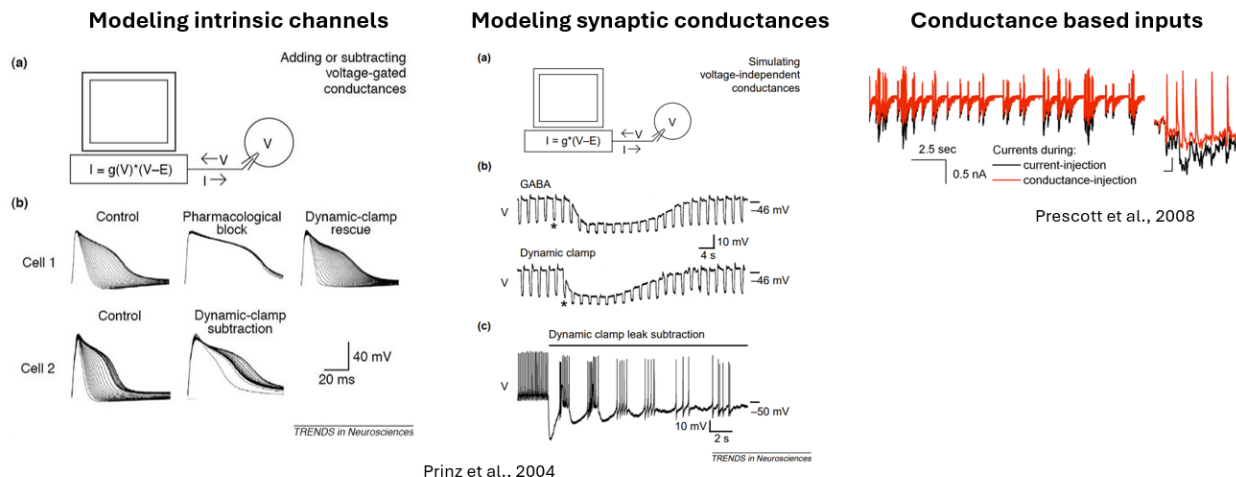


*Figure 1-7 Different applications of dynamic clamp*

Left- Modeling intrinsic ion channels. In this example, tetraethylammonium (TEA) was used to block high-voltage threshold potassium channels. Dynamic clamp then modeled in the conductance of the blocked channel and was able to rescue the action potential morphology. Additionally, negative conductance can be applied to counteract the effect of an ion channel. Adapted from Prinz et al., 2004.

Middle- Modeling synaptic conductances. In this example, dynamic clamp was used to recreate a neuron's voltage response of a synaptic conductance. This conductance can now be simulated during spiking experiments. Adapted from Prinz et al., 2004.

Right- Conductance clamp – Simulating inputs with conductance injections allows for inputs to be responsive to voltage-dependent parameters of the neuron's voltage. Adapted from Prescott et al., 2006

## Chapter 2 Low threshold voltage-gated potassium channels in the cochlear nucleus angularis

\*Note, this chapter is a slightly modified version of “Kv1 channels regulate variations in spike patterning and temporal reliability in the avian cochlear nucleus angularis,” published in the *Journal of Neurophysiology*, 2021.

Neurons in early sensory nuclei must process a wealth of incoming information to extract features that are relevant to their particular circuit. The avian cochlear nucleus is composed of two divisions, nucleus magnocellularis (NM) and nucleus angularis (NA), each of which extract unique information from auditory nerve activity in parallel (C. E. Carr & Soares, 2002). NM neurons encode timing information by phase-locking to the fine structure in the acoustic signal (Sachs et al., 1978; Sullivan & Konishi, 1984), partly enabled by specialized intrinsic properties such as a large low-threshold voltage-gated potassium conductance (GKLT) (Ohmori, 2014; Raman et al., 1994; Rathouz & Trussell, 1998; A. D. Reyes et al., 1994; Sanchez et al., 2015). This dendrotoxin-I (DTX)-sensitive conductance is attributed to the expression of the Kv1 family of potassium channels, particularly Kv1.1 and Kv1.2, that are prominent throughout the auditory brainstem of birds and mammals (Akter et al., 2018; H. Brew & Forsythe, 1995; Johnston et al., 2010; Koyano et al., 1996; Lu et al., 2004; P. Manis & Marx, 1991; S. Wu & Oertel, 1986).

In contrast to NM, NA has been understood to process information about sound intensity, or level, in service of interaural level difference computation (Konishi et al., 1985; Sullivan & Konishi, 1984; T. T. Takahashi & Konishi, 1988a; Viète et al., 1997). More broadly, however, NA neurons are also involved in spectrotemporal and amplitude modulation coding and auditory envelope processing (Fontaine et al., 2014; Steinberg & Peña, 2011). The neuronal population in

NA shows greater morphological and physiological heterogeneity than those in NM and nucleus laminaris (NL) (Fukui & Ohmori, 2003; Köppl & Carr, 2003; Soares et al., 2002). Sound-evoked responses observed in vivo in NA fall into a range of response categories, such as onset, chopper, primary-like, and “Type IV,” similar to corresponding recorded responses in the mammalian cochlear nucleus (Köppl & Carr, 2003; Sachs et al., 1978; Warchol & Dallos, 1990). Likewise, NA neurons display a range of electrophysiological phenotypes that likely arise from the expression of a more diverse array of ion channels (Ahn et al., 2014; D. H. Brown & Hyson, 2019; Fukui & Ohmori, 2003; Kreeger et al., 2012; Lubejko et al., 2019; Soares et al., 2002). Single-spiking neurons in NA most closely resemble NM neurons, whereas a broad group of repetitively firing neurons in NA can be further subdivided according to their firing patterns to step currents in vitro: early burst firing (tonic I), late or delayed firing (tonic II), and regular spiking (tonic III) (Kreeger et al., 2012; Soares et al., 2002). A DTX-sensitive conductance has been shown to be required for the single-spiking phenotype, but blocking this conductance also elevated firing rates in tonic neurons (Fukui & Ohmori, 2003). Along with immunohistochemical evidence for Kv1 channel protein expression in NA (Bloom et al., 2014; Lu et al., 2004), these data suggest that GKLT is present and active in shaping NA neuron physiology. The ion channel basis of the different tonic phenotypes is not yet known.

The parallels between the heterogeneity among in vivo response types and the heterogeneity among in vitro response types suggest that intrinsic properties may have a significant effect on the transformation of auditory information. We have recently investigated type-specific variation in sensitivity to temporally modulated stimuli in the tonic neurons in vitro and shown how diversity in intrinsic properties can enhance stimulus encoding (Ahn et al., 2014;

Kreeger et al., 2012). Temporal modulation sensitivity in vitro and bandpass feature extraction in vivo could be replicated in NA neurons using a phenomenological model of adaptive spike thresholds (Fontaine et al., 2014; Lubejko et al., 2019). Although the model was originally derived from the biophysical phenomenon of sodium channel inactivation (Platkiewicz & Brette, 2010), its ion channel basis in NA has not been empirically confirmed and could also be influenced by other subthreshold conductances, including GKLT (Higgs & Spain, 2011; Prescott, Ratté, et al., 2008; Ratté et al., 2015).

In this study, we used whole cell patch-clamp electrophysiology and DTX to pharmacologically block GKLT and test whether GKLT was needed to elicit the various spiking phenotypes among the tonic neurons. We further investigated whether GKLT was necessary for the temporal reliability of firing, high-pass filtering properties, and spike threshold adaptation that characterized a subset of tonic firing neurons.

## Materials and methods

### *Brain Slice Preparation*

All animal procedures were performed with Institutional Animal Care and Use Committee approval and according to University of Maryland guidelines on animal welfare. Chicken (*Gallus gallus*) embryos incubated to embryonic days 17–18 were cooled and rapidly decapitated, and the head section containing the brain stem blocked, placed in a chilled, oxygenated low-sodium artificial cerebrospinal fluid (ACSF) (low-Na<sup>+</sup> ACSF in mM: 97.5 NaCl, 3 KCl, 2.5 MgCl<sub>2</sub>, 26 NaHCO<sub>3</sub>, 2 CaCl<sub>2</sub>, 1.25 NaH<sub>2</sub>PO<sub>4</sub>, 10 dextrose, 3 HEPES, and 230 sucrose) and dissected out of the cranium. The brain stem tissue block was mounted with cyanoacrylate glue and supported with 5% agarose gel solution. Transverse slices (250 μm thick) containing NA were cut on a

vibrating tissue slicer (Leica Microsystems, Wetzler, Germany). Slices were incubated in normal ACSF (in mM: 130 NaCl, 3 KCl, 2 MgCl<sub>2</sub>, 26 NaHCO<sub>3</sub>, 2 CaCl<sub>2</sub>, 1.25 NaH<sub>2</sub>PO<sub>4</sub>, 10 dextrose, and 3 HEPES) at 34°C for 30 min then held at room temperature in normal ACSF until recording.

#### *Whole Cell Patch-Clamp Electrophysiology*

Slices were placed in a recording chamber and continuously perfused with oxygenated, warmed normal ACSF (1–2 mL/min, 28°C–30°C) containing synaptic blockers [3 μM strychnine, 20 μM SR95531 (gabazine), 15 μM DNQX, and 20 μM AP5; Sigma] to isolate intrinsic activity. Whole cell patch-clamp recordings were performed on visually identified NA cells using infrared differential interference contrast video microscopy. Initial glass recording pipette resistances were 3–7 MΩ. Pipettes were filled with a potassium gluconate intracellular recording solution (in mM: 110 potassium gluconate, 20 KCl, 1 EGTA, 2 MgCl<sub>2</sub>, 10 HEPES, 2 Na<sub>2</sub>ATP, 0.3 Na<sub>2</sub>GTP, 10 phosphocreatine, and 0.2% biocytin). Series resistance, cell capacitance, and resting membrane voltage were measured upon break-in in voltage-clamp mode. Voltage recordings were made with a MultiClamp 700B amplifier (Molecular Devices, Sunnyvale, CA) set to current-clamp mode. Application of the current stimulus and recording of the voltage output were controlled by an analog-to-digital board (National Instruments, Austin, TX) and a computer running custom software written in IGOR Pro (WaveMetrics, Lake Oswego, OR). A holding current was applied to maintain a constant voltage baseline of approximately –60 mV. Drug application for pharmacological manipulation of voltage response was performed by bath application of dendrotoxin-I (100 nM, Alomone Labs Cat. No. D-390), a potent antagonist of Kv1.1, 1.2, and 1.6 channels (35, 36).

Cell-type classification protocols were carried out to identify neuronal phenotypes in NA with 400-ms-duration flat current steps of varying amplitudes from  $-150$  pA up to  $750$  pA in  $50$  or  $100$  pA intervals. We collected data from  $77$  NA neurons ( $20$  single-spike,  $12$  tonic I,  $16$  tonic II,  $23$  tonic III, and  $6$  damped, see results). The patterns of action potential (AP) firing over multiple current steps were used to divide NA neurons into three broad groups: single-spiking, tonic firing, or damped. Single-spiking NA neurons resembled neurons in NM and NL, firing a single onset AP at all step amplitudes. Tonic firing neurons fired repetitively with overshooting action potentials throughout the duration of the flat current steps at most amplitudes, but could be further subdivided based on their characteristic firing at depolarizing steps just above rheobase: burst firing at the onset of current injection (tonic I), a delay followed by burst firing (tonic II), or tonic firing with uniform interspike intervals (tonic III) (see Soares et al., 2002 for more details). Damped neurons fired broad APs that progressively declined in amplitude into oscillatory subthreshold potentials. If the neuron type was ambiguous from the current levels utilized, subsequent, smaller intervals were used to distinguish the phenotype. Passive membrane properties were assessed using a small hyperpolarizing current step ( $-50$  pA).

#### *Acquisition of f-I Curve and Analysis*

Input-output functions were assessed by measuring firing-current (f-I) curves with standard flat current steps (400-ms duration as for classification protocols) or noisy current stimuli (2-s duration). Stimuli to acquire noise f-I curves were constructed by convolving Gaussian white noise with an exponential function (time constant,  $3$  ms) added to a direct current (DC) step function as described previously (Ahn et al., 2014; Kreeger et al., 2012). These noise stimuli simulate the arrival of many small, stochastic, and statistically independent synaptic currents,

both excitatory and inhibitory. To accommodate cell-to-cell differences in input resistance, a standard noise current was created by calibrating the standard deviation (around a zero mean) of the noise current to generate a 2-mV standard deviation in the membrane potential in the target neuron, designated “1 $\sigma$ .” The amount of voltage fluctuation was varied by multiplying the standard noise stimulus by a factor of 2, 4, or 8 (i.e., 4-, 8-, and 16-mV voltage fluctuation, respectively). Each trial had an interstimulus interval of 8–10 s. A hyperpolarizing conditioning prepulse (–50 pA, 1 s) was applied before each stimulus to minimize sodium channel inactivation from the prior stimulus. A complete series of stimuli in the parameter space (mean DC, noise level) was systematically generated by varying the mean current amplitude and noise level independently (3 noise levels, 5–7 DC levels). Firing rates were averaged across three stimulus repetitions over the full 2-s duration and reported as means  $\pm$  SD in hertz. After acquisition of control data, DTX (100 nM) was bath-applied to the slice and data for drug trials were acquired after a 10-min wash-in period.

Metrics to quantify differences between the lowest noise level (2 $\sigma$ ) and highest noise level (8 $\sigma$ ) curves were devised. One metric quantified the total area difference index (ADI) (Lubejko et al., 2019):

$$ADI = \frac{\sum_{i=1}^n \text{normFR}_{8\sigma,i} - \sum_{i=1}^n \text{normFR}_{2\sigma,i}}{\sum_{i=1}^n \text{normFR}_{8\sigma,i}}$$

where normFR was the firing rate at each of n steps in each noise level normalized to the maximum firing rate in whole data set. The second metric was the normalized difference in the maximum firing rate between 2 $\sigma$  and 8 $\sigma$ ,  $\Delta\text{MaxFR}$ :

$$\Delta MaxFR = \frac{MaxFR_{8\sigma} - MaxFR_{2\sigma}}{\sum_{i=1}^n normFR_{8\sigma,i}}$$

where MaxFR refers to the maximum firing rate value of each within-noise-level f-I curve. Both metrics varied from 0 (curves are identical) to 1 (maximum difference). Plotting these points (MaxFR index and the ADI index) against each other produced a spectrum of fluctuation sensitivity. Neurons closest to the origin were more “integrator-like,” whereas neurons further away from the origin were more “differentiator-like.” Using the criteria of ADI and  $\Delta MaxFR > 0.2$ , we were able to test the noise f-I curves from 15 differentiators and 5 integrators with DTX.  $\Delta MaxFR$  index and ADI index were statistically compared using Wilcoxon’s t test.

### *Spike Timing Reliability*

After noise was calibrated, a  $4\sigma$  noisy current was injected into neurons at a single DC current step amplitude (typically 150–400 pA) to produce a firing rate between 20 and 50 Hz. Repeated trials of 2-s long frozen noisy current injections were injected (usually 30 to 45 trials, or until  $>600$  spikes were collected) before and after DTX application. To quantify neuronal reliability, we calculated a shuffled autocorrelogram (SAC), a histogram of all interspike intervals between spikes across trials, excluding intervals within the same trial. The SAC is normalized by the normalizing factor (NF):

$$NF = N \cdot (N - 1) \cdot r^2 \Delta \tau D$$

where  $N$  is the number of trials,  $r$  is the average firing rate,  $\Delta\tau$  is the bin width of the correlation function (0.2 ms), and  $D$  is the length of the stimulus (2 s) (Ahn et al., 2014; Joris et al., 2006; Kreeger et al., 2012; Street & Manis, 2007). The SAC was fit with a Gaussian function, whose central peak is defined as the correlation index (CI). The precision of the firing between trials is represented in the full width at half-maximum (FWHM) of the Gaussian curve, measured by

$$FWHM = 2\sqrt{2\ln 2} \cdot \sigma_{SAC}$$

where  $\sigma_{SAC}$  represents 1 standard deviation of the Gaussian fit of the SAC. CI and FWHM, referred to as width, were quantified and compared using Wilcoxon's t test. To determine the current signal that drove the response, the spike-triggered average (STA) was also calculated. A 60-ms snippet of the current stimulus, starting 50 ms preceding each spike, was extracted and averaged for all spikes within a set.

### *Mutual Information*

To quantify the mutual information (I) between spike trains under control conditions (X) versus those recorded in DTX (Y), spike times were binned (1 ms) and their time bin distributions ( $x_i$ ,  $y_i$ ) were used to calculate Shannon's equation for mutual information (Shannon, 2001; Steveninck et al., 1997):

$$I(X; Y) = H(X) - H(X|Y)$$

where  $H(X)$  is the marginal entropy, or the observable information of X:

$$H(X) = - \sum_{i=1}^n p(x_i) \log_2 p(x_i)$$

where  $p(x_i)$  is the probability of distribution  $x_i$  and the entropy is given in bits.  $H(X|Y)$ , the conditional entropy, is the reduction of uncertainty about X given Y:

$$H(X|Y) = \sum_{i,j}^n p(x_i, y_j) \log_2 \frac{p(x_i, y_j)}{p(y_j)}$$

$$MI = 1 - H(X|Y)$$

where  $p(x_i, y_j)$  is the probability that  $X = x_i$  and  $Y = y_j$ . To control for random changes or response drift over the recording time, the experimental mutual information was compared with the mutual entropy calculated between control and “sham” conditions, where ACSF without DTX was washed into the recording chamber. Mutual information is reported in bits but bounded by 0 and 1, such that 0 implies that X and Y are completely independent and 1 implies that X is entirely predicted by Y, analogous to a similarity measure.

### *Action Potential Threshold Analysis*

The action potential threshold was defined as the voltage at which an all-or-none regenerative spike was initiated. This threshold was determined by using the first derivative of the voltage as

previously described (Fontaine et al., 2014). A criterion value of the derivative was selected and applied for the entire set of voltage responses across the f-I curve. Neither small changes in the criterion value nor the alternative of using the second derivative affected the results of within-subject analyses. Direct comparisons of absolute threshold between neurons, however, were omitted, as differences in the criterion applied could affect across-subject comparisons. The mean, median, and variance of the spike threshold measured across the action potentials for a given stimulus were calculated for each DC step amplitude  $m$  and noise level  $s$  combination. The mean and median were nearly identical in all cases, as expected for nearly normal distributions.

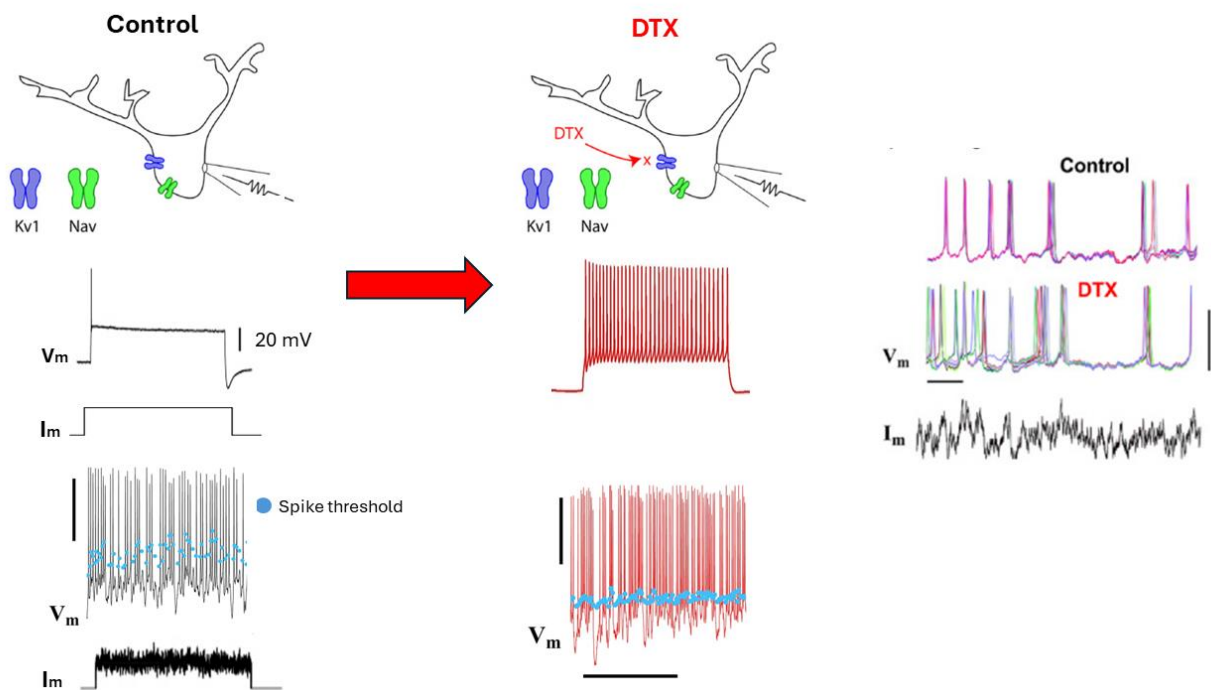


*Figure 2-1 Schematic for DTX experiment*

Neurons were recorded from in current-clamp mode. Flat current injections were used to identify the electrophysiological phenotype of the neurons being recorded and noisy current injections were used to examine temporal properties. We quantified the dynamic spike threshold seen during noisy currents. Then, we applied DTX to block Kv1 channels and repeated the experiments to determine if Kv1 channels contributed to temporal sensitivities via threshold adaptation.

## Results

### Spiking Patterns in NA Are Shaped by a DTX-Sensitive Potassium Conductance

To determine whether low-threshold potassium channel activation was involved in shaping the electrophysiological phenotypes observed in the chick cochlear nucleus NA, we recorded the voltage responses before and after bath application of DTX (100 nM), a specific antagonist of the Kv1.1, Kv1.2, and Kv1.6 channels. We characterized the firing patterns and passive membrane properties using a series of flat depolarizing current injections during whole cell patch-clamp recordings from NA neurons. As shown previously, in control conditions, NA neurons displayed heterogeneous spiking phenotypes in vitro that could be broadly classified as single spiking (Fig. 2-2Ai) or tonic firing (Fig. 2-2, Bi–Di) (Ahn et al., 2014; Kreeger et al., 2012; Soares et al., 2002). Using small current steps, tonic firing neurons can be further distinguished into three subgroups based on whether they tend to show early bursts (tonic I, Fig. 2-2Bi), late bursts (tonic II, Fig. 2-2Ci), or repetitive firing evenly spaced for the duration of the stimulus (tonic III, Fig. 2-2Di) (see also (Soares et al., 2002).

When DTX was applied, changes in the firing patterns were observed in single spiking, tonic I, and tonic II neurons. In all single-spiking neurons, which characteristically fire single-onset spikes upon depolarization in control conditions, DTX application induced repetitive firing throughout the current injection ( $n = 12$ ; Fig. 2-2Aii), in agreement with a previous study (Fukui & Ohmori, 2003). In tonic I, neurons DTX application eliminated the burst cessation in these neurons that occurred at low-amplitude steps in control and instead induced firing throughout the step duration at all step levels ( $n = 10$ , Fig. 2-2Bii). Similarly, in tonic II, neurons DTX

application eliminated the delay in firing at low-amplitude steps in control (n = 8, Fig.2-2Cii).

Tonic III neurons, in contrast, showed no apparent changes in firing pattern (n = 13, Fig.2-2 Dii).

Changes in the firing patterns also resulted in significant changes in the overall input-output functions for tonic I and tonic II neurons, as well as single-spiking neurons (single spiking: n = 12, P = 0.04 at step amplitude 0.05 nA, P < 0.001 at 0.15–0.35 nA, Fig. 2-2Aiii; tonic I: n = 10, P < 0.001 at 0.15–0.35 nA, Fig.2-1Biii; tonic II: n = 8, P < 0.001 at 0.15–0.35 nA, Fig.2-2Ciii; Sidak's multiple comparisons test). These firing rate changes were accompanied by a reduction in the threshold current amplitude (rheobase) (Fig. 2-2, Aiv–Civ; single spiking: control mean =  $0.29 \pm 0.09$  nA, DTX mean =  $0.13 \pm 0.08$  nA, P = 0.001; tonic I: control mean =  $0.21 \pm 0.07$  nA, DTX mean =  $0.078 \pm 0.4$  nA, P = 0.03; tonic II: control mean =  $0.26 \pm 0.07$  nA, DTX mean =  $0.14 \pm 0.8$  nA, P = 0.03; Wilcoxon's test). These changes in excitability were likely partly due to the increase in input resistance measured in these neurons [single-spike: n = 12, control Rin =  $101.6 \pm 17.14$  M $\Omega$  (mean  $\pm$  SD), DTX Rin =  $191.7 \pm 31.37$  M $\Omega$ , P = 0.001, Fig. 2-2Av; tonic I: n = 9, control Rin =  $243.7 \pm 29.69$  M $\Omega$ , DTX Rin =  $277.8 \pm 36.93$ , P = 0.039, Fig.2-2Bv; tonic II: n = 8, control Rin =  $230.6 \pm 29.72$  M $\Omega$ , DTX Rin =  $265.5 \pm 38.1$ M $\Omega$ , P = 0.042, Fig.2-2Cv]. In contrast, tonic III neurons showed no effects of DTX application on their firing rate, input-output function, or rheobase (Fig. 2-1Di–iv; tonic III: control mean rheobase =  $0.11 \pm 0.06$  nA, DTX mean rheobase =  $0.10 \pm 0.08$  nA, P > 0.99) nor in their input resistance (n = 13, Fig. 2-2Dv, control Rin =  $289.7 \pm 26.2$  M $\Omega$ , DTX Rin =  $291.0 \pm 24.9$  M $\Omega$ , P = 0.47, Fig. 2-2Div). Finally, a separate subset of NA neurons was characterized in control conditions as having a “damping” phenotype: broader action potentials that diminished in amplitude and whose voltage oscillates around a membrane voltage. In these neurons, DTX application had no apparent effect on the

voltage response (Fig. 2-3A). Neither the damping constant (Fig. 2-3B) nor the input resistance (Fig. 2-3C) were altered. Together, these results indicate that a DTX-sensitive conductance, the putative GLKT conductance, contributes to the spiking patterns and firing rates of a specific subset of NA neurons.

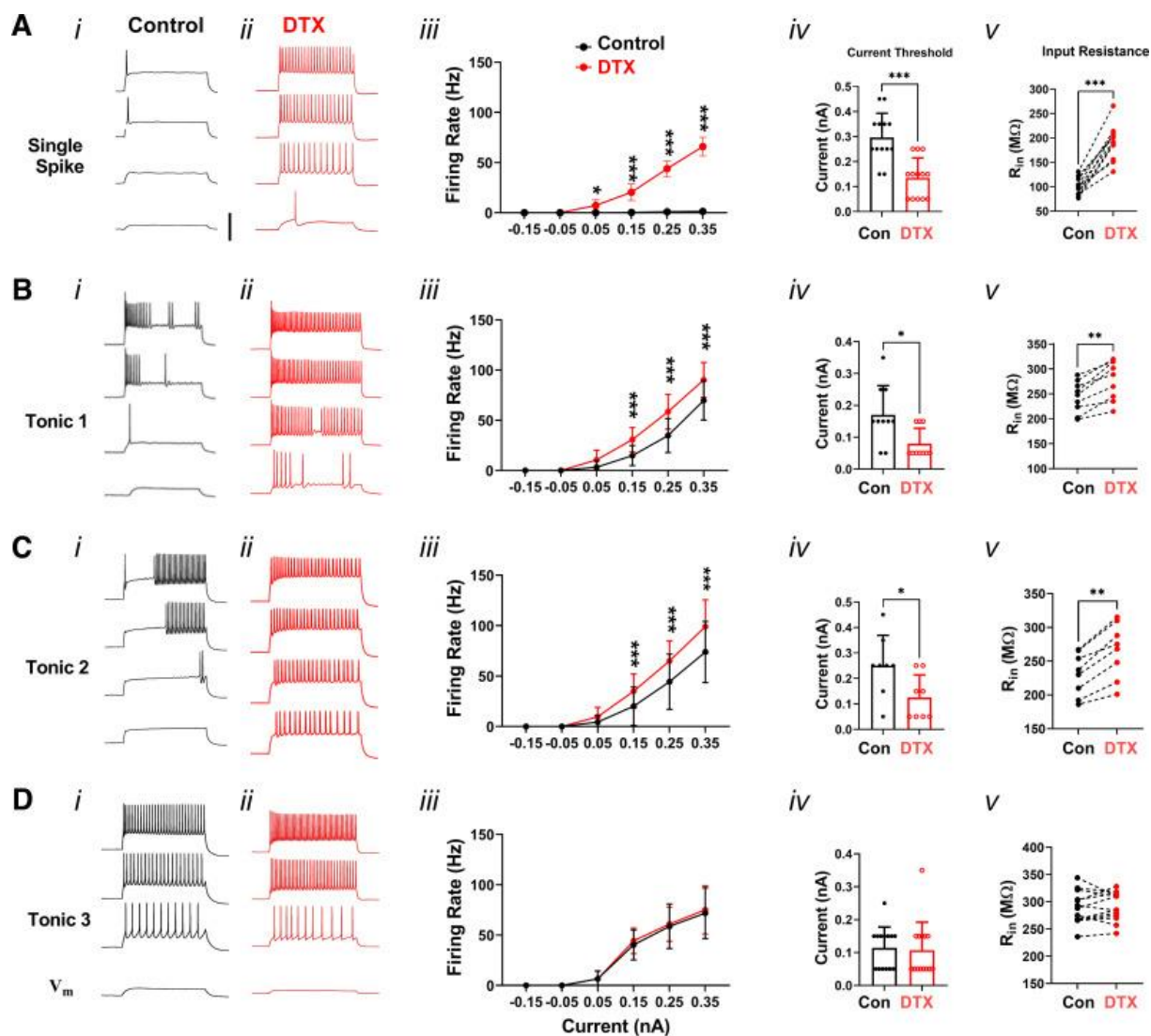


Figure 2-2 Dendrotoxin-I altered the spiking responses in a subset of nucleus angularis (NA) neurons.

Voltage responses were elicited by a set of current injections of increasing amplitude into NA neurons comprising 4 major cell types: single spiking (A) and 3 subtypes of tonic firing neurons: tonic I (B), tonic II (C), and tonic III (D). Example traces show matched responses during control conditions (Ai-Di) and following dendrotoxin-I (DTX) application (Aii-Dii). In DTX, firing rate increased in single-spike, tonic I, and tonic II neurons (Aiii:  $P < 0.001$ ; Biii:  $P < 0.001$ , Ciii:  $P < 0.001$ , 2-way ANOVA) but not in tonic III neurons (Diii,  $P = 0.25$ ). Asterisks indicate Sidak's post hoc multiple-comparisons test significance, \* $P < 0.05$ , \*\* $P < 0.01$ , \*\*\* $P < 0.001$ . The current amplitude threshold (rheobase) was also significantly reduced (Ai:  $P < 0.001$ ; Biv:  $P = 0.03$ ; Civ:  $P = 0.03$ , Wilcoxon's signed-rank test) except in tonic III neurons (Div,  $P > 0.99$ ). Input resistance increased in single-spike, tonic I, and tonic II neurons (Av:  $P = 0.001$ ; Bv:  $P = 0.039$ , and Cv:  $P = 0.042$ , Student's t test) except in tonic III neurons (Dv:  $P > 0.99$ ). Scale bar: 40 mV, current step duration: 400 ms.

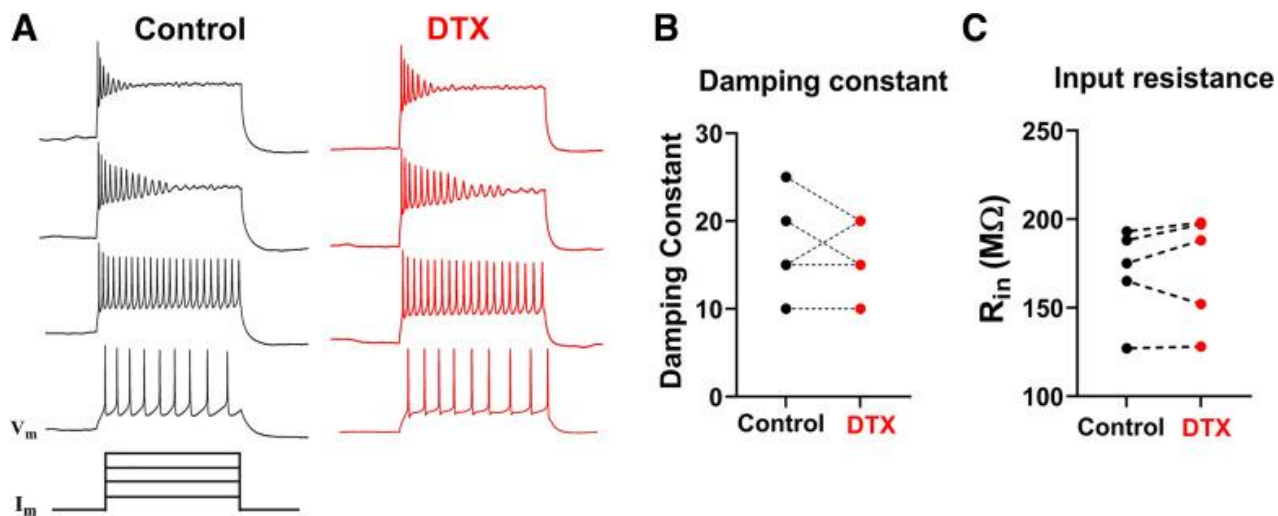


Figure 2-3 Dendrotoxin-I (DTX) did not alter firing or intrinsic properties of damped neurons.

Voltage responses in response to flat current injections (400 ms duration) showed no apparent change between control (A, left) and after DTX application (A, right). The damping constant (B) and input resistance (C) were unchanged [control damping constant =  $19.0 \pm 6.3$  (mean  $\pm$  SD), DTX damping constant =  $18.2 \pm 5.2$ ,  $P = 0.97$ ; control  $R_{in} = 168.3 \pm 22.4 M\Omega$ , DTX  $R_{in} = 174.8 \pm 26.7 M\Omega$ ,  $P > 0.99$ , Student's t test]. Vertical scale bar: 40 mV.

## The DTX-Sensitive Conductance Improves Temporal Firing Reliability and Information Content in Tonic Firing Neurons

Different subtypes of NA neurons exhibited varying levels of temporal reliability in response to frozen noise stimulation *in vitro* (Kreeger et al., 2012). To test whether GKLT regulated temporal reliability in NA, we collected voltage responses to repeated trials of frozen noise from 49 NA neurons before and after DTX application (9 tonic I, 8 tonic II, 16 tonic III, 5 damped, 11 single-spike) (Fig. 2-4, A and B). The trial-to-trial temporal firing reliability was analyzed using a shuffled autocorrelogram (SAC), a histogram of all across-trial interspike intervals excluding within-trial spike pairs (Fig. 2-4) (Kreeger et al., 2012; Joris et al., 2006). The peak (correlation index, CI) and width of the SAC indicate the degree and precision of the time locking of the spikes across trials. Application of DTX significantly reduced the SAC peak amplitudes measured in single spiking, tonic I, and tonic II neurons (single spiking: control CI =  $47.4 \pm 12.6$ , DTX CI =  $22.4 \pm 12.3$ ,  $n = 11$ ,  $P = 0.005$ ; tonic I: control CI =  $28.9 \pm 6.7$ , DTX CI =  $11.1 \pm 5.4$ ,  $n = 9$ ,  $P = 0.0059$ ; tonic II: control CI =  $13.7 \pm 4.6$ , DTX CI =  $7.0 \pm 2.4$ ,  $n = 8$ ,  $P = 0.042$ ; Fig. 2-3C; summary data in Fig. 2-4) and increased the SAC width (single spiking: control FWHM =  $0.5 \pm 0.34$  ms, DTX FWHM =  $1.2 \pm 1.0$  ms,  $P < 0.001$ ; tonic I: control FWHM =  $2.02 \pm 0.93$  ms, DTX FWHM =  $3.11 \pm 1.22$  ms,  $P < 0.001$ ; tonic II: control FWHM =  $1.97 \pm 0.32$  ms, DTX FWHM =  $3.41 \pm 0.71$  ms,  $P = 0.039$ ). In contrast, in tonic III or damped neurons, DTX application had no significant effect on the SAC peak (tonic III: CI =  $4.83 \pm 3.82$ , DTX CI =  $4.68 \pm 3.98$ ,  $n = 12$ ,  $P = 0.84$ ; damped: control CI =  $3.59 \pm 1.04$ , DTX CI =  $4.96 \pm 2.88$ ,  $n = 9$ ,  $P = 0.84$ ) or width (tonic III: FWHM =  $3.85 \pm 1.64$  ms, DTX FWHM =  $4.32 \pm 2.13$  ms,  $P = 0.41$ ; damped: control FWHM =  $6.43 \pm 3.14$  ms, DTX FWHM =  $6.01 \pm 3.55$  ms,  $P = 0.56$ ). These results indicate that GKLT contributes to precise and reliable firing in the same subset of cell

types that showed firing rate changes with DTX (single spiking and tonic I and II) but not in the tonic III or damped neurons.

Another method to quantify the similarity (or dissimilarity) of the spiking responses before and after DTX application is to measure the mutual information (MI) contained in the two sets of spike trains (see materials and methods) (Shannon, 2001; Steveninck et al., 1997). MI quantifies the predictive value of one data set toward the other in bits, where 1 indicates complete certainty and 0 indicates complete independence between the data sets. The MI between control and DTX trials was low in single-spike, tonic I, and tonic II neurons (Fig. 2-6, red markers and bars), indicating a high degree of dissimilarity. The same analysis applied to separate experiments that used sham drug application yielded an MI close to 1, significantly higher than for DTX experiments ( $P < 0.001$ ,  $P = 0.007$ ,  $P = 0.028$ , respectively, Wilcoxon's test). For tonic III neurons, the mutual information between control and DTX spike trains was similar to that during sham experiments, suggesting DTX had no specific effect on these neurons ( $P = 0.708$ ; Fig. 2-6). Together, these spike train timing analyses suggest that Kv1 channels are crucial for the specific and reliable encoding of dynamic stimuli in a subset of NA neurons.

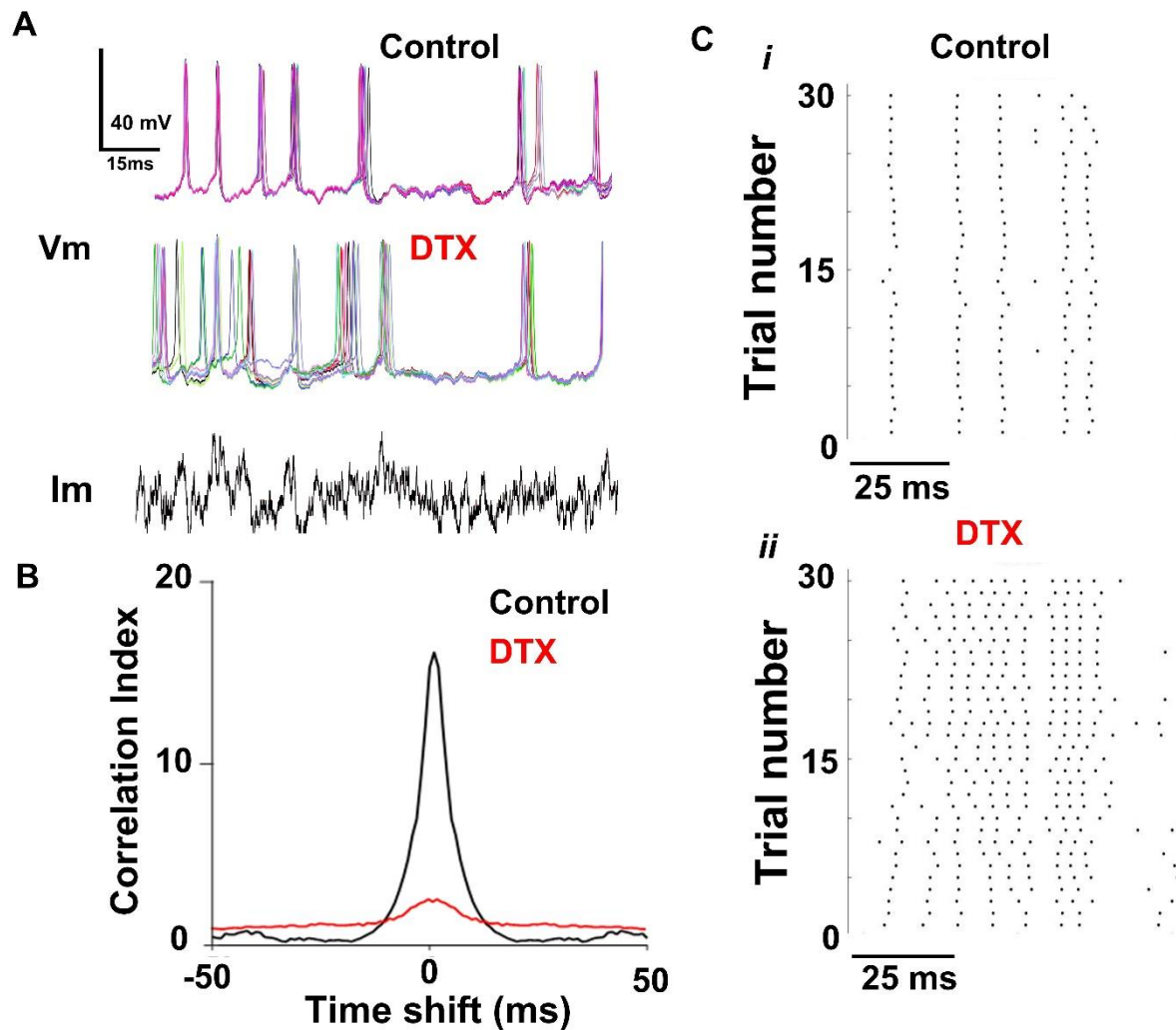


Figure 2-4 Dendrotoxin-I (DTX) reduced the spike timing reliability in a tonic II neuron in nucleus angularis (NA)

A: overlaid voltage traces ( $V_m$ ) for 7 repetitions of an identical "noisy" current ( $I_m$ ) stimulus in control and 100 nM DTX conditions. Only the first 150 ms of the 2 second long stimulus is shown. Scale bars, 40 mV, 15 ms. Bi and ii: raster plots of the first 100 ms of response for all 30 trials for each condition. Scale bar: 25 ms. C: spike timing reliability quantified with a shuffled autocorrelation showed a reduced peak correlation index and broader distribution for responses in the presence of DTX.

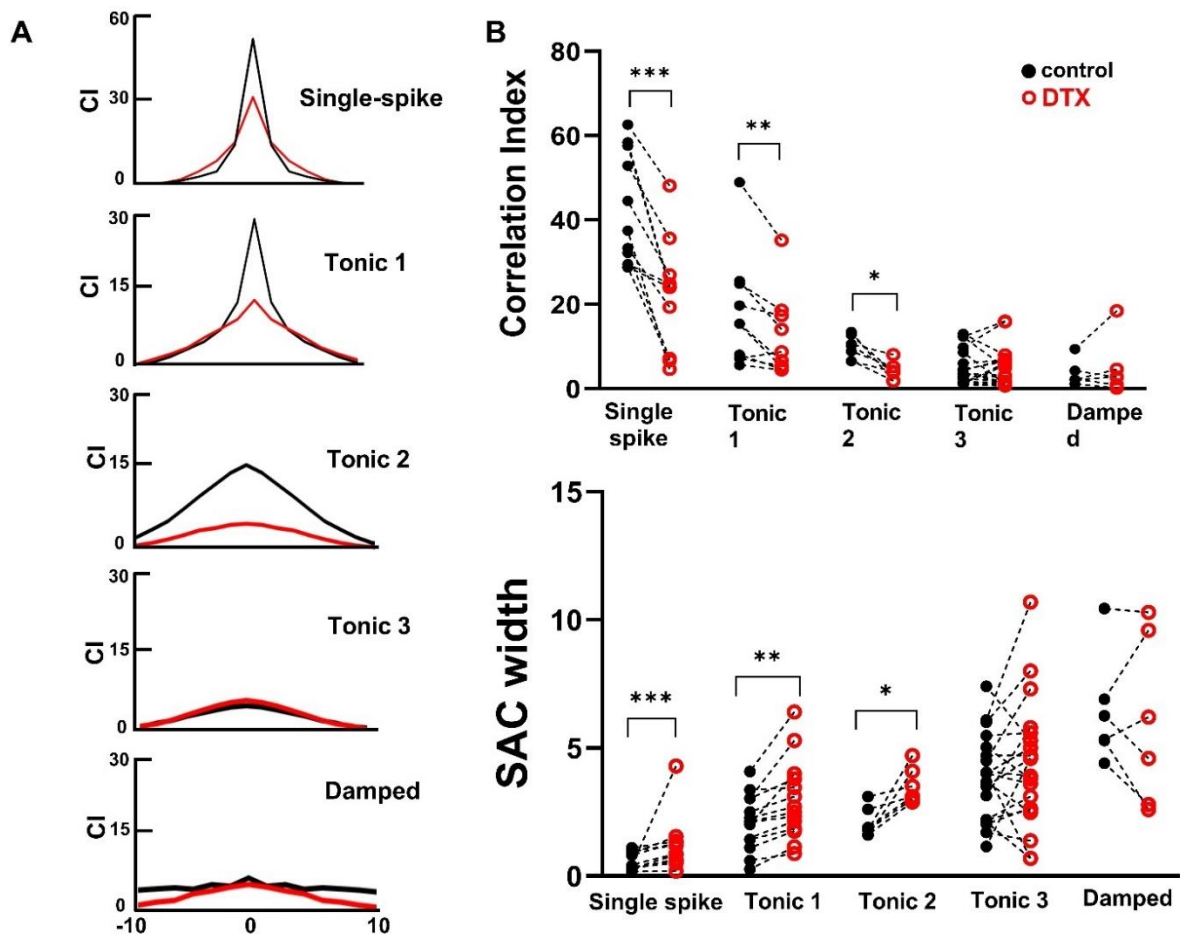


Figure 2-5 Dendrotoxin-I (DTX) reduced the spike timing reliability in cell type-specific manner.

A: averaged shuffled autocorrelogram (SAC) across all neurons recorded for each of the 5 cell types (control, black, DTX, red). B: summary data of SAC parameters peak correlation index (CI; top) and full width at half-maximum height (FWHM; bottom). Peak CI decreased in single-spike, tonic I, and tonic II neurons while corresponding FWHM values increased (\* $P < 0.05$ , \*\* $P < 0.01$ , \*\*\* $P < 0.001$ , Wilcoxon's test).

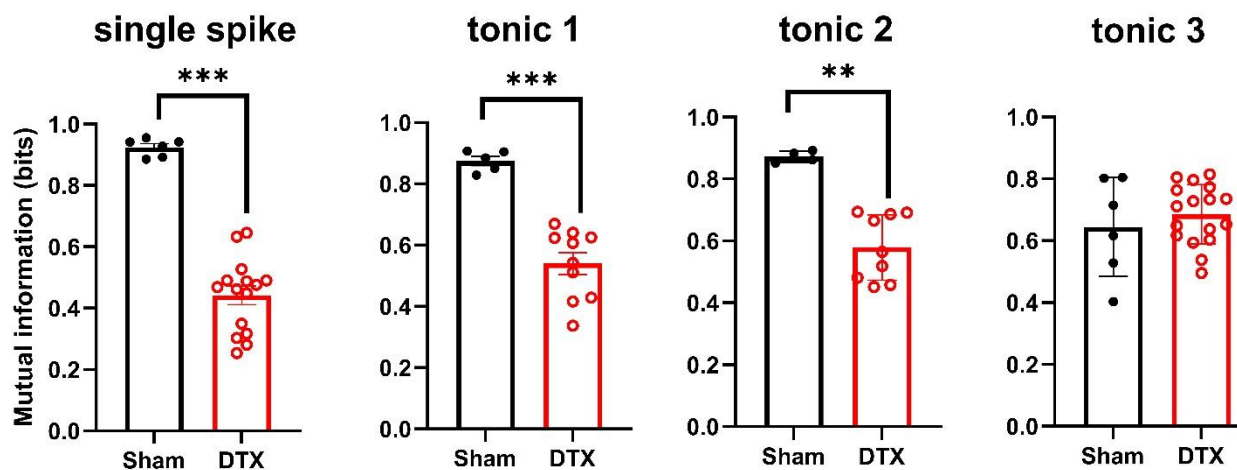
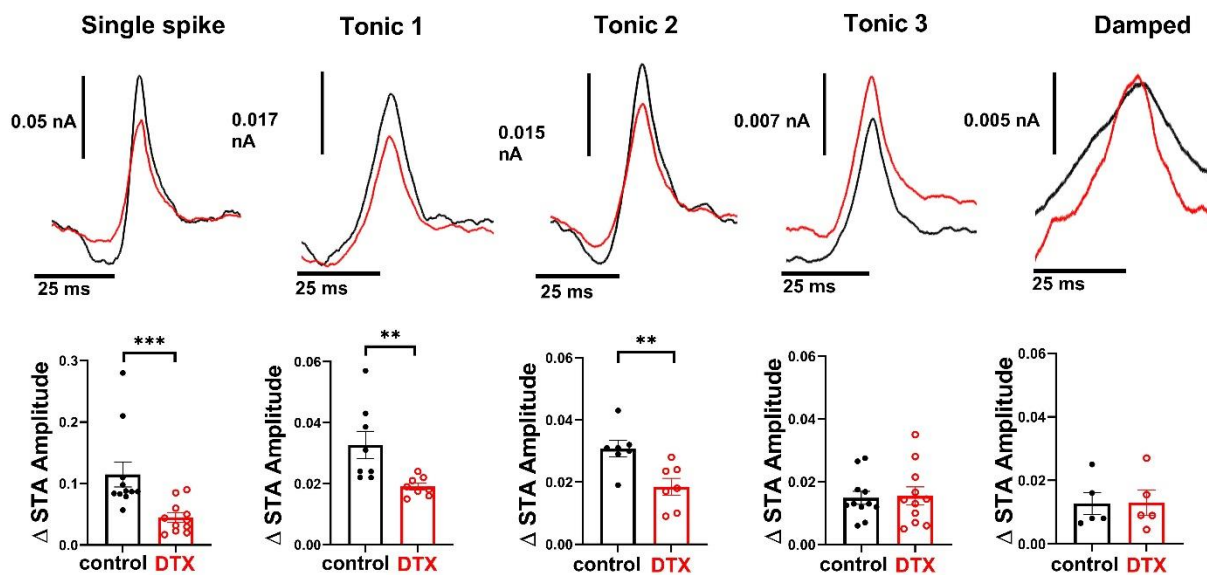


Figure 2-6 Mutual information (MI) between spike trains by cell type.

MI between control spike trains and spike trains following sham solution change was high (black markers, bars) indicating high similarity. In contrast, MI between spike trains from control vs. DTX trials was significantly lower for single-spike, tonic I, and tonic II neurons but not for tonic III neurons (Mann–Whitney test,  $**P < 0.01$ ,  $***P < 0.001$ ). Bars show means  $\pm$  SD.

## Kv1 Channel Expression Drives Fluctuation Sensitivity by Contributing to an Adaptive Spike Threshold

A key feature of coincidence detector neurons is their selective responsiveness to highly correlated synaptic inputs that cause a rapid rise in the postsynaptic voltage. To determine whether DTX affected the selectivity of NA neurons to rapid changes in their inputs, we measured the spike-triggered average current (STA) of the stimulus preceding each action potential. The peak-to-trough amplitude of the STAs were reduced by application of DTX in the single-spike, tonic I, and tonic II neurons (single spiking: control amplitude =  $0.11 \pm 0.02$  nA, DTX amplitude =  $0.044 \pm 0.01$  nA,  $n = 11$ ,  $P < 0.001$ , Wilcoxon t test; tonic I: control amplitude =  $0.032 \pm 0.005$  nA, DTX amplitude =  $0.019 \pm 0.001$  nA,  $n = 9$ ,  $P = 0.036$ ; tonic II: control amplitude =  $0.031 \pm 0.02$  nA, DTX amplitude =  $0.0185 \pm 0.0015$  nA,  $n = 8$ ,  $P = 0.014$ ; Fig. 2-7). In contrast, the peak-trough amplitudes of the STAs for the tonic III and damped neurons were unaltered (tonic III: amplitude =  $0.015 \pm 0.0013$  nA, DTX amplitude =  $0.016 \pm 0.003$  nA,  $n = 16$ ,  $P = 0.73$ ; damped: control amplitude =  $0.013 \pm 0.003$  nA, DTX amplitude =  $0.013 \pm 0.003$  nA,  $n = 5$ ,  $P = 0.95$ ). A large STA amplitude indicates that the neuron will only fire to rapidly rising inputs, so a reduction in STA amplitude implies a corresponding reduction in selectivity.



*Figure 2-7 Dendrotoxin-I (DTX) reduced the high-pass response selectivity in a subset of nucleus angularis (NA) neurons*

Top row: spike-triggered averages (STA) for each neuron type before (black traces) and after (red traces) DTX application. Traces are grand averages of the population for each cell type. Bottom row: summary statistics of peak-to-trough amplitude of STA waveforms from individual neurons. STA amplitudes were significantly reduced in the presence of DTX for single-spiking, tonic I, and tonic II neurons (\*\* $P < 0.01$ , \*\*\* $P < 0.001$ , Wilcoxon's test). Tonic III and damped neuron STAs were unchanged.

Previous studies of the input-output function of the repetitively firing neurons in NA showed that sensitivity to rapidly rising inputs leads higher firing rates to stimuli containing larger fluctuations (Fontaine et al., 2014; Kreeger et al., 2012; Lubejko et al., 2019). Neurons that showed the greatest fluctuation sensitivity have been dubbed “differentiators,” in contrast to “integrator” neurons whose firing rates reflected the mean stimulus level regardless of the size of the noise fluctuations around the mean (Higgs et al., 2006). To determine whether GKLT affected fluctuation sensitivity, we measured the f-I curves using current steps with three noise fluctuation amplitudes ( $2\sigma$ ,  $4\sigma$ , and  $8\sigma$ ) before and after DTX application. In 15 tonic firing NA neurons classified as differentiators (1 control example shown in Fig. 2-7Ai), DTX application elevated firing rates overall (the maximum measured firing rate increased from a mean across 15 neurons of 68.4 Hz in control to 83.7 Hz with DTX, data not shown). However, it also reduced the relative firing rate enhancement to larger current noise fluctuations compared with smaller noise fluctuations (Fig. 2-8Aii). These noise f-I curves were quantified by measuring the normalized difference in maximum firing rate (MaxFR index) between the low noise ( $2\sigma$ ) and high noise ( $8\sigma$ ) and the normalized firing rate difference over the entire curve (area difference index, ADI) (see materials and methods). Both these measures are larger in differentiators than in integrators (which are close to the origin, see Fig. 2-9) and decreased significantly with DTX (Fig. 2-8Bi–iii; MaxFR index control =  $0.388 \pm 0.152$ , differentiator DTX =  $0.199 \pm 0.146$ ,  $n = 15$ ,  $P < 0.001$ , Student’s t test; ADI control =  $0.455 \pm 0.175$ , DTX =  $0.273 \pm 0.158$ ,  $P < 0.001$ ). In contrast, the application of DTX had little effect on the noise f-I curves in five tonic firing NA neurons classified as integrators (Fig. 2-9, A and B, MaxFR index: control =  $0.035 \pm 0.034$ , DTX =  $0.029 \pm 0.0581$ ,  $n = 5$ ,  $P = 0.42$ , Student’s t test; ADI: control =  $0.052 \pm 0.072$ , DTX =  $0.043 \pm 0.083$ ,  $P = 0.39$ ). It should be noted that this reduction cannot be explained by a simple

proportional increase in all firing rates, which would have had no effect on the normalized indices. Thus, blocking GKLT with DTX selectively reduced the fluctuation sensitivity by the differentiator neurons, causing them to behave more like an integrator neuron.

The primary mechanism underlying the fluctuation sensitivity and high-pass behavior has been proposed to be an adaptive spike threshold (Lundstrom et al., 2009; Mensi et al., 2016; Platkiewicz & Brette, 2010). Sodium channel inactivation is a key ion channel mechanism to achieve the adaptation (Platkiewicz & Brette, 2010), but other conductances that are active in the subthreshold regime have the potential to influence the threshold (Higgs et al., 2006; Higgs & Spain, 2011; Prescott, Ratté, et al., 2008; Svirskis et al., 2004). During adaptation, the voltage threshold dynamically varies depending on the mean voltage, the rate of rise in the voltage, and the time since a preceding action potential. We asked whether the effects described are consistent with a role for GKLT in spike threshold adaptation. To measure spike threshold adaptation, we measured threshold variation during noisy current drive, as previously described in NA neurons (Lubejko et al., 2019). With DTX application, the variation in the threshold to the large noise stimulus ( $8\sigma$ ) was reduced (Fig. 2-10A), and the spike waveforms were more stereotyped (Fig. 2-10, B and C). Across 15 NA tonic firing neurons, DTX significantly reduced the threshold variation across a range of mean current amplitudes {2-way ANOVA, main effect by drug [F(20,345) = 10.95, P = 0.001]; P = 0.003 at 0.20 nA, P = 0.0021 at 0.25 nA, P < 0.001 at 0.30 and 0.35 nA, Sidak's multiple-comparisons test; Fig. 2-9D}. These data show that consistent with the reduction in filtering, DTX affects fluctuation sensitivity at least in part due to reduced threshold adaptation. These results suggest that Kv1 channels are involved in threshold adaptation at higher noise levels, possibly in conjunction with sodium channel inactivation.

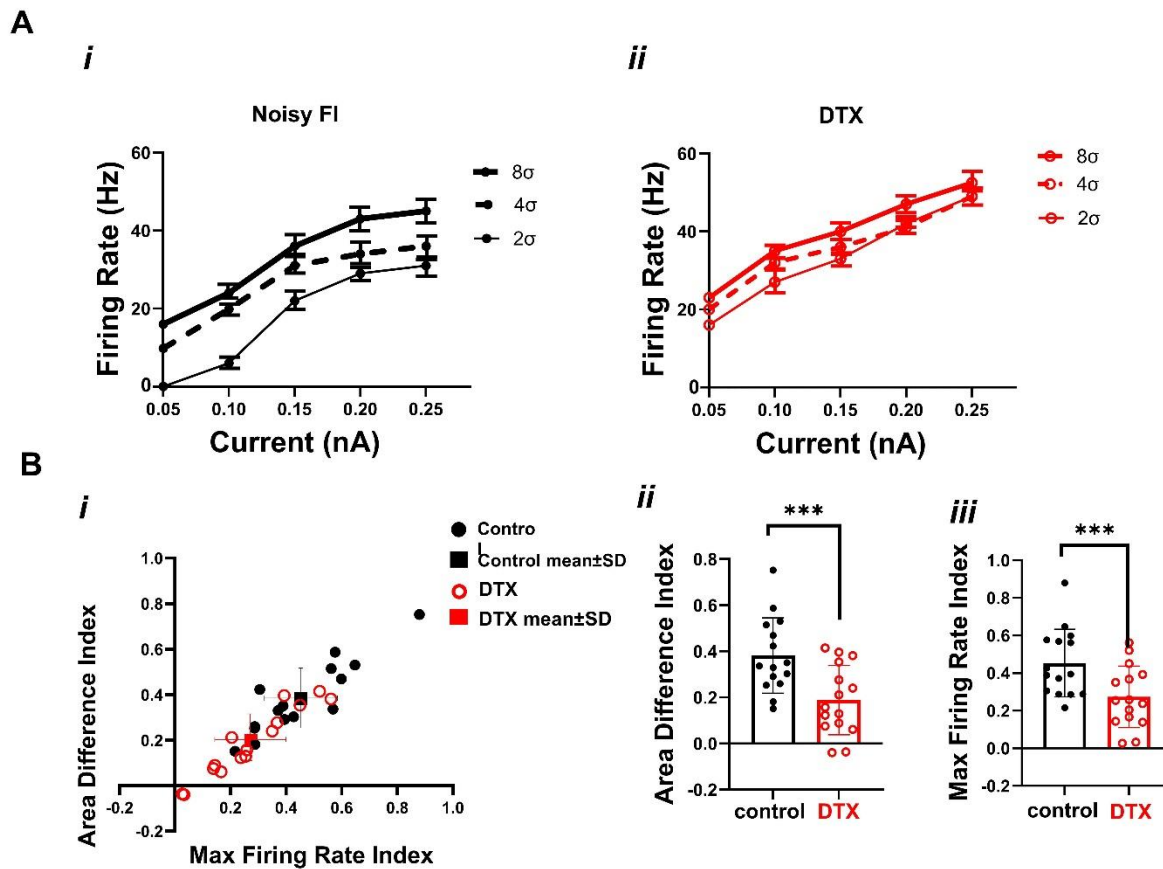


*Figure 2-8 Dendrotoxin-I (DTX) diminished fluctuation sensitivity in differentiators*

A: an example of 1 differentiator neuron's input-output function with 3 levels of noise before (i) and after (ii) DTX application. Example traces in response to the largest step current (0.25 nA) with smallest ( $2\sigma$ ) and largest ( $8\sigma$ ) noise fluctuations in control (iii) and DTX (iv). Scale bars: vertical, 30 mV; horizontal, 500 ms. B: summary plot of f-I curve metrics for 15 differentiator neurons. Markers represent individual neurons before (black solid) and after (red open) DTX application; square markers with error bars are group mean  $\pm$  SD for control (black) and DTX (red) conditions. Area difference index (control ADI =  $0.391 \pm 0.17$ , DTX ADI =  $0.187 \pm 0.15$ ; ii) and maximum firing rate index (control  $\Delta_{\text{maxFR}} = 0.422 \pm 0.19$ , DTX  $\Delta_{\text{maxFR}} = 0.261 \pm 0.15$ ; iii) were reduced upon DTX application. \*\*\* $P < 0.001$ , Student's t test.

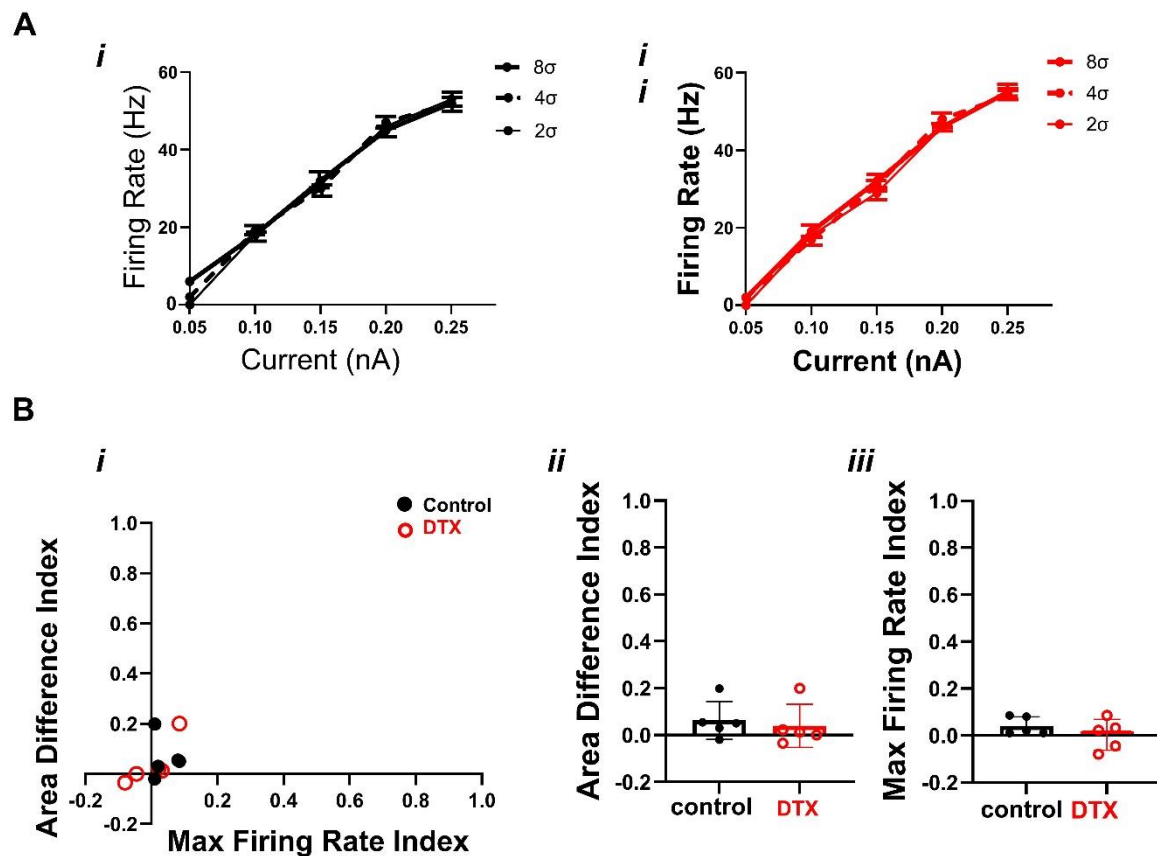
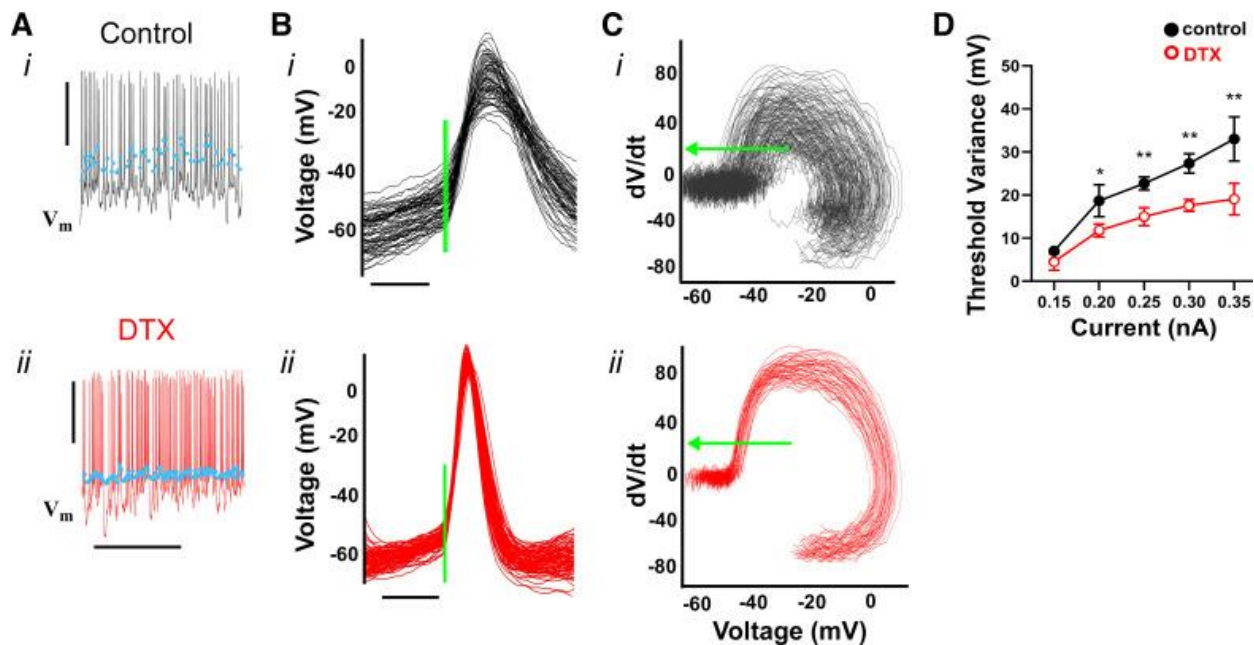


Figure 2-9 Dendrotoxin-I (DTX) had no impact on fluctuation sensitivity metrics in integrators

A: an example of 1 integrator neuron's input-output function with 3 levels of noise before (i) and after (ii) DTX application. Example traces in response to the largest step current (0.25 nA) with smallest (2 $\sigma$ ) and largest (8 $\sigma$ ) noise fluctuations in control (iii) and DTX (iv). Scale bars: vertical, 30 mV; horizontal, 500 ms. Bi: summary plot of f-I curve metrics for 5 integrator neurons indicated no DTX effects. Markers as in Fig. 7Bi. Area difference index (control ADI = 0.042  $\pm$  0.14, DTX ADI = 0.032  $\pm$  0.025; ii) and maximum firing rate index (control  $\Delta$ maxFR = 0.036  $\pm$  0.017, DTX  $\Delta$ maxFR = 0.008  $\pm$  0.072; iii) showed no changes with DTX.



*Figure 2-10 Dendrotoxin-I (DTX) altered the dynamics of action potential initiation and threshold variability during periods of high current fluctuation.*

A: example spike trains with spike thresholds indicated by blue dots in a control (i) and post-DTX application (ii). Scale bars, 20 mV, 500 ms. B: action potentials overlaid for control (i) and DTX (ii) trials aligned on spike threshold (green bar). Scale bar, 2 ms. C: phase trajectory of voltage derivative vs. voltage for action potentials (Aps) in B for control (i) and DTX (ii).  $dV/dt$  threshold is labeled with a green arrow. D: threshold variability was significantly diminished in DTX trials relative to control for noise fluctuation level  $8\sigma$  {2-way ANOVA, main effect by drug [ $F(20,345) = 10.95, P = 0.001$ ]}. Multiple-comparisons test showed significant differences at current steps  $> 0.2$  nA (Sidak's test, 0.2 nA:  $*P < 0.05$ ; 0.25–0.35 nA:  $**P \leq 0.001$ ).

## Discussion

The role of the low-threshold gated potassium conductance (GKLT) in the temporal processing of auditory signals has been extensively studied. The GKLT conductance is attributed to the expression of members of the Kv1 family of voltage-gated potassium channels, particularly Kv1.1 and Kv1.2, that are prevalent throughout the auditory brainstem structures of birds and mammals (H. Brew & Forsythe, 1995; Dodson et al., 2003; Fukui & Ohmori, 2003; Johnston et al., 2010). Distinct from the Kv3 family associated with a high-threshold conductance responsible for action potential repolarization (Choudhury et al., 2020; Parameshwaran et al., 2001; L. Wang et al., 1998), *in vitro* studies showed that GKLT activates at membrane potentials near rest and is responsible for the single-spiking behavior and outward rectification characteristic of many auditory neurons (Kuba et al., 2002a; Kuba, 2007; Rathouz & Trussell, 1998; A. D. Reyes et al., 1994; Zhang & Trussell, 1994). Activation of GKLT results in a short membrane time constant that prevents the temporal summation of synaptic potentials (Akter et al., 2018; Fukui & Ohmori, 2003; Yang et al., 1999). Thus, the GKLT conductance is a key component to phase locking to the fine temporal structure in the acoustic signal and high-fidelity sensory encoding in the cochlear nucleus NM (Ashida et al., 2017; Sullivan & Konishi, 1984; Warchol & Dallos, 1990). In the avian interaural time difference (ITD) circuit, dynamic activation of this conductance is crucial for the spike initiation properties that underlie the coincidence detection in the NL (C. Carr & Konishi, 1990; Fukui & Ohmori, 2003; Higgs et al., 2006; Higgs & Spain, 2011; Kuba et al., 2005; Nishino et al., 2008; Ohmori, 2014; Rathouz & Trussell, 1998; A. Reyes et al., 1996; A. D. Reyes et al., 1994). Similar effects can be observed in

the analogous mammalian circuit (Khurana et al., 2011, 2012; Matthews & Fuchs, 2010; Svirskis et al., 2002, 2004).

Pharmacological and immunohistochemical studies, however, have suggested that Kv1 channels are not exclusively expressed in these timing pathways but are also present in the sister cochlear nucleus, NA (Bloom et al., 2014; Fukui & Ohmori, 2003; Lu et al., 2004). In this study, we found that pharmacological blockade of GKLT, with the Kv1.1/1.2-specific antagonist DTX, dramatically altered the firing phenotypes of some NA neuronal subtypes but not others. Specifically, the single-spiking neurons and the tonic I and tonic II phenotypes lost their unique onset or bursting firing patterns, whereas the tonic III phenotype that only displayed regular spiking was unchanged. In addition, we found that the temporal reliability of firing, high-pass filtering characteristics, and spike threshold adaptation were all partially reliant on the DTX-sensitive conductance. These results suggest that Kv1 channels make important contributions to the intrinsic physiological diversity and functional heterogeneity of NA neurons.

## Ionic Basis of Electrophysiological Diversity in NA

Previous work showed that DTX application not only converted single-spiking NA neurons into repetitive firing neurons, but it also caused an increase in firing rate in NA tonic firing neurons (Fukui & Ohmori, 2003). We confirmed and extended these results to show that DTX-sensitive changes in firing pattern and rate are related to the physiological classifications in the chick embryonic brain stem described previously (Soares et al., 2002). The DTX effects were limited to tonic firing neurons that show bursting behavior at lower current stimulus levels. We conclude that the burst termination (tonic I) and delayed burst (tonic II) behaviors both require

the presence of a DTX-sensitive conductance, but it remains unclear what causes the differences in their response patterns. One explanation could be a difference in the activation or inactivation kinetics of the Kv1 channel conductance; a slow inactivation of IKLT has been shown in NM neurons (Kuznetsova et al., 2008). Since multiple isoforms, Kv1.1, Kv1.2, and Kv1.6, are DTX-I sensitive, there may be differences in subunit compositions or modulation. Alternatively, there may be some other subthreshold conductance present in one type of tonic neuron that interacts with the DTX-sensitive current [e.g., an A-type current that could enhance early bursting (Prescott, Ratté, et al., 2008; Ratté et al., 2015) or other inward current (Swensen & Bean, 2003)]. Two neuron types in NA appeared unaffected by DTX: tonic III neurons, which best represent canonical rate-coding integrators, and damped neurons, a potential immature phenotype (D. H. Brown & Hyson, 2019; Fukui & Ohmori, 2003). In the presence of DTX, the blockade of bursting resulted in responses by all three tonic firing subtypes more closely resembling each other. Because these subtype differences have not been observed in the hatchling (Fukui & Ohmori, 2003), it is possible that the increase in excitability and reduction in phenotypic diversity that occurs with development could be due to a downregulation of GKLT. Examining these neuronal subtypes is important because computational approaches have shown that increased population heterogeneity is directly correlated with increased information encoding capacity (Ahn et al., 2014).

## Neurons in the NA Utilize Kv1 Channels to Encode the Temporal Dynamics of Their Inputs

Multiple features demonstrated as archetypal in NA appear to be at odds with a presumed role for GKLT in temporal processing: multispiking intrinsic firing properties (Fukui & Ohmori,

2003; Kreeger et al., 2012; Soares et al., 2002), poorer phase-locking in vivo to the acoustic fine structure, and a role in interaural-level coding (Konishi et al., 1985; Sullivan & Konishi, 1984; Warchol & Dallos, 1990). However, a more complex picture of sound processing in NA has been emerging. First, the heterogeneity of in vivo response properties and morphology suggested that NA is not a monolithic rate-coding nucleus, but a diverse population of neurons (Soares et al., 2002; Soares & Carr, 2001), some of which show temporal sensitivity, dynamic feature selectivity, and auditory envelope processing (Fontaine et al., 2014; Kreeger et al., 2012; Lubejko et al., 2019; Steinberg & Peña, 2011). Second, in vitro studies showed a diversity of intrinsic features across the population, some of which also demonstrated greater temporal sensitivity than others (Kreeger et al., 2012; Lubejko et al., 2019; Soares et al., 2002). In another study, the differentiator-type intrinsic properties of a subset of NA neurons could account for the intensity-dependent bandpass behavior in vivo (Fontaine et al., 2014). In their model, the high-pass filtering due to active intrinsic membrane properties of the tonic firing, coincidence-detector-like neurons combined with the low-pass filter behavior of the synaptic inputs, and passive membrane properties resulted in the overall bandpass filtering. Interestingly, variation in the properties across the neuronal population produced an array of bandpass properties spanning the physiological response space. The results presented in the present study provides direct evidence that variations in Kv1 conductances contribute to the variations in temporal processing properties in vitro; it remains to be tested whether a mature circuit in vivo would also require these properties to encode spectrotemporal auditory information. Neurons with high reliability should be capable of encoding more rapidly changing components of the acoustic signal, such the onsets and gaps that are key features of speech and other communication signals. Neurons with less reliability are likely to be important for encoding the more slowly changing aspects of

the acoustic signal, such as slower envelope variations or ongoing interaural-level cues. Together, these studies suggest that NA neurons function on a spectrum of operating modes, ranging from pure integrators to pure coincidence detectors (Prescott, Ratté, et al., 2008).

### Spike Threshold Adaptation in NA Neurons May Rely on the Low-Threshold Potassium Conductance

The operating mode diversity observed across NA specifically appears to arise from a mechanism known as spike-threshold adaptation, a phenomenon by which the voltage threshold is modulated by spike history and membrane voltage mean and rate of rise (Fontaine et al., 2014; Hodgkin & Huxley, 1952a, 1952b; Huang et al., 2016; Kobayashi & Kitano, 2016). This form of adaptation is the probable mechanism underlying the selective responsiveness of NA neurons to rapid rises in the postsynaptic voltage, acting like a high-pass filter and enhancing the firing response to temporally modulated inputs. Spike threshold adaptation is a process that occurs throughout the brain, particularly in cortical pyramidal neurons, and auditory brainstem neurons (Fontaine et al., 2014; Higgs & Spain, 2011; Howard & Rubel, 2010; Lubejko et al., 2019; Monsivais & Rubel, 2001; Platkiewicz & Brette, 2011). In NA, threshold adaptation drives NA neurons to encode amplitude modulations with higher fidelity than auditory nerve fibers (Fontaine et al., 2014), as well as diversifies their operating modes (Lubejko et al., 2019). Phenomenological models based on sodium channel inactivation as a mechanism were successful at recapitulating the firing responses (Fontaine et al., 2014; Lubejko et al., 2019); however, these models use abstract conductance representations that do not specifically rule out other non-sodium, subthreshold conductances, such as the Kv1 channel. In a study of cortical

neurons, blockade of Kv1 channels with DTX largely eliminated spike threshold adaptation (Higgs & Spain, 2011). Our results suggest a similar role for Kv1 in NA neurons.

## Functional Analogs of NA Neurons in the Mammalian Cochlear Nucleus

The mammalian auditory brain stem is not anatomically homologous to the avian auditory brain stem. The mammalian ventral cochlear nucleus (VCN) has functionally similar cell types to those in NA, but there does not appear to be a one-to-one match for each type. For example, the spherical bushy cells of the VCN are analogous to the avian NM neurons in that both have high levels of Kv1 expression, receive calyceal inputs from auditory nerve fibers, generate precise spiking phase-locked to the fine structure in auditory signals, and project to analogous coincidence detection circuits (Oertel, 1997). The T-stellate cells of the VCN appear to be the closest functional analog to NA neurons, in that they have reduced phase-locking relative to auditory nerve inputs, repetitive intrinsic firing properties, encode envelope and intensity information for spectrotemporal coding, and project directly to the midbrain inferior colliculus (Cao & Oertel, 2010; C. E. Carr & Soares, 2002; Frisina et al., 1990; P. Manis & Marx, 1991; Palmer et al., 2003; Rhode, Oertel, et al., 1983; Rhode & Greenberg, 1994; Xie & Manis, 2017). Identified T-stellate neurons lack any significant low-threshold potassium channel conductance and are insensitive to DTX (Cao & Oertel, 2010; Ferragamo et al., 1998; McGinley & Oertel, 2006; Oertel et al., 1990). These results suggest that the T-stellate neurons of the VCN are not functionally analogous to the DTX-sensitive neurons in NA (tonic I/tonic II subtypes), but instead may be more similar to the DTX-insensitive, integrator-like neurons of NA (tonic III subtype). Another study, using acutely dissociated neurons and voltage-clamp, suggested there

was a population of neurons in the VCN with intermediate levels of DTX-sensitive, lower-threshold conductances, possibly corresponding to the radiate (or D-stellate) type of multipolar neurons, a less common type of repetitively firing neuron in the AVCN that projects to the dorsal cochlear nucleus (Rothman & Manis, 2003a, 2003b, 2003c; Xie & Manis, 2017). The recent discovery in the VCN of a third stellate neuron population, dubbed L-stellate, which appears to provide narrowband inhibition and operates within a feedback loop with T-stellate neurons (Ngodup et al., 2020), further suggests that there may be greater phenotypical diversity than previously appreciated. How these cell types may correspond to NA cell types remains to be seen. These multispiking neurons in VCN can entrain to high-frequency stimuli *in vitro*, but the reliability of responses to the noisy, temporally modulated stimuli that we describe in the present study have only been tested in DCN neurons (Street & Manis, 2007). Comparisons between NA and VCN are complicated by the fact that VCN contains a dense network of lateral connectivity and local inhibition, whereas NA appears to be a strictly feedforward circuit without local inhibition, so their feature selectivity and computational roles are likely to be quite dissimilar. Also limiting comparisons of intrinsic properties across studies are species differences (chick vs. guinea pig vs. mouse) and the possible confounding effect of temperature on the kinetics of the ion channels (Cao & Oertel, 2010; Ranjan et al., 2019).

## Summary

In summary, we have demonstrated that dendrotoxin-sensitive conductances are prevalent in a subpopulation of NA neurons and are critical for the temporal response properties in these neurons. By enhancing spike threshold adaptation, this conductance underlies the spike timing reliability, high-pass membrane filtering, and fluctuation sensitivity properties of the

differentiator subtypes. The regulation of the Kv1 family of channels may be a key driver of intrinsic electrophysiological diversity in the avian cochlear nucleus and contribute to spectrotemporal auditory feature selectivity in vivo.

## Chapter 3 Electrophysiological properties and anatomy of the avian superior olivary nucleus

\*Note, this chapter is a slightly modified version of “Electrophysiological correlates of divergent projections in the avian superior olivary nucleus,” posted on BioRxiv, 2024. Minor revisions were recommended from the Journal of Neurophysiology

Inhibition is crucial for processing auditory information in central nervous system circuits (Beiderbeck et al., 2018; Caspary et al., 2005; Chanda & Xu-Friedman, 2010; Keine et al., 2016). In the auditory brainstem, inhibition sharpens phase locking for frequency tuning (Al-Yaari et al., 2019; Dehmel et al., 2010; Fukui et al., 2010; Keine & Rübsamen, 2015; Kuenzel et al., 2011; Monsivais et al., 2000), boosts gap detection capability (Middleton et al., 2011; Williamson et al., 2015), and improves amplitude modulation coding (Dugue et al., 2007; Keine et al., 2016). The firing rates of inhibitory neurons in early auditory structures were shown to be proportional with sound intensity (Coleman et al., 2011; Ferragamo et al., 1998; Moiseff & Konishi, 1983; Ngodup et al., 2020; Yang et al., 1999), thus their feedback can function as an intensity-dependent gain-control mechanism that regulates disparities in binaural sound levels (See review by (Burger et al., 2015; Nishino et al., 2008). Despite the multifaceted roles of inhibition, birds do not rely much on local inhibitory interneurons in their auditory brainstem nuclei. Instead, inhibition originates primarily in a nucleus, the superior olivary nucleus (SON) (Bartheld et al., 1989; C. E. Carr et al., 1989; Lachica et al., 1994; Westerberg & Schwarz, 1995) that is anatomically segregated from the ascending excitatory nuclei. To determine how the SON may underlie the multiple functions of inhibition in the auditory brainstem, we examined the intrinsic physiological properties of SON neurons.

In birds, the auditory nerve synapses onto two anatomically distinct cochlear nuclei: the intensity-coding nucleus angularis (NA) and the phase-, or time-, coding nucleus magnocellularis (NM) (C. E. Carr & Boudreau, 1993; Parks & Rubel, 1975, 1978). NM projects bilaterally to the nucleus laminaris (NL), which performs coincidence detection to calculate interaural time differences (ITD) (C. Carr & Konishi, 1990)(C. Carr & Konishi, 1990). Both NA and NL have excitatory projections to the ipsilateral SON (C. E. Carr & Boudreau, 1991; T. T. Takahashi & Konishi, 1988b). which in turn projects either to the ipsilateral NM, NL, and NA, or to the contralateral SON (SONc). These projections come from two, non-overlapping populations of SON neurons (Burger et al., 2005). *In vitro* studies of SON neurons have revealed two response types: 1) a single spiking phenotype wherein a single action potential is fired at the onset of a current injection, and 2) a tonic spiking phenotype wherein a series of action potentials are produced throughout the duration of the current injection (Carroll et al., 2018; Coleman et al., 2011; Yang et al., 1999). It was unclear whether these two response phenotypes underlay the divergent projections from SON onto its targets.

*In vivo* recordings showed that SON neurons could generate a number of firing patterns in response to simple tone or noise sound stimuli. In these studies, most SON units were classified as either “onset” and produced action potentials only at the beginning of sound presentation, or “sustained” and produced action potentials throughout sound presentation(Coleman et al., 2011). These were primarily monaural responses, but some studies displayed subset had similar excitatory drive from both ipsilateral and contralateral stimuli (Moiseff & Konishi, 1983). While in earlier studies SON neurons were not thought to encode temporal features of sounds(Lachica et al., 1994; Monsivais et al., 2000; Yang et al., 1999), more recent work has demonstrated robust phase locking in sustained responses(Coleman et al., 2011).

The underlying drivers of these variations could be from differential weighting of inputs from either NA or NL, variations in synaptic properties, or, as shown in both mammalian and avian cochlear nucleus neurons, diversity of intrinsic membrane properties (Baldassano & MacLeod, 2022; D. H. Brown & Hyson, 2019; Hirsch & Oertel, 1988; Hong & Sanchez, 2018; Kuo et al., 2012; P. B. Manis et al., 2019; Rothman & Manis, 2003c). In fact, temporally responsive intrinsic properties of a subset of NA neurons allow them to reliably encode features of the acoustic envelope (Baldassano & MacLeod, 2022; Fontaine et al., 2014; Kreeger et al., 2012; Lubejko et al., 2019; Steinberg & Peña, 2011). We hypothesized that intrinsic properties of SON neurons were the primary driver of their temporal responsiveness. Furthermore, if we found that SON biophysical phenotypes corresponded to postsynaptic targeting, that might provide some functional insight into how diversity in SON could relate to the variety of roles for inhibition.

To investigate these properties *in vitro*, we used naturalistic current steps to expand the characterization of SON intrinsic phenotypes and axonal trajectory tracing to determine the cell-type specific projections of SON neurons. We demonstrate the presence of a second tonic firing phenotype that displays sensitivity to the temporal features of inputs. Furthermore, we determined that the firing phenotype was highly indicative of the neuron's axonal projection. These results suggest that efferent and contralateral inhibitory signals may reflect different functional outputs and that intrinsic features of SON neurons may drive the different temporal properties seen *in vivo*.

## Materials and Methods

### *Brain slice preparation*

All animal procedures were performed with Institutional Animal Care and Use Committee approval and according to University of Maryland guidelines on animal welfare. White leghorn chicken (*Gallus gallus*) embryos (sex undetermined) incubated to embryonic day 17-18 were cooled and rapidly decapitated, and the head section containing the brain stem blocked, placed in a chilled, oxygenated low-sodium artificial cerebrospinal fluid (ACSF) (low-Na<sup>+</sup> ACSF; in mM: 97.5 NaCl, 3 KCl, 2.5 MgCl<sub>2</sub>, 26 NaHCO<sub>3</sub>, 2 CaCl<sub>2</sub>, 1.25 NaH<sub>2</sub>PO<sub>4</sub>, 10 dextrose, 3 HEPES, and 230 sucrose) and dissected out of the cranium. The brain stem tissue block was mounted with cyanoacrylate glue and supported with 5% agarose gel. Standard transverse slices (250 μm thick) containing SON were cut on a vibrating tissue slicer (Leica Microsystems, Wetzler, Germany). For neuronal reconstruction experiments, “wedge” slices were cut to preserve the maximal amount of the recorded neuron’s axonal projection. After advancing through the tissue and just prior to collecting the section containing SON, the mounting platform was angled approximately 15°, such that the slice containing SON was approximately 400 μm at the dorsal edge and 200 μm at the ventral edge. We used wedge slices with a thick dorsal end and a thinner ventral end as opposed to slices that were uniform thickness in order to allow for maximum visibility under DIC within the SON while recording. Slices were incubated in normal ACSF (in mM: 130 NaCl, 3 KCl, 2 MgCl<sub>2</sub>, 26 NaHCO<sub>3</sub>, 2 CaCl<sub>2</sub>, 1.25 NaH<sub>2</sub>PO<sub>4</sub>, 10 dextrose, and 3 HEPES) at 34°C for 30 min then held at room temperature in normal ACSF until recording.

#### *Whole cell patch-clamp electrophysiology*

Slices were placed in a recording chamber and continuously perfused with oxygenated, warmed normal ACSF (1–2 mL/min, 28–30°C) containing synaptic receptor blockers (3 μM strychnine, 20 μM SR95531 (gabazine), 15 μM 6,7-dinitroquinoxaline-2,3-dione (DNQX), and 20 μM D-

AP5 (D-2-amino 5-phosphovalerate); Sigma) to isolate intrinsic activity. Whole cell patch-clamp recordings were performed on visually identified SON cells using infrared differential interference contrast video microscopy. Initial glass recording pipette resistances were 3–7 M $\Omega$ . Pipettes were filled with a potassium gluconate intracellular recording solution (in mM: 110 potassium gluconate, 20 KCl, 1 EGTA, 2 MgCl<sub>2</sub>, 10 HEPES, 2 Na<sub>2</sub>ATP, 0.3 Na<sub>2</sub>GTP, 10 phosphocreatine and 0.2% biocytin). Series resistance, cell capacitance, and resting membrane voltage were measured upon break-in in voltage clamp mode. Voltage recordings were made with a MultiClamp 700B amplifier (Molecular Devices, Sunnyvale, CA) set to current-clamp mode. Application of the current stimulus and recording of the voltage output were controlled by an analog-to-digital board (National Instruments, Austin, TX) and a computer running custom software written in IGOR Pro (WaveMetrics, Lake Oswego, OR). A holding current was applied to maintain a constant voltage baseline of approximately -65 mV. A maximum current of -100 pA would be applied before the cell was considered unhealthy. Cell type classification protocols were carried out to identify neuronal phenotypes in SON with 400-ms-duration flat current steps of varying amplitudes from -150 pA up to 550 pA in 50 or 100 pA intervals. We collected data from 93 SON neurons (34 single spike, 23 regular tonic, 34 chattering tonic) across experiments. All datasets were checked for normality using a Shapiro-Wilk test.

### *Regularity analysis*

Tonic neurons fired multiple action potentials throughout the duration of a flat current injection but could be subdivided into at least 2 subtypes of tonic firing- regular and chattering based on the regularity of their spiking. Regularity was estimated from the coefficient of variation (CV) of

the interspike intervals over the 400-ms response duration, such that the closer the CV was to zero, the more regular the firing. CV was calculated as the ratio of the standard deviation( $\sigma$ ) of the intervals over the mean ( $\mu$ ) of the intervals:

$$CV = \frac{\sigma_{intervals}}{\mu_{intervals}}$$

We used the CV for the first step above rheobase when determining the cell type, because that is the current level where the patterning emerges.

#### *Acquisition of f-I Curve and Analysis*

Input-output functions were assessed by measuring firing-current (f-I) curves with standard flat current steps (400-ms duration as for classification protocols) or noisy current stimuli (2-s duration), as previously described (Kreeger et al., 2012; Lubejko et al., 2019). Noise stimuli were constructed by convolving Gaussian white noise with an exponential function (time constant, 3-ms) added to a direct current (DC) step function. These noise stimuli simulate the arrival of many small, stochastic, and statistically independent synaptic currents, both excitatory and inhibitory. To accommodate cell-to-cell differences in input resistance, a standard noise current was created by calibrating the standard deviation (around a zero mean) of the noise current to generate a 2-mV standard deviation in the membrane potential in the target neuron, designated “ $1\sigma$ .” The amount of voltage fluctuation was varied by multiplying the standard noise stimulus by a factor of 2, 4, or 8 (i.e., 4-, 8-, and 16-mV voltage fluctuation, respectively). Each trial had an

interstimulus interval of 8 seconds. A hyperpolarizing conditioning pre-pulse (−50 pA, 1-s duration) was applied before each stimulus to minimize sodium channel inactivation from the prior stimulus. A complete series of stimuli in the parameter space (mean DC, noise level) was systematically generated by varying the mean current amplitude and noise level independently (3 noise levels, 5–10 DC levels). Firing rates were averaged across one to three stimulus repetitions over the full 2 second duration and reported as means  $\pm$  SD in Hertz.

Metrics to quantify differences between the lowest noise level ( $2\sigma$ ) and highest noise level ( $8\sigma$ ) curves were devised in Kreeger et al. (2012) and utilized here. One metric quantified the total area difference index (ADI) :

$$ADI = \frac{\sum_{i=1}^n normFR_{8\sigma,i} - \sum_{i=1}^n normFR_{2\sigma,i}}{\sum_{i=1}^n normFR_{8\sigma,i}}$$

where normFR was the firing rate at each of n steps in each noise level normalized to the maximum firing rate in the whole data set. The second metric was the normalized difference in the maximum firing rate between  $2\sigma$  and  $8\sigma$ ,  $\Delta maxFR$ :

$$\Delta MaxFR = \frac{MaxFR_{8\sigma} - MaxFR_{2\sigma}}{\sum_{i=1}^n normFR_{8\sigma,i}}$$

where MaxFR refers to the maximum firing rate value of each within-noise-level f-I curve. Both metrics varied from 0 (curves are identical) to 1 (maximum difference). Plotting these points (MaxFR index and the ADI index) against each other produced a spectrum of fluctuation sensitivity. Neurons closest to the origin were more “integrator-like,” whereas neurons further away from the origin were more “differentiator-like.” Using the criteria of ADI and  $\Delta\text{MaxFR} > 0.2$ , we were able to test the noise f-I curves from 15 differentiators and 5 integrators with DTX.  $\Delta\text{maxFR}$  index and ADI index were statistically compared using Wilcoxon’s t test.

### *Spike Timing Reliability*

After noise was calibrated, a  $4\sigma$  noisy current was injected into neurons at a single DC current step amplitude (typically 150–400 pA) to produce a firing rate between 20 and 50 Hz. Repeated trials of 2-s long frozen noisy current injections were injected (usually 30 to 45 trials, or until  $>600$  spikes were collected) before and after DTX application. To quantify neuronal reliability, we calculated a shuffled autocorrelogram (SAC), a histogram of all interspike intervals between spikes across trials, excluding intervals within the same trial. The SAC is normalized by the normalizing factor (NF):

$$NF = N \cdot (N - 1) \cdot r^2 \Delta\tau D$$

where N is the number of trials, r is the average firing rate,  $\Delta\tau$  is the bin width of the correlation function (0.2-ms), and D is the length of the stimulus (2-s). The SAC was fit with a Gaussian function, whose central peak is defined as the correlation index (CI). The precision of the firing

between trials is represented in the full width at half-maximum (FWHM) of the Gaussian curve, measured by

$$FWHM = 2\sqrt{2\ln 2} \cdot \sigma_{SAC}$$

where  $\sigma_{SAC}$  represents 1 standard deviation of the Gaussian fit of the SAC. CI and FWHM, referred to as width, were quantified and compared using Wilcoxon's t test. To determine the current signal that drove the response, the spike-triggered average (STA) was also calculated. A 60-ms snippet of the current stimulus, starting 50 ms preceding each spike, was extracted and averaged for all spikes within a set.

#### *Neuronal reconstruction and determination of postsynaptic target*

Slices containing biocytin fills were fixed in 4% paraformaldehyde in 0.1 M phosphate buffer overnight and processed with Vectastain ABC (avidin-biotinylated HRP complex) Elite Kit (Vector Labs, Burlingame, CA). The shape of the slice, the boundary of SON, the location of filled neurons, and their morphological reconstructions were drawn using the computer-assisted tracing program NeuroLucida (MicroBrightfield, Williston, VT). Cytoarchitectural features and the shape of the slice were used to determine where the recording was in the rostral-caudal axis. Larger medial vestibular nuclei (MVN) and NM indicated more rostral and smaller, or a lack of, MVN and lower order nuclei (NA, NM, and NL) indicated more caudal.

Axons were able to be identified from dendrites due to their lack of branching, thinner diameter, and near constant diameter. Neurons were only used for analysis if their axon was a minimum of

50 micrometers in length and exited the boundary of the SON. Neuronal fills were superimposed onto a singular representative SON to determine emergent anatomical properties.

## Results

### SON contains heterogeneous electrophysiological phenotypes

Using simple current steps, we observed three action potential firing phenotypes in the voltage responses of SON neurons. First, a tonic firing phenotype (Fig. 3-1Ai) that fired tonically throughout the current step with firing rates that increased linearly with larger amplitude current steps (n=14; Fig. 3-1Aii, mean for population in Fig. 3-1Aiii), referred to here as “regular tonic.” Second, we observed a single spiking phenotype (Fig. 3-1Ci) that produced only one spike on the onset despite increasing the amplitude of the current injection (n=16; Fig. 3-1Cii, population in Fig 3-1Ciii). These two phenotypes align with those previously described 16,17,32. In addition, we observed a 3rd phenotype that was characterized by staggered or irregular bursts of action potentials (Fig. 3-1Bi), which we denote as “chattering” tonic neurons. The bursts increased in spike count and duration with larger current injections (n=14; Fig. 3-1Bii, population in Fig. 3-1Biii). The f-I relationship of chattering neurons was more sinusoidal than for regular firing neurons.

To determine whether regular firing and chattering neurons could be divided into distinct groups, we quantified the regularity of spiking with the coefficient of variation (CV) (see Methods) of the interspike intervals. The measured CV for the initial step above rheobase appeared to be bimodal with a clear gap at 0.3 (Fig. 3-2Ai). These groups corresponded to the

visually observed chattering and regular phenotypes, respectively, supporting the division of these phenotypes into groups for further analysis.

Previous analyses of ‘bursting’ and tonic firing groups have shown that increasing current drive regularizes the firing across the stimulus step<sup>41</sup>. When we analyzed the CV with increasing steps, we found that both the chattering tonic CV (Fig. 3-2Aii) and the regular tonic (Fig. 3-2Aiii) did decline, but chattering tonic were still significantly higher than regular firing neurons at all step levels (Fig. 3-2Ai. 2-way ANOVA, main effect by cell type [ $F(1, 157) = 131.9, P < 0.001$ ];  $P < 0.001$  at 0.05 nA,  $P < 0.001$  at 0.15 nA,  $P = 0.0061$  at 0.15 nA,  $P = 0.0041$  at 0.2 nA,  $P = 0.0029$  at 0.25 nA,  $P = 0.003$  at 0.3 nA,  $P = 0.007$  at 0.35 nA,  $P = 0.0042$  at 0.4 nA,  $P = 0.022$  at 0.45 nA, Sidak’s multiple-comparisons test).

To determine if the onset mechanics of spikes differed between these two phenotypes, we quantified the threshold (Fig. 3-2B) and the latency to first spike after current injection (Fig. 3-2C). Interestingly, chattering tonic neurons had comparable thresholds with regular tonic neurons at lower current levels but significantly lower latency. Increasing current increased the threshold in both phenotypes, however the slope of the threshold sensitivity (i.e. the change in threshold with input current) in chattering neurons (slope = 55.7 mV/nA) was significantly higher than the slope for regular tonic neurons (slope = 32.82 mV/nA) (ANCOVA, [ $F(1, 175) = 12.31, P = 0.004$ ]). Increasing current level also reduced the latency in both phenotypes, with the latency in regular tonic significantly higher at lower current levels than chattering tonic. (2-way ANOVA, main effect by cell type [ $F(4, 84) = 69.37, P < 0.001$ ];  $P = 0.001$  at 0.05 nA,  $P = 0.001$  at 0.1 nA, Sidak’s multiple-comparisons test). That difference became non-significant at higher current levels.

We then measured the intrinsic membrane properties of each SON phenotype (Fig 3-3). Chattering neurons had lower whole cell capacitance ( $n=26$ ,  $WCC= 50.4\pm 10.3$  pF) than regular tonic ( $n=33$ ,  $WCC =69.5\pm18.8$  pF) or single spiking phenotypes ( $n=23$ ,  $WCC =57.6\pm18.6$  pF) (Student's t-test,  $P=0.0028$  chattering vs. regular,  $P=0.0042$ , chattering vs single spike,  $P<0.001$ , regular vs single spike). Single spiking neurons had the largest afterhyperpolarization (AHP) ( $12.0\pm5.3$  mV). Chattering tonic neurons had the second largest AHP ( $4.99\pm1.19$ mV) and regular tonic had the smallest amplitude AHP ( $2.09\pm2.86$  mV) (Student's t-test,  $P= 0.0016$  chattering vs. regular,  $P<0.001$ , chattering vs single spike,  $P <0.0001$ , regular vs single spike). Finally, single spiking cells had the highest rheobase ( $0.30\pm0.11$  nA), chattering tonic had the second largest ( $0.23\pm0.12$  nA), and regular tonic had the lowest ( $0.12\pm0.007$  nA) (Student's t-test,  $P= 0.003$  chattering vs. regular,  $P<0.001$ , chattering vs single spike,  $P <0.0001$ , regular vs single spike).

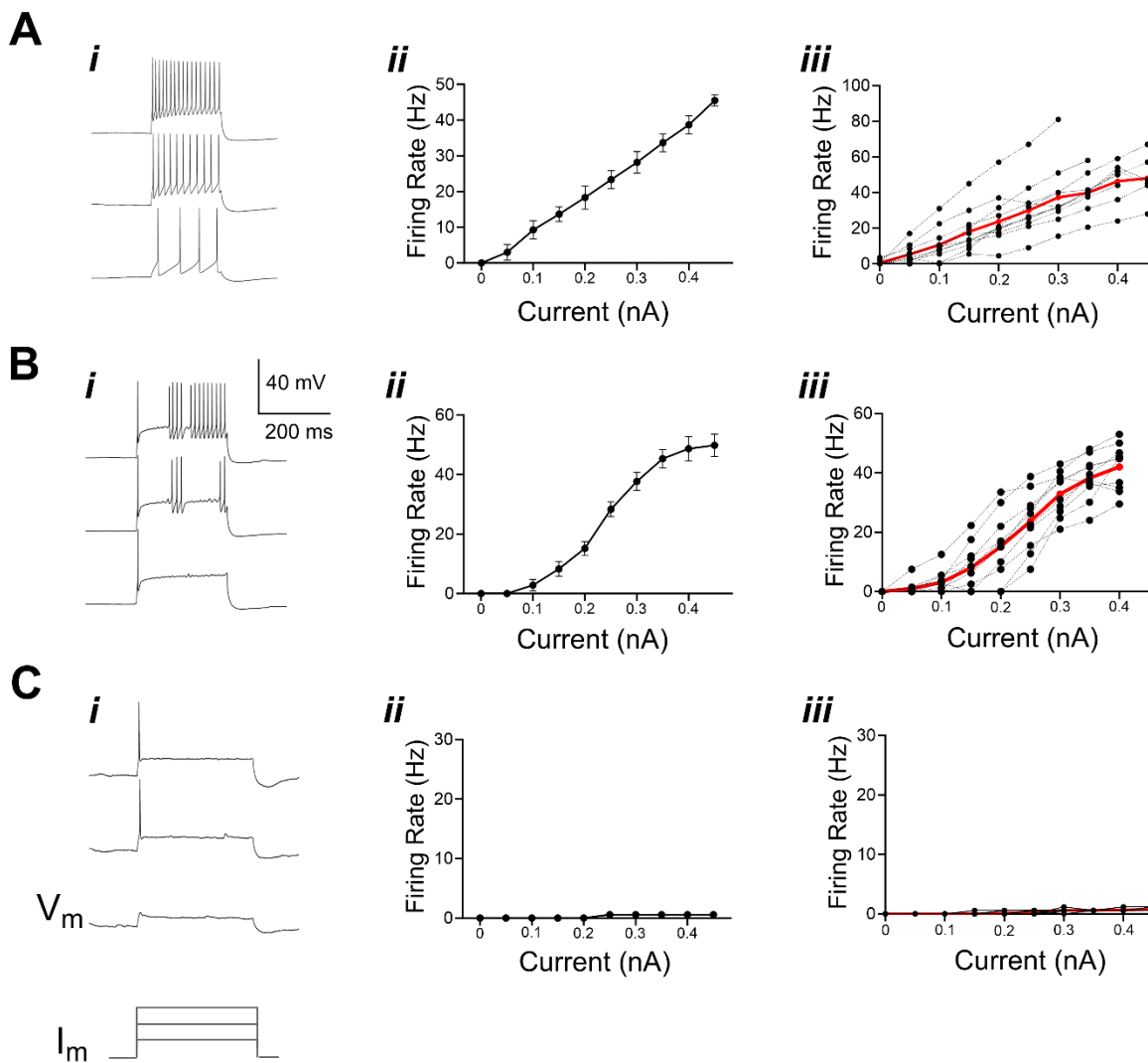
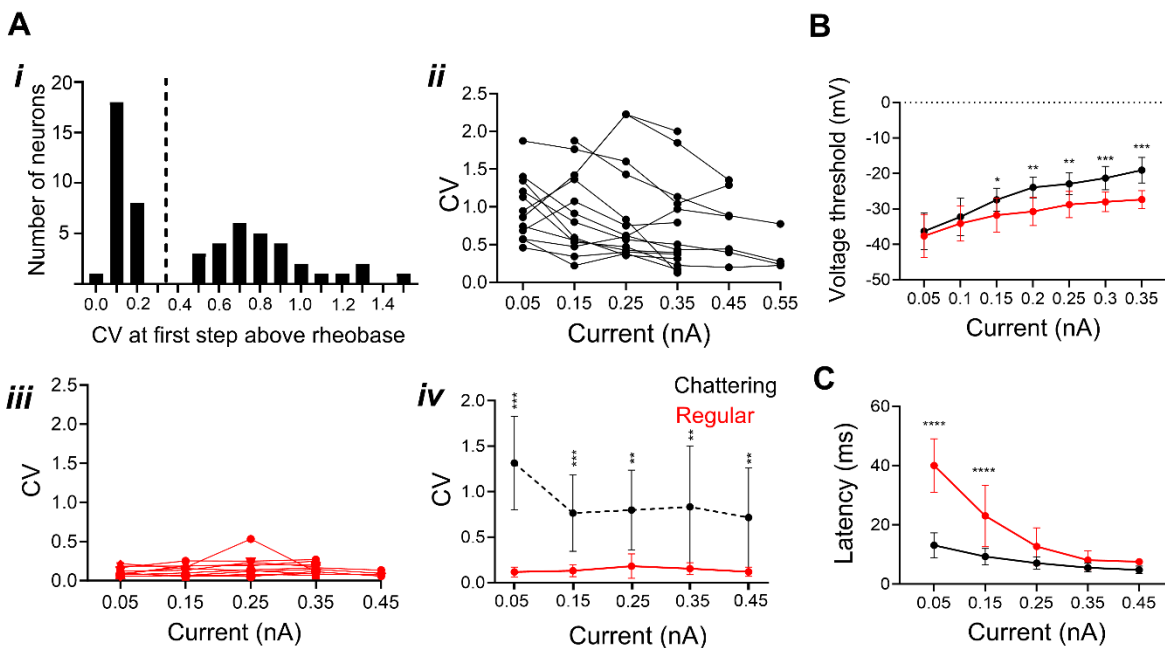


Figure 3-1 Intrinsic physiological phenotypes of SON neurons.

Three phenotypes of responses were identified by their voltage response to current step stimulation: (Ai) regular tonic firing, (Bi) chattering tonic firing and (Ci) single spiking. Qualitative differences were observed in action potential firing patterns (*i*; traces show voltage responses to current steps of three different amplitudes; bottommost traces in first column illustrate timing and relative amplitude of current steps). Shapes of the firing rate-current amplitude (FI) curves of the two types of tonic firing neurons were linear for regular tonic and sigmoidal for chattering (*ii*) (mean $\pm$ s.d. across trials). Matching example individual recordings in columns (*i*) and (*ii*); column (*iii*) overlays FI curves from all individual recordings (black markers) and group averages (red line)(all error bars omitted for clarity). Scale bar A-C: vertical 40 mV; horizontal, 200 ms.  $V_m$ , membrane voltage;  $I_m$ , membrane current.



**Figure 3-2 Chattering and regular firing phenotypes were quantifiably differentiable by regularity analysis.**

A) Histogram of coefficient of variation (CV) of the interspike intervals calculated for the action potentials fired in response to the one current step above rheobase. A clear gap around 0.3-0.4 was used as a criterion for the division of regular and chattering cell types (dashed vertical). CV versus current step amplitude for chattering neurons (Aii; N=14) and regular (Aiii; N=14) neurons. CVs were significantly different between chattering and regular tonic cell types across all stimulus amplitudes, although spiking may regularize with increased stimulus level (Aiv) (2-way ANOVA, main effect by cell type [ $F(1, 157) = 131.9, P < 0.001$ ]; post-hoc comparisons at each step:  $P < 0.001$  at 0.05 nA;  $P < 0.001$  at 0.15 nA;  $P = 0.0061$  at 0.15 nA;  $P = 0.0041$  at 0.2 nA;  $P = 0.0029$  at 0.25 nA;  $P = 0.0030$  at 0.3 nA;  $P = 0.0070$  at 0.35 nA;  $P = 0.0042$  at 0.4 nA;  $P = 0.022$  at 0.45 nA, Sidak's multiple-comparisons test. \*\*\*,  $P < 0.001$ ; \*\*,  $P < 0.01$ ). B) Chattering tonic neurons showed an increase in action potential threshold with step amplitude slightly more than regular tonic neurons (ANCOVA, [ $F(1, 175) = 12.31, P = 0.004^{***}$ ]). C) First spike latency was delayed in regular tonic neurons compared to chattering neurons, which typically fired a spike at the onset. Latency decreased with step amplitude (2-way ANOVA, main effect by cell type [ $F(4, 84) = 69.37, P < 0.001$ ];  $P = 0.001$  at 0.05 nA<sup>\*\*\*</sup>,  $P = 0.001$  at 0.1 nA<sup>\*\*\*</sup>, Sidak's multiple-comparisons test).

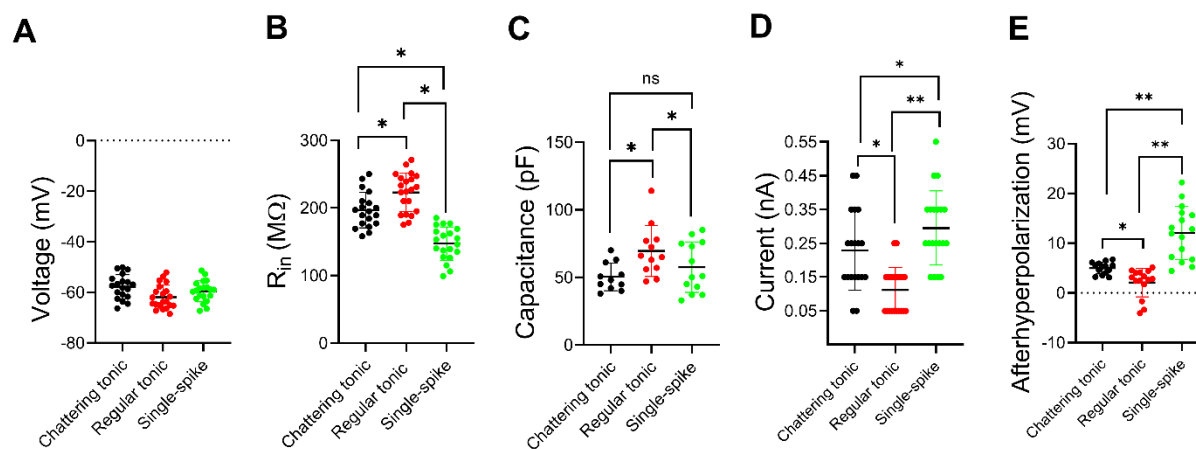


*Figure 3-3 Intrinsic membrane properties differ between SON phenotypes*

- A. Resting membrane voltages did not differ amongst electrophysiological phenotypes
- B. Input resistances were highest in regular tonic, then chattering tonic, and lowest in single spiking neurons
- C. Capacitance was highest in regular tonic neurons, but not different amongst chattering tonic and single spiking
- D. Rheobase was lowest in regular tonic, then chattering tonic, and finally single spike
- E. Afterhyperpolarization was largest in single spikes, then chattering tonics, and finally regular tonic

## SON neurons display varied levels of temporal reliability

We next wanted to explore if intrinsic membrane properties of the three SON phenotypes engendered different levels of temporal capabilities. To investigate how well the SON neurons locked to the current stimulus, we pharmacologically blocked synaptic activity (see Materials & Methods) and measured their responses to frozen noise over repeated trials to analyze the spike timing. We recorded timing data from 78 SON neurons: 33 regular tonic, 20 single spiking, and 25 chattering tonic neurons. A single DC current step amplitude was chosen to generate firing levels in the tens of Hz range. White noise was added to the current step amplitude ( $4\sigma$ , see Methods). All SON phenotypes produced reliable firing patterns upon noisy current injection (Fig 3-4Ai-iii, iv). The trial-to-trial temporal firing reliability was analyzed using a shuffled autocorrelogram (SAC), a histogram of all across-trial interspike intervals, excluding within-trial spike pairs (Fig. 3-4Bi-iii). An example voltage trace is shown in figure 3-4C. The peak value (measured as correlation index, or CI) and width of the SAC indicate the degree and precision of the time locking of the spikes across trials, respectively. Single spiking neurons were the most reliable, with the highest CI ( $n=20$ , mean =  $81.34\pm 24.9$ ) and the narrowest SAC (FWHM mean =  $1.04\pm 0.53$  ms). Chattering tonic neurons displayed the second highest CI values and the second narrowest SAC ( $n=25$ , CI mean =  $26.11\pm 9.17$ , FWHM mean =  $2.7\pm 1.11$  ms). Regular tonic neurons had the lowest CI values and the widest SAC ( $n=33$ , CI mean =  $7.33\pm 2.58$ , FWHM =  $7.53\pm 1.99$  ms). Both the CI (one-way ANOVA- [F (2, 59) = 109.7],  $P<0.001$ ) and the FWHM (one-way ANOVA [F (DFn, DFd) = 8.731 (2, 59)],  $P<0.001$ ) were statistically different between the three phenotypes (Figure 3-4Di, ii). These results suggest that different SON phenotypes are intrinsically capable of encoding differing levels of temporal information.

## SON tonic phenotypes exist along a spectrum of fluctuation sensitivity

We next considered the effects of naturalistic noisy current injections on the input-output functions of the two types of tonically firing SON neurons. Characterizing noise sensitivity means quantifying neurons on a spectrum of integrators to differentiators. Fluctuation insensitive neurons are integrators, which increase spiking monotonically with mean current but not with noise level. Comparatively, fluctuation sensitive neurons behave as differentiators, increasing spiking with current level, but also with noise level (Baldassano & MacLeod, 2022; Kreeger et al., 2012; Lubejko et al., 2019). We recorded 69 neurons for these experiments: 30 regular tonic neurons and 39 chattering tonic neurons. The addition of noise altered the input-output functions of chattering tonic neurons (Fig. 3-5A) increased firing rates to the larger voltage swings in the noisy currents, thus responding as differentiators. The addition of noise did not alter the input-output functions of the regular tonic neurons, whose firing rates were unaffected by the noise level, thus responding as integrators (Fig. 3- 5B). To quantify the noise responses of tonic SON neurons, we measured the area of the curve between the highest and lowest levels of noise at each current step (Fig.3-5Ci) and as well as the difference in firing between high and low noise levels at the highest level of current. We determined that chattering and regular tonic neurons displayed different levels of fluctuation sensitivities (Fig. 3-5Cii, chattering tonic ADI mean =  $0.35 \pm 0.09$ , n= 39, regular tonic ADI mean=  $0.08 \pm 0.08$ , n =30, unpaired t-test,  $P < 0.001$ ). These results suggest that tonic neurons in SON encode temporal variations along a spectrum of sensitivity.

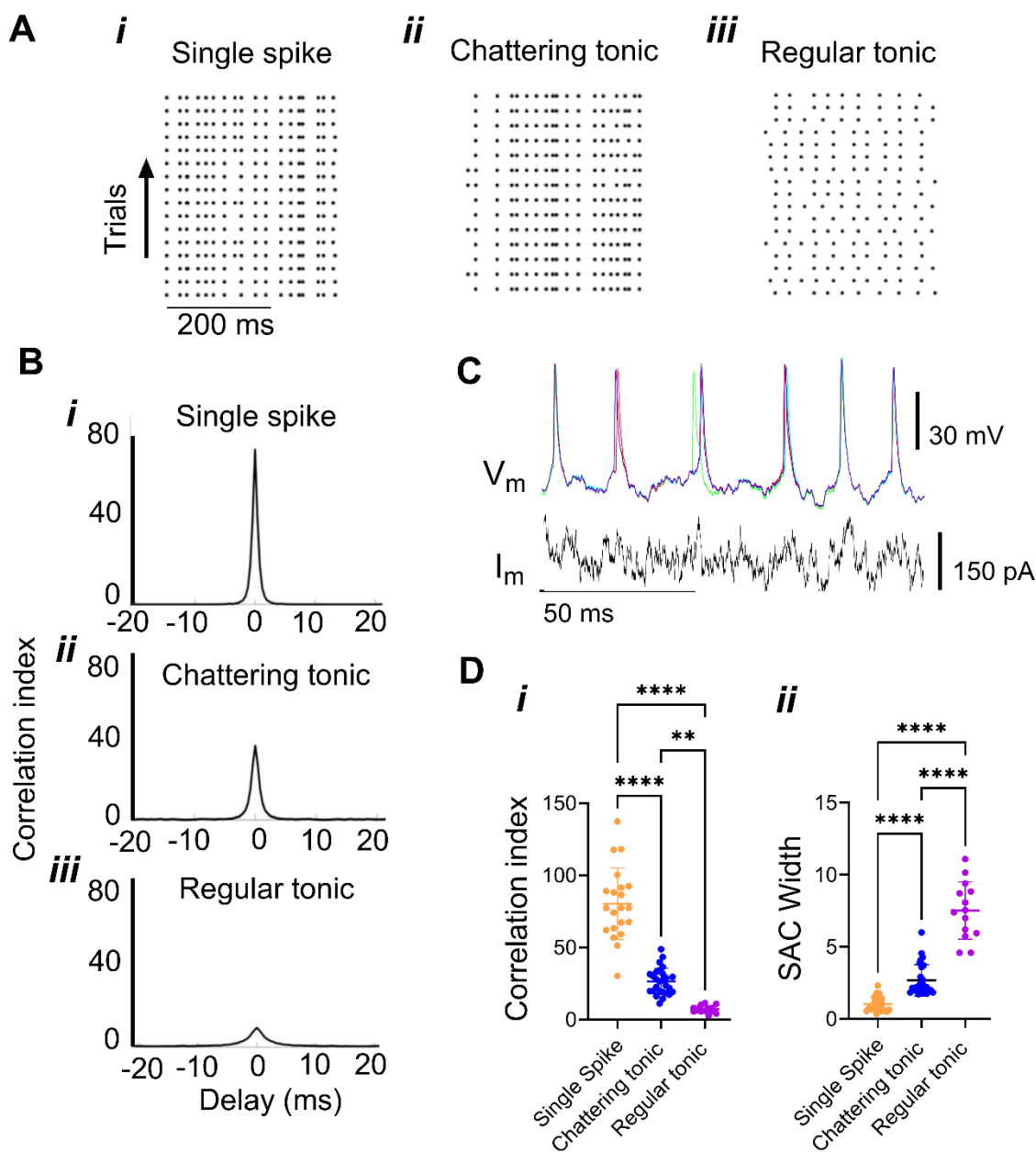
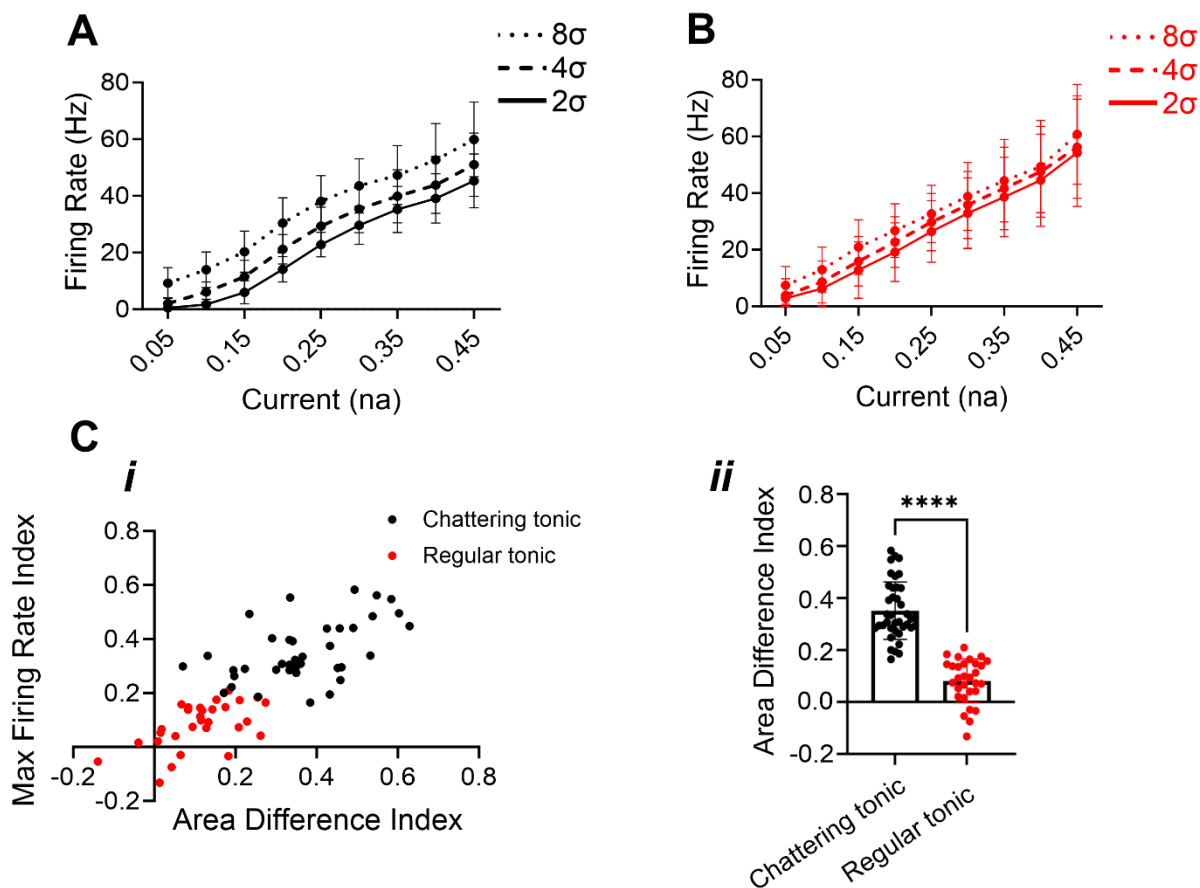


Figure 3-4 Spike timing reliability depends on cell type.

A) Raster plots in response to a noisy current stimuli (not shown). An example neuron (i-iii) of each cell type show reliable firing to repeated presentations of the same stimulus B) Example of a shuffled autocorrelogram (SAC) for each cell demonstrated in A. C) Voltage responses ( $V_m$ ) of 5 repeated iterations of identical noisy current injections ( $I_m$ ) from a chattering tonic neuron. D) Quantifying the SAC parameters, peak correlation index (CI) and full-width at half-max (FWHM) of each cell type. i Cell types in SON have distinct CI peaks: i single spiking cells,  $CI=81.34\pm 24.9$ ,  $n=20$ ; ii chattering tonic,  $CI= 26.11\pm 9.2$ ,  $n=25$ ; iii regular tonic neurons  $CI=7.33\pm 2.7$ ,  $n=33$ . One-way ANOVA [ $F(2, 59) = 109.7$ ,  $P<0.001^{***}$ ]. ii Cell types in SON have distinct autocorrelogram (single spiking cells,  $FWHM = 1.04\pm 0.53$  ms; chattering tonic  $FWHM = 2.7\pm 1.11$  ms; regular tonic cells,  $FWHM = 7.53\pm 1.99$ ms, (one-way ANOVA [ $F(2, 59) = 123.6$ ,  $P<0.001^{***}$ ])



*Figure 3-5 Temporal fluctuation sensitivity depends on cell type*

FI curves of tonic firing SON neurons in response to noisy currents were measured at three different noise fluctuation amplitudes (standard deviation around the mean:  $2\sigma$ ,  $4\sigma$  or  $8\sigma$ ; see Methods) were measured. Abscissa represents the mean current amplitude for each stimulus. (A) In one chattering neuron, increasing the noise fluctuation amplitude elicited higher firing rates. (B) In one regular neuron, there was little effect of noise amplitude on the firing rates (B). Ci) Comparative analysis of FI curves sensitivity by plotting the difference in maximum firing rate and the integrated difference between the curves for largest ( $8\sigma$ ) versus smallest ( $2\sigma$ ) noise conditions (see Methods). Chattering and regular tonic neurons comprised different ends of a continuum of sensitivity to fluctuations. Cii) Grouped values were statistically different (chattering,  $N=39$ ; regular,  $N=30$ , Student's t-test,  $p<0.001$ ).

## SON neurons exited nucleus in at least three distinct fiber tracts and correlated with physiological phenotype

Here, we explore the anatomy of the fiber tracts that exited SON neurons. We recorded from individual neurons in vitro and dialyzed cells with biocytin. We visualized the biocytin and were able to reconstruct the neurons, focusing on the cell body and axon. We reconstructed neurons using NeuroLucida software and were able to identify axons from their uniform thickness and lack of branching. Axons needed to extend a minimum of 400  $\mu\text{m}$  beyond the boundary of the SON to be included in the analysis. Thirty-five neurons were recovered whose reconstructed axonal projections met the criteria and for which physiological data were collected: 14 single spiking, 10 regular tonic, and 11 chattering tonic neurons.

To visualize populations or clusters, all reconstructed neurons were superimposed onto a single representative left SON (Fig. 3-6Ai). Three fiber tracts were visually distinguishable. We quantified these projections by measuring the angle between the center of the cell body with the point on the SON boundary where the axon crossed, with due lateral as a reference angle of  $0^\circ$  (Fig.3-6Aii) Three distinct fiber tracts could be differentiated on the basis of this crossing angle: an ipsilateral lateral tract (between  $30^\circ$  and  $70^\circ$ ,  $n=5$ ), an ipsilateral medial tract (between  $90^\circ$  and  $135^\circ$ ,  $n=17$ ) and a contralateral tract (between  $180^\circ$  and  $280^\circ$ ,  $n=13$ ).

To explore the relationship between SON response types and postsynaptic targets, we matched 35 reconstructed neurons with data from electrophysiological recordings and found that specific SON phenotypes underlie the separate observed fiber tracts. Chattering tonic neurons exited solely via the ipsilateral medial projection ( $n=11$ ) (Fig. 3-6Ci-v). Single spiking neurons composed the entirety of the contralateral projection ( $n=14$ ) (Fig. 3-6Di-iv). Finally, regular tonic neurons composed the entirety of the ipsilateral lateral projections ( $n=5$ ). However, they also

exited via the ipsilateral medial projections (n=5) (Fig3-6. Bi-iv). These results suggest that SON phenotypes underlie the divergent projections.

### Cells in SON are clustered by their electrophysiological phenotype

We then asked if SON phenotypes were organized within the anatomy of the nucleus. We analyzed the fills of neurons that met the axon length criteria for the projection analysis (Fig. 3-7, n=35) and the cell bodies of all filled neurons (Fig. 3-7- bottom row. n=135). These clusters revealed some loose organization of SON phenotypes. Single spiking neurons tended to exist in the ventral areas of the SON (12/14 of neurons that had sufficient axon length Fig. 3-7Ai, 33/45 of all single spiking neurons), while both tonic phenotypes tended to exist in the dorsal area. For chattering tonic neurons, 30/46 existed in dorsal areas. Regular tonic neurons ended up being identical in proportion, with 30/44 existing in dorsal sections of the SON. We were not able to differences in the dendritic arbors amongst the neuron types. These results indicate that SON neurons tend to cluster within regions of the SON.

### Rostrocaudal distribution of SON phenotypes.

The three observed fiber tracts exited SON along a rostral-to-caudal axis. Using cytoarchitectural references (NL, NM, NA, and medial vestibular size), we split these fiber tracts into caudal, medial, and rostral sections. 11/17 (64.7%) of ipsilateral medial axons and a 1/ 5 (20%) of the ipsilateral lateral axons exited in the most caudal plane. 5/17 (29.4%) of the ipsilateral medial axons, 4/ 5 (80%) of ipsilateral lateral axons, and 1/16 (6.3%) of contralateral axons exited in the

medial plane. 1/17 of the ipsilateral medial axons and 15/16 contralateral axons exited in the rostral plane (Fig. 3-8). These results suggest that the axons of SON neurons are organized and “bundle” into specific planes, depending on their postsynaptic targets.

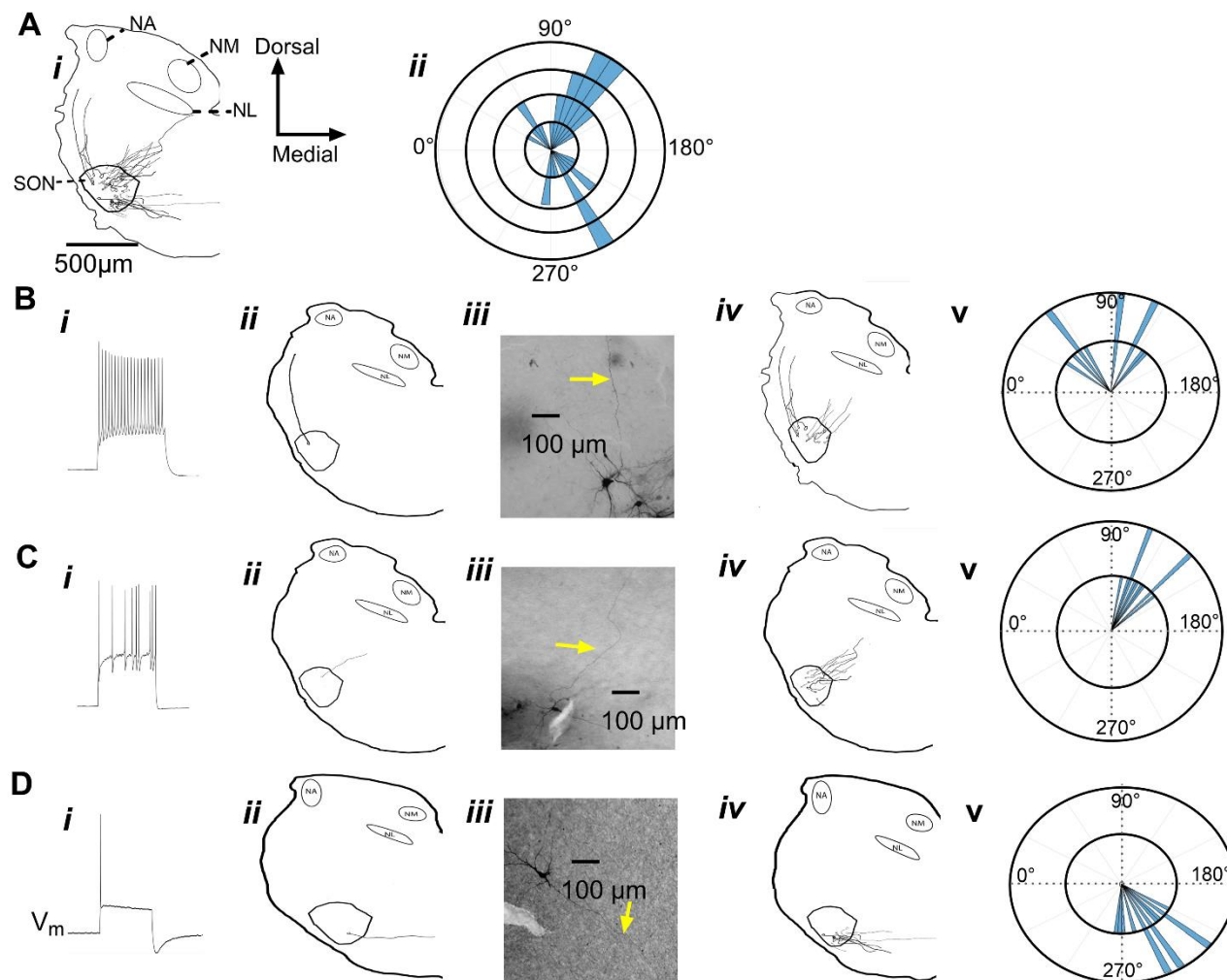


**Figure 3-6 Morphological analysis of axonal projection patterns.**

Physiologically recorded SON neurons were intracellularly labeled with biocytin, processed and reconstructed partial morphology to locate the cell body and determine the projection pattern of the axon as it leaves the SON. Axons appeared to exit the SON in three directed fascicles.

- A) (Top Left) Compiled overlay of 39 separate recovered neuron in 30 slices onto a typical anatomical outline of the ventral left quadrant of the chick brainstem.  
 (Top Right) When the angle of the efferent axon was measured to quantify these tracts such that lateral =  $0^\circ$ , dorsal =  $90^\circ$ , we could identify an ipsilateral lateral tract ( $30^\circ \leq x \leq 70^\circ$ ;  $n=5$ ), an ipsilateral medial tract ( $90^\circ \leq x \leq 135^\circ$ ;  $n=17$ ) and a putative contralateral tract (between  $180^\circ \leq x \leq 280^\circ$ ;  $n=13$ ). Radius indicates axon counts (each concentric ring = 1 count).

B-D) Physiological cell types showed preferential efferent projection angles. For each cell type, example voltage traces (i), reconstructed axon shown relative to SON and brain stem outlines (ii), photomicrograph of the cell body and axon (iii), polar plot of axonal projections of cell type group (iv), and overlay summary of all axon reconstructions for the group (v) polar histogram quantifying the distribution of axons exiting the SON at particular angles. B) Axons from regular tonic cell type fell within one of the two ipsilateral tracts. C) Axons from chattering tonic cell type SON neurons all fell within the ipsilateral medial tract. D) Axons from single spiking SON neurons all fell within the contralateral tract.

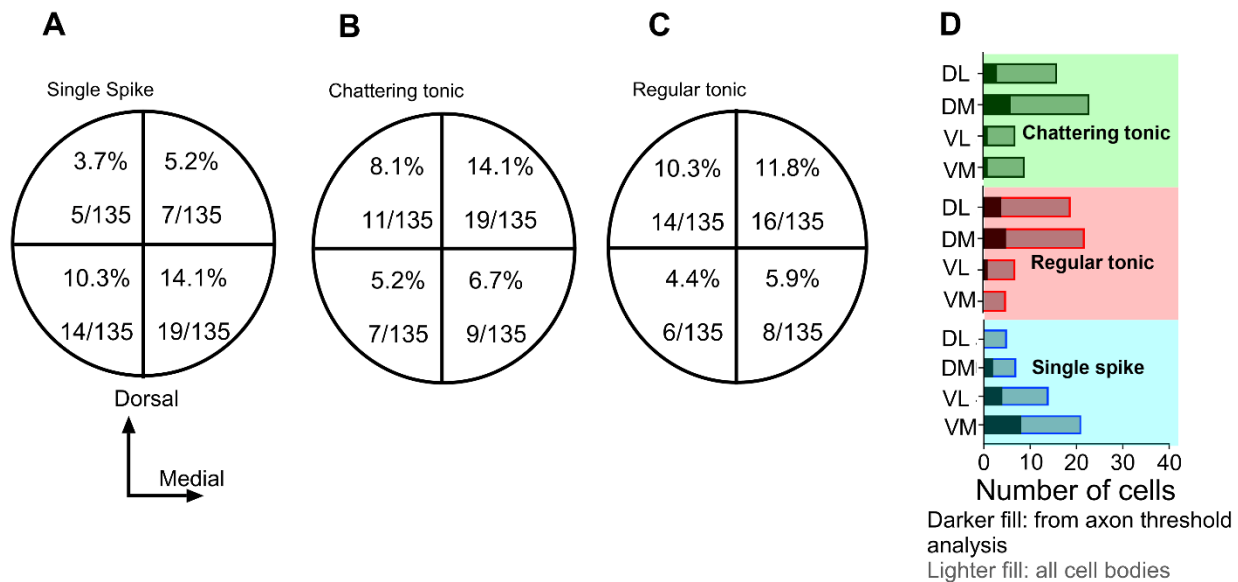


*Figure 3-7 Distribution of the location of cell bodies within SON differs with physiological type*

A-C) Diagram of the coronal section of SON into dorsoventral and mediolateral quadrants with the number of cell bodies located in each out of a total of 135 recovered and corresponding physiological types. Percentages expressed as percent of total. D) M, Medial; L, Lateral; D, Dorsal; V, Ventral. Same data as a bar plot shows the relative distributions of both tonic types were similar and preferentially in dorsal quadrants, while single spiking neurons were preferential in ventromedial. Distribution of SON neurons for which axonal reconstructions were recovered as well and shown as darker shaded regions within bars and had a similar distribution.

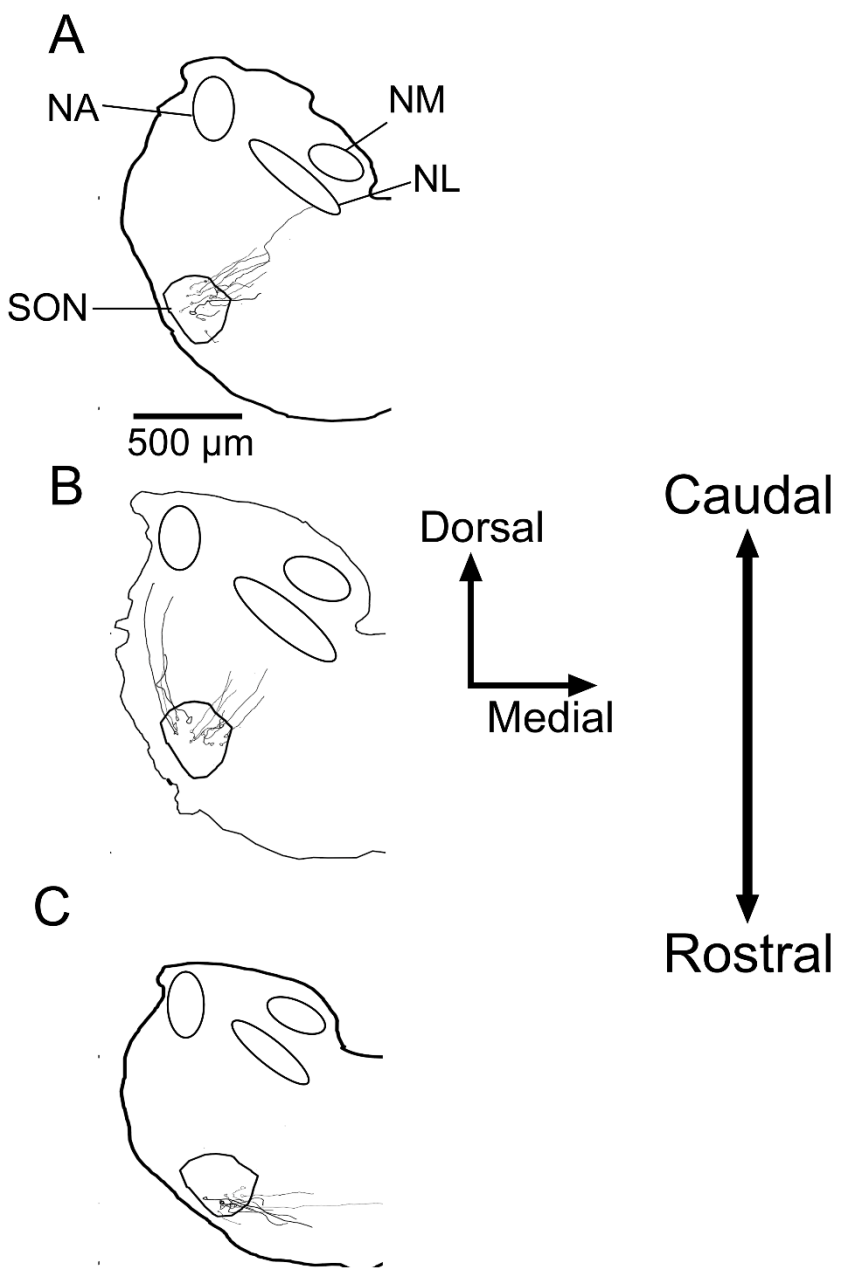


*Figure 3-8 Axonal projection patterns differed across the rostrocaudal extent of SON.*

A) In the caudal most sections axonal projections were mostly via the ipsilateral medial tract (10/10) ipsilateral medial, 4 regular tonic & 6 chattering tonic)

B) Middle sections contained axonal projections either via the ipsilateral medial tract (8/13, 5 chattering tonic and 3 regular tonic) or the ipsilateral lateral tract (5/13, all 5 regular tonic)

C) Rostral most sections contained axonal projections almost entirely oriented contralaterally (16, all single spiking).

## Discussion

Neural inhibition contributes to numerous computational functions in auditory brainstem circuits, such as intensity-dependent gain-control (Al-Yaari et al., 2019; Keine et al., 2016; Nishino et al., 2008), phase locking (Al-Yaari et al., 2019; Dehmel et al., 2010; Fukui et al., 2010; Keine et al., 2016; Kuenzel et al., 2011; Monsivais et al., 2000), ITD & gap detection (Middleton et al., 2011; Williamson et al., 2015), and amplitude modulation coding (Dugue et al., 2007; Keine et al., 2016). Synaptic inhibition in the avian auditory brainstem originates largely from the SON, which projects to the ipsilateral NA, NM, and NL, or to the SONc (Burger et al., 2005). These projections arise from distinct SON populations. The inhibition these SON neurons provide is diversified enough to perform all these functions, suggesting underlying specializations within SON. Two phenotypes based on intrinsic physiological firing elicited *in vitro* have been described in the SON: a tonic firing phenotype and a single spiking phenotype (Carroll et al., 2018; Coleman et al., 2011; Yang et al., 1999), however the functional role for each phenotype is not clear. We investigated whether specific cell types underlie the divergent projections from SON as a first step toward relating intrinsic properties to circuit function.

### Two tonic firing phenotypes in SON.

In this study, we describe a third, previously undescribed, phenotype which we term a “chattering” tonic neuron, distinct from the “regular” tonic neurons. To distinguish tonic firing phenotypes, we quantified each neuron’s interspike interval CV as a measure of the regularity of firing and found a bimodal distribution in the population of tonic neurons that corresponded to the qualitative spiking pattern of chattering and regular. Using CV as a grouping criterion, we

tested other electrophysiological properties and found differences in spike latency, rheobase, input resistance, and afterhyperpolarization, indicating that there are two distinct phenotypes within our sample of tonic neurons.

Variations in excitability and spiking properties may emerge from the differential expression, kinetics, and densities of ion channels (See Prescott et al. (Prescott, Koninck, et al., 2008) for summary). The Kv1 family of channels is a class of low threshold activated voltage-dependent potassium channels that are prevalent in auditory regions, particularly in temporally sensitive areas (Goldberg et al., 2008; Jan & Jan, 2012; Pliego & Pedroarena, 2020; Shu et al., 2007; Storm, 1987) and are critical for coincidence detection neurons across numerous species (Akter et al., 2018; Dodson et al., 2002; Fukui & Ohmori, 2003; Grigg et al., 2000; Kopp-Scheinflug et al., 2003; P. Manis & Marx, 1991). While most prominent in avian NL neurons (see review by (Kuba, 2007), they are also present in subsets of NA neurons, including distinct tonic phenotypes in which dendrotoxin, a Kv1 channel antagonist, abolished all firing response patterning (Baldassano & MacLeod, 2022). The chattering phenotype could also result from sodium channels inactivating after a burst of firing, while Kv1 channel activity acts to prevent further spiking until the sodium channels de-inactivate. Alternatively, another subthreshold voltage-dependent delayed rectifier potassium current, labeled M-type, contributes to burst firing in vivo in the substantia nigra and chattering phenotypes in entorhinal cortex (Drion et al., 2010; Koyama & Appel, 2006), but this current type has not yet been identified as present in avian auditory neurons.

The novel observation of a chattering phenotype in this study compared to previous in vitro studies of SON could be due to differences in temperature, age, or stimulus protocol. At near physiological temperatures (or as in our experiments  $\sim 34^{\circ}\text{C}$ ) stimulation can elicit more complex

firing behavior compared to that at room temperature (Carroll et al., 2018; Yang et al., 1999). Low temperatures slow the kinetics of channels that contribute to variation in spike patterns (Moran & Conti, 1995; Ranjan et al., 2019). While age-dependent effects on spiking have also been well-documented (Fukui & Ohmori, 2003; Hong et al., 2016), this is unlikely to explain the differences here as age ranges in previous studies overlapped with the ages we used here (Carroll et al., 2018; Coleman et al., 2011; Rothman et al., 1993; Y. Wang & Manis, 2005; Yang et al., 1999). Finally, differences in stimulus protocol could obscure spiking patterns that are most apparent at current levels just above rheobase, as we find with the chattering phenotype. Increasing current leads to an increase in the number of spikes in each burst, eventually leading to tonic firing throughout the duration of the current injection. Yang et al. ((Yang et al., 1999) did not report their current step intervals, however Carroll et al. (Carroll et al., 2018) reported using intervals smaller or equal to the intervals we used, thus we believe that temperature was a primary driver in the differences in phenotypes observed.

### SON neurons encode temporal features of sound

The capability of neurons to encode temporal features is dependent on synaptic dynamics (Rothman et al., 1993; Sanchez et al., 2015; Y. Wang & Manis, 2005) and intrinsic membrane properties (Higgs & Spain, 2011; Kreeger et al., 2012; Lubejko et al., 2019; A. D. Reyes et al., 1994). Temporal features emerge at different timescales. Phase locking, or the firing at a particular phase of a modulated stimulus, is important for pitch perception (Winter, 2005) and for binaural ITD computations (T. C. T. Yin, 2002). Envelope coding, or firing to instantaneous changes in amplitude, is important for sound recognition (Nelson & Takahashi, 2010; Schneider & Woolley, 2010; Singh & Theunissen, 2003). Historically, SON neurons were not thought to

encode temporal features and merely rate code, but a subset of in vivo recordings from SON neurons showed phase locking in neurons up to 4 kHz. However, the strength of the phase locking varied considerably amongst neurons (Coleman et al., 2011).

Our study investigated intrinsic sensitivity of SON neurons to temporally modulated inputs in vitro using fluctuating noisy current injections (Mainen & Sejnowski, 1995), where fluctuation size likely relates to the amplitude and timing of synaptic inputs. Each SON phenotype was found to have a different level of temporal sensitivity, with single spiking neurons being the most reliable, regular tonic neurons the least reliable, and chattering tonic neurons in between. These different phenotypes may underlie the spectrum of temporal sensitivity demonstrated in Coleman et al. ((Coleman et al., 2011). We also varied the level of fluctuation to determine if SON neurons differentially responded to fluctuation size. We found that chattering tonic neurons increased their firing with larger fluctuations, but regular tonic neurons did not. These results suggest that input synchrony, as well as mean input, drive the level of inhibitory output from the SON.

### SON neurons provide inhibition to divergent postsynaptic targets organized by intrinsic spiking properties.

In previous studies, retrograde labeling revealed distinct SON populations that send axons either ipsilaterally towards the lower order nuclei (NA, NL, and NM) or to SONc (Burger et al., 2005). Whether these divergent projections represented different electrophysiological types was not known. To address this issue, we reconstructed the axons of recorded neurons and found a clear pattern. Each neuron had an axon that exited the SON in one of three directions: as an ipsilateral projection that followed the olivary-trapezoid tract toward NM and NL, an ipsilateral projection

that followed a lateral tract, potentially in the same region as the inferior cerebellar peduncle toward NA, or a contralateral projection fiber tract, which crosses along the trapezoid body decussation that headed toward SONc (Puelles & Martinez, 2013). The firing response phenotype of each neuron correlated with its preferred axonal fiber projection: axons in the ipsilateral medial projection originated from both chattering tonic and regular tonic neurons; axons in the ipsilateral lateral tract originated exclusively from regular tonic neurons; and axons in the contralateral projection originated exclusively from single spiking neurons.

### Role of inhibition in the avian auditory brain stem.

The critical role of inhibition in sound encoding by the timing nuclei has been well established. Blocking inhibition worsens phase locking in NM (Fukui et al., 2006, 2010) and compresses the dynamic range, or range of sound intensities encoded before saturating, of low frequency NM neurons (Al-Yaari et al., 2019). In NL, inhibition shortens the window for coincidence detection, improving ITD calculation (Nishino et al., 2008; Yang et al., 1999) demonstrated that low frequency NL neurons (<1 kHz) had improved contrast between their best and worst frequencies during increased sound levels due to increased levels of inhibition. Inhibitory postsynaptic currents (IPSCs) in NM are slow and temporally summing (Howard et al., 2007; Howard & Rubel, 2010; Kuo et al., 2009; Monsivais et al., 2000; Yang et al., 1999), however the kinetics of IPSCs are more rapid in NL than NM, indicating a preference towards maintaining temporal structure (Kuo et al., 2009). Although summation effects would blunt temporal precision, the arrival of SON-driven synaptic inputs from temporally-sensitive chattering tonic neurons could influence temporal processing in NL, especially in low frequency regions.

Less is known about the function of inhibition in the so-called intensity pathways of avian brainstem, but some evidence from synaptic studies suggests differential processing. Kuo et al. (Kuo et al., 2009) demonstrated the kinetics of IPSCs in NA (putative SON inputs) are more rapid than in either NM or NL and vary amongst tonic and single spiking neurons in NA. The function of inhibition in NA has not yet been studied using pharmacological methods, but feedback integrator-like regular tonic SON neurons suggests a negative gain-control as a primary function. Such a gain control function would be consistent with the projection of the regular tonic, ‘integrator’-like neurons found in our study. On the other hand, the rapid synaptic kinetics could indicate a role in spectrotemporal processing. This would be consistent with NA’s enhanced envelope coding, compared to nerve inputs or that in the timing pathway (Fontaine et al., 2014; Steinberg & Peña, 2011).

Coleman et al. (Coleman et al., 2011) demonstrated both glycinergic and GABAergic signaling between the two SON and that pharmacologically blocking either increased the firing rate to sound stimuli, while blocking glycinergic signaling worsened phase locking. Binaural coupling of the two SON is theorized to be critical for ITD processing within NL, particularly during large interaural level differences (ILD) (see review by (Burger et al., 2015)). In short, NL must differentiate excitatory drive from a strong monaural stimulus or a well-timed binaural stimulus. Contralateral auditory drive disinhibits NL, boosting ITD computation. Our study suggests that the primary source of contralateral inhibition may be the single spiking neurons from the opposite SON. The phasic and temporally locked nature of these single spiking neurons could selectively bolster activity being used for ITD detection during large contrasts of ILDs.

Notably, the location of cell bodies of these neurons within the SON lined up with previous retrograde labeling experiments (Burger et al., 2005), where contralaterally projecting neurons were positioned ventrally and ipsilateral projecting neurons were positioned dorsally.

A limitation of this experiment lies in the inability to follow axons entirely to their postsynaptic target. It is possible that axons could turn and synapse in a location that is not apparent to by the length of axon measured. Burger et al. ((Burger et al., 2005) demonstrated that ipsilateral projections from SON provided input to all three of the lower brain stem nuclei, NA, NL, and NM. Therefore, this ipsilateral lateral projection could synapse on NM and NL as well, though how that is accomplished is not clear. Alternatively, this population could project outside of the brainstem.

### Mammalian vs avian inhibitory architecture.

Birds utilize sounds to accomplish the same sensory tasks as mammals, but with simpler circuitry (Grothe & Pecka, 2014). In birds, inhibition in the auditory brainstem primarily originates from the SON. Importantly, there is no local inhibition within NA, NM, or NL. However, phasic inhibition from GABAergic neurons outside of the low-CF region of NL has been described. The exact function of this population is not well understood, but they likely shorten the window for bilateral EPSP summation and enhance ITD-tuning ((Yamada et al., 2013). Comparatively, inhibition in the mammalian auditory brainstem arises from multiple sources and is utilized in several different processes, with several sources arising from within the cochlear nucleus (Altschuler et al., 1986; Caspary et al., 1994; Gai & Carney, 2008; Keine & Rübsamen, 2015; Kopp-Scheinflug et al., 2002; Ngodup et al., 2020; Oertel et al., 2011; Xie & Manis, 2013). D-stellate cells in the ventral cochlear nucleus (VCN) utilize large dendritic arbors to span auditory nerve fibers and provide broadband local inhibition, the dorsal cochlear

nucleus (DCN), and to bushy cells in the contralateral VCN (Cant & Gaston, 1982; Needham & Paolini, 2003; W. Wang et al., 2019; Wickesberg et al., 1994). Tuberculo-ventral cells in DCN receive AN input and project to the ipsilateral VCN (Zhang & Oertel, 1993). Finally, L-stellate cells in the VCN receive narrowband excitatory inputs and project to ipsilateral T-stellate and bushy cells (Ngodup et al., 2020).

In addition to the sources from within the cochlear nucleus, inhibition arises from other brainstem structures as well during binaural computations. The ventral nucleus of the trapezoid body (VNTB) provides both GABAergic & glycinergic (although the GABAergic component declines during development) to the medial nucleus of the trapezoid body (MNTB), which itself is a source of rapid feed-forward glycinergic inhibition that is important for ITD computation.

The exact mechanism of ITD computation in mammals is still debated. One proposed mechanism is a balance of excitatory-inhibitory inputs. Excitatory inputs from bushy cells in the VCN drive activity in contralaterally projecting glycinergic neurons, shifting the ITD preference towards the contralateral ear (Brand et al., 2002; Pecka et al., 2008). However, other experiments, such as those in Franken et al. (Franken et al., 2015) propose that internal delay lines give rise to ITD computation, which would be closer to the avian model. Additionally, interaural level difference (ILD) calculations occur in higher order circuits within birds, occurring within lemniscal nuclei (Adolphs, 1993; Mogdans & Knudsen, 1994; T. T. Takahashi et al., 1995), while mammalian ILDs are calculated largely in the brainstem (Kyweriga et al., 2014).

## Chapter 4 : The impact of GABAergic-like conductances on intensity coding and using conductance clamp to measure operating modes

### Introduction

In chapter 4 of this dissertation, we utilize a computational simulation of synaptic conductances through dynamic clamp to 1) determine the effect of inhibition on the intensity coding neurons of the cochlear nucleus angularis (NA) and 2) recreate noisy currents using a conductance-based model. NA neurons are physiologically diverse, and likely have different functional roles (especially single spiking neurons), however a primary role to encode intensity cues from ANF inputs. As mentioned in chapters 1 & 2, NA neurons encode intensity cues by receiving numerous small bouton-like excitatory synapses from the auditory nerve, allowing them to have a graded level of input that can reflect mean presynaptic levels. The range of sound intensities NA neurons can encode, or the difference between the softest sound capable of producing action potentials and the point at which firing rate saturates, is referred to as the neuron's "dynamic range."

It is important to maximize the range of sound intensities for several functions, such as distinguishing the proximity of sound sources. In both birds and mammals, individual cochlear neurons tend to have a dynamic range that spans ~25-30 dB ((Köppl & Carr, 2003), which is not likely to encode the ~120 dB range of intensities that animals can encode (Colburn et al., 2003). Instead, the statistics of a sound stimulus shape the firing rate of intensity coding auditory neurons, which adapt their firing rate to encode a range of relevant sound intensities (Dean et al.,

2005). Inhibition has been shown to expand dynamic range of NM neurons (Al-Yaari et al., 2020) and is a mechanism of neural adaptation (reviewed in (Benda, 2021).

However, the effect of inhibitory conductances on how NA neurons process inputs has not yet been established. Immunohistochemical studies show inhibitory synapses are distributed throughout NA, both clustered on the cell bodies and within the neuropil ((MacLeod & Pandya, 2022). In order to explore the effect of inhibition on intensity coding in NA, we used dynamic clamp to simulate GABAergic conductances during whole cell-patch clamp recordings where a series of current injections were administered to determine the rheobase, as well as the point of firing saturation.

In the same experiments, we utilized conductance clamp to model *in vivo*-like synaptic barrages to NA neurons. Conductance clamp circumvents issues in current clamp, as described in chapter 1, section IV (Prescott et al., 2006). Using noisy currents as a method for investigating integrative properties of neurons is easier because traditional patch-clamp systems were capable of producing frozen current stimuli, where a conductance clamp approach requires specialized hardware. However, it is unclear whether the results of noisy current experiments can be recreated using a conductance based approach. We performed conductance clamp experiments as a method of experimental verification for noisy current-clamp experiments by systematically altering mean levels of conductance and the standard deviation of conductance using dynamic clamp.

## Materials and methods

### Brain slice preparation

Brain slices were collected in the same manner described in chapters 2 & 3.

### Whole cell patch-clamp electrophysiology

Electrophysiological recordings were done similarly to chapters 2 & 3, however application of the current stimulus and recording of the voltage output were controlled by an analog-to-digital board from CED1401 (Cambridge, UK) instead of National Instruments (Austin, TX) and a computer running Signal software (Cambridge, UK) instead of IGOR Pro (WaveMetrics, Lake Oswego, OR) was used. A holding current was applied to maintain a constant voltage baseline of approximately -65 mV. Cell type classification protocols were carried out to identify neuronal phenotypes in NA with 400-ms-duration flat current steps of varying amplitudes from -150 pA up to 550 pA in 50 or 100 pA intervals. Due to the nature of the experiments, we only recorded from tonic firing neurons, therefore we discarded data from single spiking recordings. We collected data from 20 tonic firing NA neurons (8 tonic 1 neurons, 7 tonic 2 neurons, 5 tonic 3 neurons) across all experiments in this section.

### Modeling GABAergic-like inputs

To simulate inhibitory-like conductances, we utilized an alpha synapse model which simulates the presence of a synapse between two cells using the Alpha function to generate the post-synaptic conductance profile,  $g(t)$ , using the equation:

$$g(t) = Gmax * \left(\frac{t}{\tau}\right) * e^{(1-\frac{t}{\tau})}$$

where  $G_{\max}$  is the maximum synaptic conductance in nanosiemens,  $t$  is the time since the synapse was triggered, and  $\tau$  is the conductance time constant. A  $\tau$  of 7 ms was selected based on IPSC kinetics of tonic firing NA neurons IPSC kinetics Kuo et al. ((Kuo et al., 2009). A Goldman-Hodgkin-Katz (GHK) model was used to simulate a GABAergic-like conductance by recreating the current produced by ion diffusion through membrane ion channels, driven by concentration differences. GABAergic inhibition has been shown to elicit depolarizing synaptic potentials in NA (Kuo et al., 2009). Therefore, our simulation was conducted assuming an intracellular chloride concentration of 12.5 mM and an extracellular chloride concentration of 5 mM, generating a calculated reversal potential  $E_{Cl}$  of -40 mV (reversal potential for  $E_{Cl}$  is -41mV in (Kuo et al., 2009).

Direct square-pulse current injections were applied, with a range of amplitudes increasing in 50 pA intervals to firing rate saturation. To model the inhibitory component, a 20 Hz train of pulses was modeled to occur simultaneously with the direct current injection (with an onset delay of 50 ms after depolarizing current). These pulses simulated the inhibitory presynaptic element firing action potentials (presumed SON) that triggered a train of inhibitory conductances. To compare strength of inhibition,  $G_{\max}$  conductance was set at 20 nS or 40 nS and the model was turned off during control conditions.

### Dynamic range

To quantify the dynamic range of NA neurons, we first determined the rheobase i.e. the lowest amount of current required to produce spikes, referred to as  $I_{\min}$ . Next, we determined the maximum current required to produce a saturating number of action potentials i.e. increasing the

current level either caused the firing rate to decrease or increased firing by less than 3% in response to a 100 pA current level increase. This maximal point is referred to as  $I_{MAX}$ .

In the control condition (no GABAergic conductance), all neurons saturated their firing rates. However, 2 neurons did not have their firing rates saturate in the modeled GABAergic conditions. This was an experimental oversight that occurred because these experiments were performed with a new system and firing rate was only quantified after the experiment was over, therefore the saturating was determined qualitatively during the recording. For these neurons, the  $I_{MAX}$  was the highest tested current level.

$$I_{MAX} - I_{MIN} = I_{DYN}$$

Where  $I_{DYN}$  is the resulting dynamic range of an NA neuron.

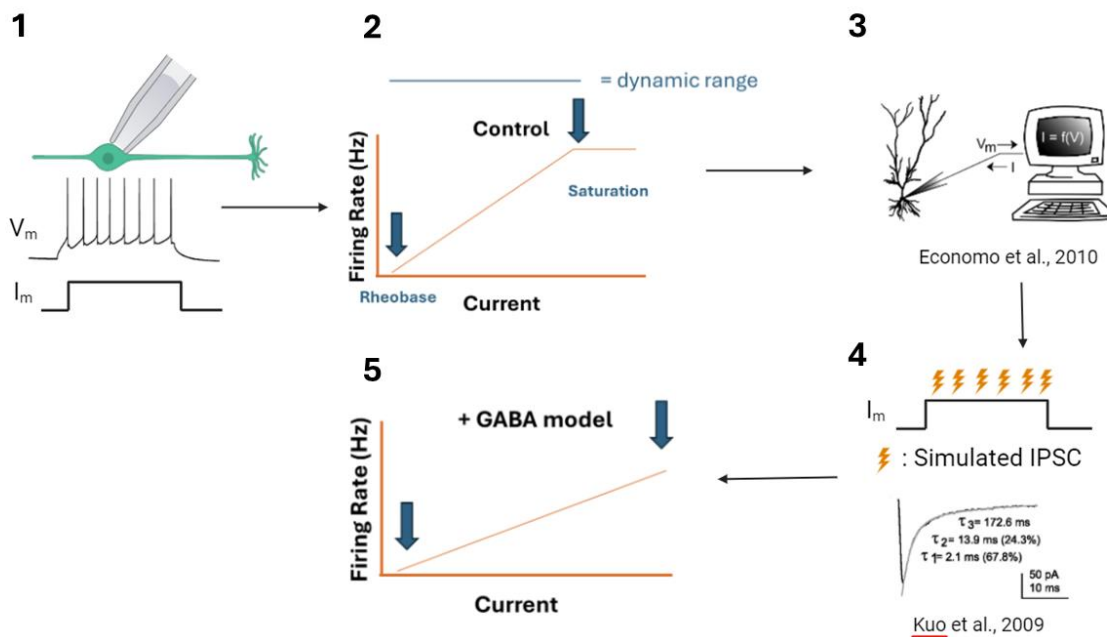


Figure 4-1 Schematic of experimental design for GABAergic experiment

- 1- Patch a neuron and identify its firing pattern (tonic vs. non-tonic)
- 2- Record an F-I, noting the rheobase & point of saturation
- 3- Turn on dynamic clamp software and set parameters for model
- 4- Recollect F-I with modeled IPSCs throughout the current injection
- 5- Quantify the rheobase and point of saturation

## Conductance clamp model of noise

Models of noisy currents simulate *in vivo* like behaviors, which are increasingly recognized as important for understanding neuronal behavior in dynamic systems. The standard noise generation mechanism uses an Ornstein-Uhlenbeck (O/U) process to model the noisy behavior. The O/U noise model is a stochastic process using the following stochastic differential equation

$$dG_t = \frac{1}{\tau((G_{base} - G_t)dt)} + \sigma N$$

Where  $G_t$  is the noisy conductance at time “t,”  $\tau$  is the time constant controlling the decay of the noise back to a baseline conductance value set by  $G_{base}$ ,  $\sigma$  scales the standard deviation of the noise, and  $N$  is a random value obeying Gaussian statistics with a mean of zero and a standard deviation of 1. A reversal potential of -30 mV was used to model a combination of both excitatory and inhibitory conductances.

The  $G_{base}$  was systematically altered from 0 nS to 100 nS in 10 nS intervals. At each  $G_{base}$ , 3 different standard deviation values were selected in order to replicate the different noise levels. Each sweep included a 1 sec hyperpolarizing step (to de-inactivate sodium channels) and a 2 second noisy duration. Spiking was quantified entirely post-hoc using Signal’s automated spike detection software. The area difference index (ADI), described in chapter 2 & 3, was utilized to quantify the level of fluctuation sensitivity.

## Results

### Modeled GABAergic conductances expand the dynamic range of tonic firing NA neurons

We recorded F-I curves from 10 tonic firing NA neurons and determined the rheobase and the saturating current level to measure the intrinsic dynamic range of the neuron, then replot the F-I while applying a GABAergic-like conductance (example in Fig. 4-1Ai of control and while the conductance was simulated, Fig. 4-1 Aii). Quantification of the F-I curve is in Fig. 4-1B. After applying simulated GABAergic conductances, the dynamic range expanded from  $0.53 \pm 0.15$  nA in control conditions to  $0.74 \pm 0.21$  nA when 20 nS of conductance was simulated ( $p = 0.013^*$ , Student's t-test) and  $0.73 \pm 0.18$  nA when 40 nS of conductance was simulated ( $p = 0.015^*$ , Student's t-test) (Average of F-I curves in Fig. 4-2A. Dynamic range demonstrated in 4-2B). There was no difference between the 20 nS & 40 nS conditions ( $p = 0.39$ , Student's t-test). Notably, the rheobase was not altered (Fig. 4-2 Ci. Control neurons,  $0.1 \pm 0.04$  nA, 20 nS GABA,  $0.12 \pm 0.04$  nA, 40 nS GABA,  $0.12 \pm 0.06$  nA), nor was the maximum firing rate produced (Fig. 4-2 Cii. Control,  $59 \pm 20.8$  Hz, 20 nS GABA  $62.8 \pm 18.2$  Hz, 40 nS GABA  $61.8 \pm 18.1$  Hz). However, the current at which this firing rate was elicited was significantly increased (Fig. 4-2 Ciii. Control  $0.52 \pm 0.08$  nA, 20 nS GABA  $0.76 \pm 0.11$  nA, 40 nS GABA  $0.77 \pm 0.1$  nA). These results indicate that GABAergic conductances could work to expand the dynamic range of NA neurons.

Qualitatively, the characteristic spiking phenotype was not altered by addition of GABAergic conductances, as demonstrated by the voltage response of the tonic 2 neuron seen in Fig. 4-1Aii maintaining its pause in firing at the onset of a current injection. Additionally, in

control conditions, spiking at saturating current levels tended to have reduced spike amplitudes, while spike height seemed to be unaffected at saturating levels in the modeled GABAergic conditions.

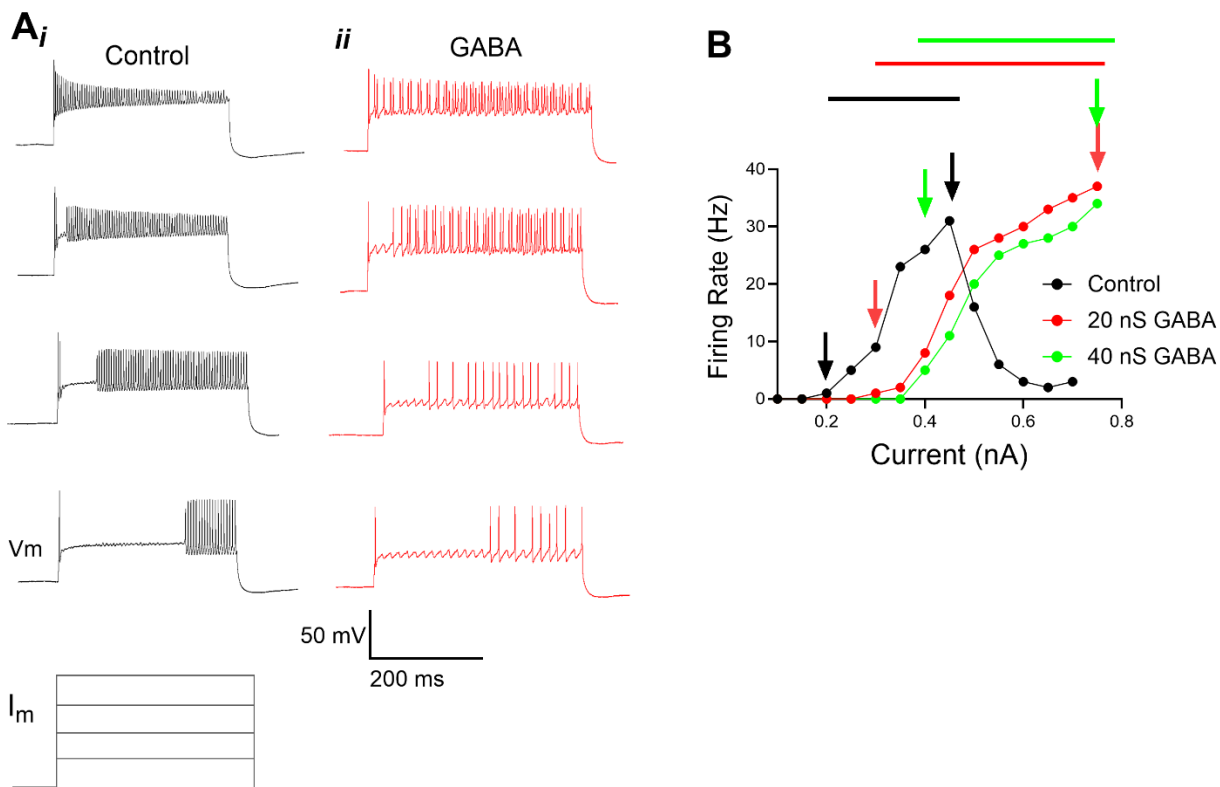


*Figure 4-2 Example of the influence of GABAergic-like conductance on F-I functions*

*Ai-ii*) Voltage responses from a tonic 2 neuron in response to flat current injections & with 20 nS of GABAergic conductances modeled at 20 Hz. B) a representative current-firing function of a neuron in control (black), 20 nS of GABAergic conductance (red), and 40 nS of GABAergic conductance. Arrows of respective colors denote rheobase and firing saturation, lines correspond to the dynamic range of the corresponding F-I

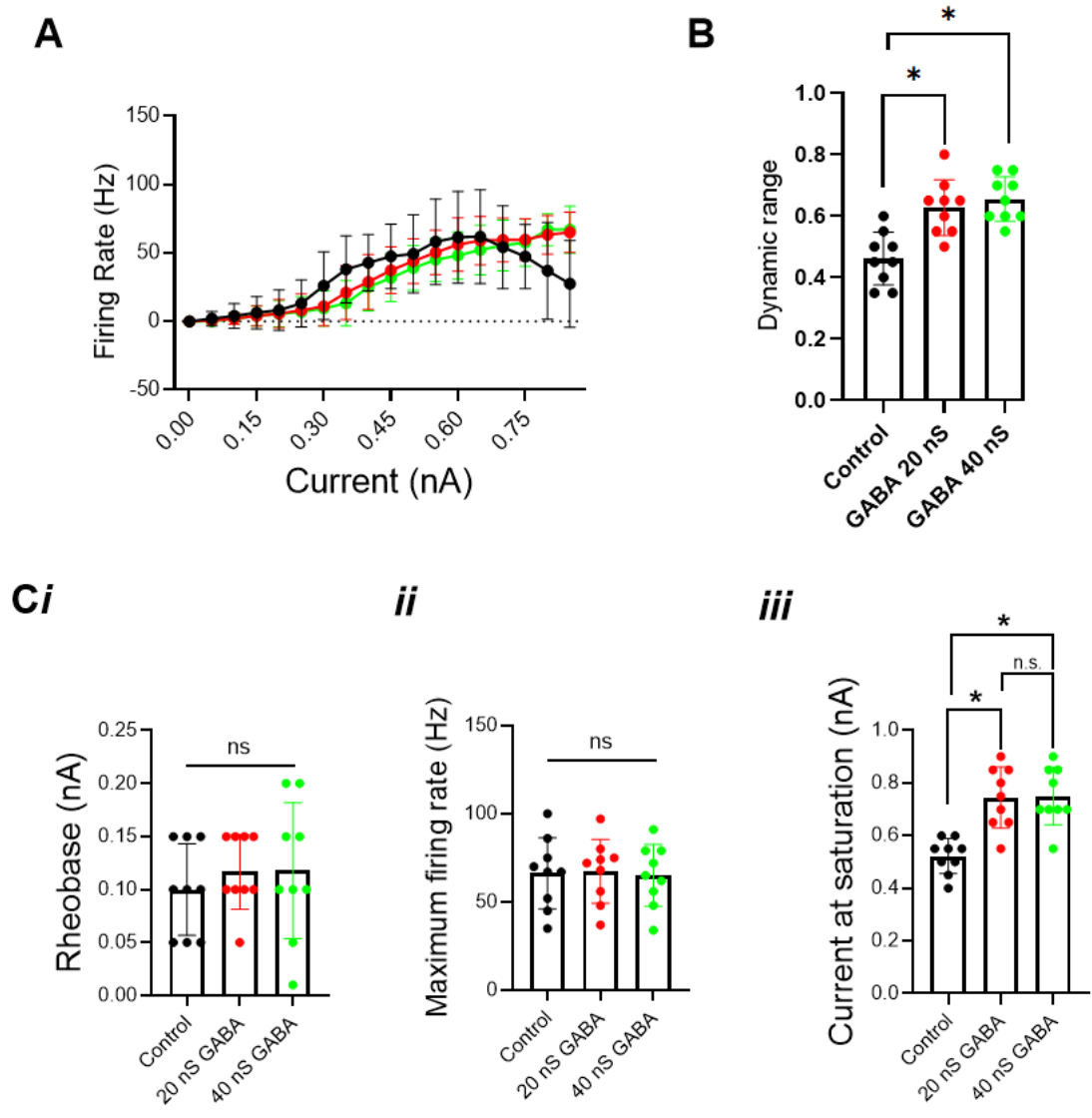


Figure 4-3 GABAergic-like conductances expand the dynamic range of NA neurons by increasing the current required to produce saturation

- A) Average F-Is across control (black), 20 nS of GABA (red), and 40 nS of GABA (green) across 9 neurons.
- B) Dynamic range of the population F-I curves for each condition
- C) No changes were observed across in the rheobase (i), nor the maximum firing rate (ii), but the current that produced saturating responses was elevated by GABAergic-like conductances (iii).

## Conductance clamp firing responses maintain fluctuation sensitivity

A critique of noisy current clamp experiments is that the frozen noise currents do not respond to changing membrane parameters in a realistic way (Prescott et al., 2006). This is an issue that is circumvented using conductance clamp. In order to determine if noisy current experiments accurately captured the operating modes of neurons, we recorded noisy conductance clamp F-I recordings from 10 tonic firing NA neurons (3 tonic 1, 4 tonic 2, 3 tonic 3 neurons) and quantified their area difference index (ADI) (see Methods, chapter 2) and then compared the ADI values of these F-I curves (Fig. 4-2Ai shows a “differentiator,” Fig 4-2Aii shows an “integrator”) to the ADI values of neurons recorded from using current clamp (Fig 4-2Bi, ii show a differentiator & an integrator. Recordings & values were taken from (Baldassano & MacLeod, 2022). We found that there were no significant differences in the distribution of ADI values from conductance clamp recordings and noisy current clamp recordings (Fig. 2C, unpaired Student’s t-test,  $p = 0.29$ ).

A limitation with this experiment was the inability to match noisy current paradigms within the same neuron- this limitation was due to the separate software for each paradigm. Noisy current paradigms ran through custom IGOR software, where the conductance clamp paradigm utilized Signal software. It was not possible to utilize both systems while recording from a single neuron.

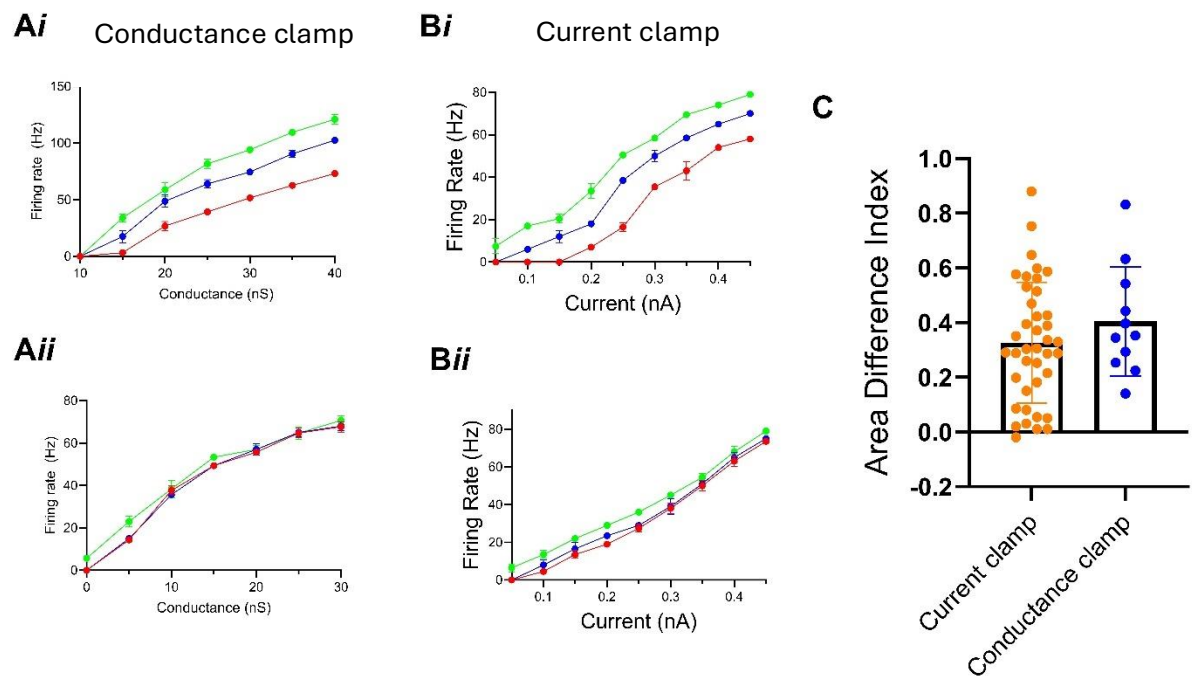


Figure 4-4 *Integrative properties are captured similarly in conductance clamp & current clamp.*

Ai, ii) Firing rates from a differentiator and integrator, respectively, recorded from using conductance clamp. Bi, ii) Firing rates from a differentiator and integrator, respectively, using current clamp (values taken from Baldassano & MacLeod, 2021). C) Comparing the ADI from each population of neurons found no difference in integrative capabilities ( $p = 0.29$ ).

## Discussion

Dynamic clamp is a powerful technique that allows for simulated conductances, such as synaptic and intrinsic channels. Here we used *in vitro* electrophysiology and computational simulations in a dynamic clamp to answer two questions. 1) Will modeling GABAergic-like conductances expand the dynamic range of tonic firing NA neurons? 2) Will using conductance-clamp models of noise sensitivity verify the fluctuation sensitivity seen in experiments using noisy currents?

We found that modeling GABAergic-like inputs caused the dynamic range to significantly increase in tonic firing NA neurons by preventing firing saturation at higher current levels. We also found that using conductance clamp models of noise produced a range of fluctuation sensitivities similar to those produced in current clamp, thus further verifying the efficacy of noisy currents in determining a neuron's fluctuation sensitivity.

### Inhibition in intensity coding

Hearing can occur over an incredible range of sound intensities. At 0 dB sound pressure level (SPL), which is the lower threshold of vertebrate hearing ranges, the tympanic membrane may only move the distance equivalent to a fraction of an atom (Kirk & Smith, 2003). The upper threshold can be 120 dB, an increase of 12 orders of magnitude, with sensitivities to ~1 dB changes (Houtsma et al., 1980; Viemeister, 1974, 1983). These intensities are reflected in neural firing rates, however, given the low threshold and the ~35 dB dynamic range of most cochlear

neurons, it is not likely that this can account for the significantly larger range of sound intensities that are encoded by the brain (Colburn et al., 2003).

While sounds can vary over extended periods of time, over shorter periods they tend to fluctuate over a limited range (Kirk & Smith, 2003). *In vivo* recordings in the inferior colliculus (IC) demonstrated that the firing rate of intensity coding neurons is dependent on the context of the stimulus, rather than responding strictly to the mean level of the stimulus because the neuron's firing rate would adapt to the statistics of the preceding auditory stimulus (Dean et al., 2005). This adaptation occurred over varying timescales, but on average occurred within ~160 ms, although some neurons showed adaptation on much longer scales (Dean et al., 2008). While numerous processes can underlie this adaptation, inhibition likely plays a role (reviewed in (Benda, 2021). A primary target of NA is the SON, which projects back to NA (Burger et al., 2005), meaning that intensity information is a driver of the firing rate of the SON. Our results in chapter 3 demonstrate that tonic firing SON neurons likely project to NA and act as gain-control neurons. This feedback-loop can modulate the output response of NA neurons such that their firing rate is contained within a set range.

Additionally, inhibition could shape the temporal sensitivities of NA neurons. Experiments in cortical neurons have demonstrated that inhibition expands their dynamic range capabilities while preserving the spike timing required for temporal coding (Khubieh et al., 2016). GABA receptors have been shown to be both in the neuropil and clustered on the cell bodies of NA neurons (MacLeod & Pandya, 2022) and NA neurons have a spectrum of temporal sensitivities (Ahn et al., 2014; Baldassano & MacLeod, 2022; Kreeger et al., 2012; Lubejko et al., 2019). GABAergic inputs could act to sharpen the temporal processing while also expanding the level of input intensity being coded. GABA is depolarizing in NA, and inhibits through

shunting (Kuo et al., 2009). GABAergic synapses that are clustered near the soma likely influence temporal selectivity by increasing spike thresholds while synapses located on distal dendrites are more likely involved in dampening responses and reducing the amplitude of EPSPs that get integrated at the soma (Jadi et al., 2012). It is unclear if specific NA phenotypes have different synapse locations. Future experiments can validate these trains of thought.

### Conductance and current models – when to use them?

Examining the integrative properties of neurons *in vitro* allows for robust control of the inputs to neurons. Traditionally, fixed current injections have been used to measure these integrative properties because they are technically simpler to use (Prescott et al., 2006). However, it is debated how natural these fixed current injections are. These inputs fail to reflect the changing membrane potential, and therefore the voltage-dependent conductances, in a naturalistic manner. An example of this is when a spike occurs in current clamp, the current is not impacted by the spike, which should have a shunting effect. Spike morphology is impacted by this, as current clamp tends to produce taller and wider spikes (Prescott et al., 2006).

Utilizing conductance clamp circumvents these issues, however, it requires a more computationally advanced recording system. We showed here that, while the morphology of individual spikes is different, that integrative properties are conserved between conductance clamp and current clamp models. Therefore, each system can be utilized depending on the question being answered. The simplicity of current clamp models is more accessible and effectively captures integrative properties of neurons. Additionally, using frozen noise stimuli, as we have done here in chapters 2 & 3, allows for quantifying of temporal reliability in a manner that would not be possible in conductance clamp. The responsiveness of the conductance model

would cause the input to change based on minute differences in membrane voltages, meaning a small change in firing would lead to runaway alterations in firing patterns. However, the morphology of spikes during *in vivo*-like synaptic barrages is likely better captured using conductance clamp models.

## Conclusions

In this dissertation, we have discussed auditory coding in brainstem structures by examining both the literature and novel discoveries. The primary conclusions from this body of work are as follows: 1) Kv1 channels shape the characteristic responses of NA neurons and likely contribute to envelope coding by intrinsically driving temporal responsiveness, 2) inhibitory neurons in the SON are more diverse than previously thought and these distinct phenotypes have distinct temporal characteristics and project to divergent targets within the brainstem, and 3) modeled GABAergic conductances expanded the dynamic range of NA neurons and conductance clamp models of noise capture integrative properties similarly to current clamp models. These experiments have contributed to the understanding of molecular and electrophysiological techniques of auditory processing, particularly of temporally modulated stimuli. Additionally, these experiments have opened the doors for numerous future experiments, such as exploring sodium channel inactivation kinetics in specific phenotypes in NA, determining the role of temporally sensitive inhibitory SON neurons in auditory processing, and the role of inhibition in specific NA neurons using both modeling and pharmacology.

## References

- Adolphs, R. (1993). Bilateral inhibition generates neuronal responses tuned to interaural level differences in the auditory brainstem of the barn owl. *The Journal of Neuroscience*, *13*(9), 3647–3668. <https://doi.org/10.1523/jneurosci.13-09-03647.1993>
- Ahn, J., Kreeger, L. J., Lubejko, S. T., Butts, D. A., & MacLeod, K. M. (2014). Heterogeneity of intrinsic biophysical properties among cochlear nucleus neurons improves the population coding of temporal information. *Journal of Neurophysiology*, *111*(11), 2320–2331. <https://doi.org/10.1152/jn.00836.2013>
- Akter, N., Adachi, R., Kato, A., Fukaya, R., & Kuba, H. (2018). Auditory Input Shapes Tonotopic Differentiation of Kv1.1 Expression in Avian Cochlear Nucleus during Late Development. *The Journal of Neuroscience*, *38*(12), 2967–2980. <https://doi.org/10.1523/jneurosci.2472-17.2018>
- Alibardi, L. (2000). Cytology of large neurons in the guinea pig dorsal cochlear nucleus contacting the inferior colliculus. *European Journal of Histochemistry : EJH*, *44*(4), 365–375.
- Altschuler, R. A., Betz, H., Parakkal, M. H., Reeks, K. A., & Wenthold, R. J. (1986). Identification of glycinergic synapses in the cochlear nucleus through immunocytochemical localization of the postsynaptic receptor. *Brain Research*, *369*(1–2), 316–320. [https://doi.org/10.1016/0006-8993\(86\)90542-1](https://doi.org/10.1016/0006-8993(86)90542-1)
- Al-Yaari, M., Yamada, R., & Kuba, H. (2019). Excitatory-Inhibitory Synaptic Coupling in Avian Nucleus Magnocellularis. *The Journal of Neuroscience : The Official Journal of the Society for Neuroscience*, *40*(3), 619–631. <https://doi.org/10.1523/jneurosci.1124-19.2019>
- Art, J. J., Wu, Y. C., & Fettiplace, R. (1995). The calcium-activated potassium channels of turtle hair cells. *The Journal of General Physiology*, *105*(1), 49–72. <https://doi.org/10.1085/jgp.105.1.49>
- Ashida, G., & Carr, C. E. (2011). Sound localization: Jeffress and beyond. *Current Opinion in Neurobiology*, *21*(5), 745–751. <https://doi.org/10.1016/j.conb.2011.05.008>
- Ashida, G., Tollin, D. J., & Kretzberg, J. (2017). Physiological models of the lateral superior olive. *PLoS Computational Biology*, *13*(12), e1005903. <https://doi.org/10.1371/journal.pcbi.1005903>
- Ashmore, J. (2020). A maturing view of cochlear calcium. *The Journal of Physiology*, *598*(1), 7–8. <https://doi.org/10.1113/jp279215>

- Azouz, R., & Gray, C. M. (2000). Dynamic spike threshold reveals a mechanism for synaptic coincidence detection in cortical neurons in vivo. *Proceedings of the National Academy of Sciences*, 97(14), 8110–8115. <https://doi.org/10.1073/pnas.130200797>
- Bal, R., & Oertel, D. (2001). Potassium Currents in Octopus Cells of the Mammalian Cochlear Nucleus. *Journal of Neurophysiology*, 86(5), 2299–2311. <https://doi.org/10.1152/jn.2001.86.5.2299>
- Baldassano, J. F., & MacLeod, K. M. (2022). Kv1 channels regulate variations in spike patterning and temporal reliability in the avian cochlear nucleus angularis. *Journal of Neurophysiology*, 127(1), 116–129. <https://doi.org/10.1152/jn.00460.2021>
- Barnes-Davies, M., Barker, M. C., Osmani, F., & Forsythe, I. D. (2004). Kv1 currents mediate a gradient of principal neuron excitability across the tonotopic axis in the rat lateral superior olive. *European Journal of Neuroscience*, 19(2), 325–333. <https://doi.org/10.1111/j.0953-816x.2003.03133.x>
- Bartheld, C. S. V., Code, R. A., & Rubel, E. W. (1989). GABAergic neurons in brainstem auditory nuclei of the chick: Distribution, morphology, and connectivity. *Journal of Comparative Neurology*, 287(4), 470–483. <https://doi.org/10.1002/cne.902870406>
- Baydyuk, M., Xu, J., & Wu, L.-G. (2015). The calyx of Held in the auditory system: Structure, function, and development. *Hearing Research*, 338, 22–31. <https://doi.org/10.1016/j.heares.2016.03.009>
- Begum, R., Bakiri, Y., Volynski, K. E., & Kullmann, D. M. (2016). Action potential broadening in a presynaptic channelopathy. *Nature Communications*, 7(1), 12102. <https://doi.org/10.1038/ncomms12102>
- Beiderbeck, B., Myoga, M. H., Müller, N. I. C., Callan, A. R., Friauf, E., Grothe, B., & Pecka, M. (2018). Precisely timed inhibition facilitates action potential firing for spatial coding in the auditory brainstem. *Nature Communications*, 9(1), 1771. <https://doi.org/10.1038/s41467-018-04210-y>
- Benda, J. (2021). Neural adaptation. *Current Biology: CB*, 31(3), R110–R116. <https://doi.org/10.1016/j.cub.2020.11.054>
- Bloom, S., Williams, A., & MacLeod, K. M. (2014). Heterogeneous Calretinin Expression in the Avian Cochlear Nucleus Angularis. *Journal of the Association for Research in Otolaryngology*, 15(4), 603–620. <https://doi.org/10.1007/s10162-014-0453-0>
- Boord, R. L. (1961). The efferent cochlear bundle in the caiman and pigeon. *Experimental Neurology*, 3(3), 225–239. [https://doi.org/10.1016/0014-4886\(61\)90014-0](https://doi.org/10.1016/0014-4886(61)90014-0)

- Boord, R. L., & Rasmussen, G. L. (1963). Projection of the cochlear and lagenar nerves on the cochlear nuclei of the pigeon. *Journal of Comparative Neurology*, *120*(3), 463–475. <https://doi.org/10.1002/cne.901200305>
- Boudreau, J. C., & Tsuchitani, C. (1968). Binaural interaction in the cat superior olive S segment. *Journal of Neurophysiology*, *31*(3), 442–454. <https://doi.org/10.1152/jn.1968.31.3.442>
- Brand, A., Behrend, O., Marquardt, T., McAlpine, D., & Grothe, B. (2002). Precise inhibition is essential for microsecond interaural time difference coding. *Nature*, *417*(6888), 543–547. <https://doi.org/10.1038/417543a>
- Brenowitz, S., & Trussell, L. O. (2001). Maturation of Synaptic Transmission at End-Bulb Synapses of the Cochlear Nucleus. *The Journal of Neuroscience*, *21*(23), 9487–9498. <https://doi.org/10.1523/jneurosci.21-23-09487.2001>
- Brew, H., & Forsythe, I. (1995). Two voltage-dependent K<sup>+</sup> conductances with complementary functions in postsynaptic integration at a central auditory synapse. *The Journal of Neuroscience*, *15*(12), 8011–8022. <https://doi.org/10.1523/jneurosci.15-12-08011.1995>
- Brew, H. M., Hallows, J. L., & Tempel, B. L. (2003). Hyperexcitability and reduced low threshold potassium currents in auditory neurons of mice lacking the channel subunit Kv1.1. *The Journal of Physiology*, *548*(1), 1–20. <https://doi.org/10.1111/j.2003.t01-1-00001.x>
- Brown, D. A. (1988). M currents. *Ion Channels*, *1*, 55–94. [https://doi.org/10.1007/978-1-4615-7302-9\\_2](https://doi.org/10.1007/978-1-4615-7302-9_2)
- Brown, D. A., & Adams, P. R. (1980). Muscarinic suppression of a novel voltage-sensitive K<sup>+</sup> current in a vertebrate neurone. *Nature*, *283*(5748), 673–676. <https://doi.org/10.1038/283673a0>
- Brown, D. A., & Passmore, G. M. (2009). Neural KCNQ (Kv7) channels. *British Journal of Pharmacology*, *156*(8), 1185–1195. <https://doi.org/10.1111/j.1476-5381.2009.00111.x>
- Brown, D. H., & Hyson, R. L. (2019). Intrinsic physiological properties underlie auditory response diversity in the avian cochlear nucleus. *Journal of Neurophysiology*, *121*(3), 908–927. <https://doi.org/10.1152/jn.00459.2018>
- Brückner, S., & Hyson, R. L. (1998). Effect of GABA on the processing of interaural time differences in nucleus laminaris neurons in the chick. *European Journal of Neuroscience*, *10*(11), 3438–3450. <https://doi.org/10.1046/j.1460-9568.1998.00353.x>
- Burger, R. M., Cramer, K. S., Pfeiffer, J. D., & Rubel, E. W. (2005). Avian superior olivary nucleus provides divergent inhibitory input to parallel auditory pathways. *Journal of Comparative Neurology*, *481*(1), 6–18. <https://doi.org/10.1002/cne.20334>

- Burger, R. M., Forsythe, I. D., & Kopp-Scheinflug, C. (2015). Editorial: Inhibitory function in auditory processing. *Frontiers in Neural Circuits*, 9, 45. <https://doi.org/10.3389/fncir.2015.00045>
- Caird, D., & Klinke, R. (1983). Processing of binaural stimuli by cat superior olivary complex neurons. *Experimental Brain Research*, 52(3), 385–399. <https://doi.org/10.1007/bf00238032>
- Calvin, W. H. (1974). Three modes of repetitive firing and the role of threshold time course between spikes. *Brain Research*, 69(2), 341–346. [https://doi.org/10.1016/0006-8993\(74\)90012-2](https://doi.org/10.1016/0006-8993(74)90012-2)
- Camino, E., Garcia-Pino, E., Martinez-Galan, J. R., & Juiz, J. M. (2007). The potassium channel KCNQ5/Kv7.5 is localized in synaptic endings of auditory brainstem nuclei of the rat. *Journal of Comparative Neurology*, 505(4), 363–378. <https://doi.org/10.1002/cne.21497>
- Cant, N. B., & Gaston, K. C. (1982). Pathways connecting the right and left cochlear nuclei. *Journal of Comparative Neurology*, 212(3), 313–326. <https://doi.org/10.1002/cne.902120308>
- Cant, N. B., & Hyson, R. L. (1992). Projections from the lateral nucleus of the trapezoid body to the medial superior olivary nucleus in the gerbil. *Hearing Research*, 58(1), 26–34. [https://doi.org/10.1016/0378-5955\(92\)90005-8](https://doi.org/10.1016/0378-5955(92)90005-8)
- Cao, X.-J., & Oertel, D. (2010). Auditory nerve fibers excite targets through synapses that vary in convergence, strength, and short-term plasticity. *Journal of Neurophysiology*, 104(5), 2308–2320. <https://doi.org/10.1152/jn.00451.2010>
- Cao, X.-J., & Oertel, D. (2017). Genetic perturbations suggest a role of the resting potential in regulating the expression of the ion channels of the KCNA and HCN families in octopus cells of the ventral cochlear nucleus. *Hearing Research*, 345, 57–68. <https://doi.org/10.1016/j.heares.2017.01.001>
- Carr, C. E., & Boudreau, R. E. (1991). Central projections of auditory nerve fibers in the barn owl. *Journal of Comparative Neurology*, 314(2), 306–318. <https://doi.org/10.1002/cne.903140208>
- Carr, C. E., & Boudreau, R. E. (1993). Organization of the nucleus magnocellularis and the nucleus laminaris in the barn owl: Encoding and measuring interaural time differences. *Journal of Comparative Neurology*, 334(3), 337–355. <https://doi.org/10.1002/cne.903340302>
- Carr, C. E., Fujita, I., & Konishi, M. (1989). Distribution of GABAergic neurons and terminals in the auditory system of the barn owl. *Journal of Comparative Neurology*, 286(2), 190–207. <https://doi.org/10.1002/cne.902860205>
- Carr, C. E., & Soares, D. (2002). Evolutionary Convergence and Shared Computational Principles in the Auditory System. *Brain, Behavior and Evolution*, 59(5–6), 294–311. <https://doi.org/10.1159/000063565>

- Carr, C., & Konishi, M. (1990). A circuit for detection of interaural time differences in the brain stem of the barn owl. *The Journal of Neuroscience*, *10*(10), 3227–3246. <https://doi.org/10.1523/jneurosci.10-10-03227.1990>
- Carroll, B. J., Bertram, R., & Hyson, R. L. (2018). Intrinsic physiology of inhibitory neurons changes over auditory development. *Journal of Neurophysiology*, *119*(1), 290–304. <https://doi.org/10.1152/jn.00447.2017>
- Casparly, D. M., Backoff, P. M., Finlayson, P. G., & Palombi, P. S. (1994). Inhibitory inputs modulate discharge rate within frequency receptive fields of anteroventral cochlear nucleus neurons. *Journal of Neurophysiology*, *72*(5), 2124–2133. <https://doi.org/10.1152/jn.1994.72.5.2124>
- Casparly, D. M., Schattman, T. A., & Hughes, L. F. (2005). Age-Related Changes in the Inhibitory Response Properties of Dorsal Cochlear Nucleus Output Neurons: Role of Inhibitory Inputs. *The Journal of Neuroscience*, *25*(47), 10952–10959. <https://doi.org/10.1523/jneurosci.2451-05.2005>
- Chanda, S., & Xu-Friedman, M. A. (2010). Neuromodulation by GABA converts a relay into a coincidence detector. *Journal of Neurophysiology*, *104*(4), 2063–2074. <https://doi.org/10.1152/jn.00474.2010>
- Choudhury, N., Linley, D., Richardson, A., Anderson, M., Robinson, S. W., Marra, V., Ciampani, V., Walter, S. M., Kopp-Scheinflug, C., Steinert, J. R., & Forsythe, I. D. (2020). Kv3.1 and Kv3.3 subunits differentially contribute to Kv3 channels and action potential repolarization in principal neurons of the auditory brainstem. *The Journal of Physiology*, *598*(11), 2199–2222. <https://doi.org/10.1113/jp279668>
- Clack, J. A., & Anderson, J. S. (2016). Evolution of the Vertebrate Ear. *Springer Handbook of Auditory Research*, 71–105. [https://doi.org/10.1007/978-3-319-46661-3\\_4](https://doi.org/10.1007/978-3-319-46661-3_4)
- Code, R. A., & Rubel, E. W. (1989). Glycine-immunoreactivity in the auditory brain stem of the chick. *Hearing Research*, *40*(1–2), 167–172. [https://doi.org/10.1016/0378-5955\(89\)90109-3](https://doi.org/10.1016/0378-5955(89)90109-3)
- COETZEE, W. A., AMARILLO, Y., CHIU, J., CHOW, A., LAU, D., McCORMACK, T., MORENA, H., NADAL, M. S., OZAITA, A., POUNTNEY, D., SAGANICH, M., MIERA, E. V. D., & RUDY, B. (1999). Molecular Diversity of K<sup>+</sup> Channels. *Annals of the New York Academy of Sciences*, *868*(1), 233–255. <https://doi.org/10.1111/j.1749-6632.1999.tb11293.x>
- Colburn, H. S., Carney, L. H., & Heinz, M. G. (2003). Quantifying the Information in Auditory-Nerve Responses for Level Discrimination. *Journal of the Association for Research in Otolaryngology*, *4*(3), 294–311. <https://doi.org/10.1007/s10162-002-1090-6>
- Colburn, H. S., Yan-an, H., & Culotta, C. P. (1990). Coincidence model of MSO responses. *Hearing Research*, *49*(1–3), 335–346. [https://doi.org/10.1016/0378-5955\(90\)90112-3](https://doi.org/10.1016/0378-5955(90)90112-3)

- Coleman, W. L., Fischl, M. J., Weimann, S. R., & Burger, R. M. (2011). GABAergic and glycinergic inhibition modulate monaural auditory response properties in the avian superior olivary nucleus. *Journal of Neurophysiology*, *105*(5), 2405–2420. <https://doi.org/10.1152/jn.01088.2010>
- Cook, D. L., Schwindt, P. C., Grande, L. A., & Spain, W. J. (2003). Synaptic depression in the localization of sound. *Nature*, *421*(6918), 66–70. <https://doi.org/10.1038/nature01248>
- Corey, D., & Hudspeth, A. (1983). Kinetics of the receptor current in bullfrog saccular hair cells. *The Journal of Neuroscience*, *3*(5), 962–976. <https://doi.org/10.1523/jneurosci.03-05-00962.1983>
- Corey, D. P., & Hudspeth, A. J. (1979). Ionic basis of the receptor potential in a vertebrate hair cell. *Nature*, *281*(5733), 675–677. <https://doi.org/10.1038/281675a0>
- Couchman, K., Grothe, B., & Felmy, F. (2010). Medial Superior Olivary Neurons Receive Surprisingly Few Excitatory and Inhibitory Inputs with Balanced Strength and Short-Term Dynamics. *The Journal of Neuroscience*, *30*(50), 17111–17121. <https://doi.org/10.1523/jneurosci.1760-10.2010>
- Curry, R. J., & Lu, Y. (2016). Synaptic Inhibition in Avian Interaural Level Difference Sound Localizing Neurons. *ENeuro*, *3*(6), ENEURO.0309-16.2016. <https://doi.org/10.1523/eneuro.0309-16.2016>
- Dean, I., Harper, N. S., & McAlpine, D. (2005). Neural population coding of sound level adapts to stimulus statistics. *Nature Neuroscience*, *8*(12), 1684–1689. <https://doi.org/10.1038/nn1541>
- Dean, I., Robinson, B. L., Harper, N. S., & McAlpine, D. (2008). Rapid Neural Adaptation to Sound Level Statistics. *The Journal of Neuroscience*, *28*(25), 6430–6438. <https://doi.org/10.1523/jneurosci.0470-08.2008>
- Dehmel, S., Kopp-Scheinflug, C., Weick, M., Dörrscheidt, G. J., & Rübsamen, R. (2010). Transmission of phase-coupling accuracy from the auditory nerve to spherical bushy cells in the Mongolian gerbil. *Hearing Research*, *268*(1–2), 234–249. <https://doi.org/10.1016/j.heares.2010.06.005>
- Dijkstra, C. D. (2003). [The Nobel Prize in Chemistry 2003 awarded for discoveries concerning molecular channels in cell membranes]. *Nederlands Tijdschrift Voor Geneeskunde*, *147*(52), 2570–2572.
- Dodson, P. D., Barker, M. C., & Forsythe, I. D. (2002). Two Heteromeric Kv1 Potassium Channels Differentially Regulate Action Potential Firing. *The Journal of Neuroscience*, *22*(16), 6953–6961. <https://doi.org/10.1523/jneurosci.22-16-06953.2002>
- Dodson, P. D., Billups, B., Rusznák, Z., Szucs, G., Barker, M. C., & Forsythe, I. D. (2003). Presynaptic Rat Kv1.2 Channels Suppress Synaptic Terminal Hyperexcitability Following

- Action Potential Invasion. *The Journal of Physiology*, 550(1), 27–33.  
<https://doi.org/10.1113/jphysiol.2003.046250>
- Doyle, D. A., Cabral, J. M., Pfuetzner, R. A., Kuo, A., Gulbis, J. M., Cohen, S. L., Chait, B. T., & MacKinnon, R. (1998). The Structure of the Potassium Channel: Molecular Basis of K<sup>+</sup> Conduction and Selectivity. *Science*, 280(5360), 69–77.  
<https://doi.org/10.1126/science.280.5360.69>
- Drion, G., Bonjean, M., Waroux, O., Scuvée-Moreau, J., Liégeois, J., Sejnowski, T. J., Sepulchre, R., & Seutin, V. (2010). M-type channels selectively control bursting in rat dopaminergic neurons. *European Journal of Neuroscience*, 31(5), 827–835.  
<https://doi.org/10.1111/j.1460-9568.2010.07107.x>
- Dugue, P., Jeannes, R. L. B., & Faucon, G. (2007). Improving the Dynamics of Responses to Amplitude Modulated Stimuli by Modeling Inhibitory Interneurons in Cochlear Nucleus. *2007 29th Annual International Conference of the IEEE Engineering in Medicine and Biology Society*, 2007, 1286–1289. <https://doi.org/10.1109/iembs.2007.4352532>
- Eisenbach, S. L., Soueidan, S. E., & MacLeod, K. M. (2019). Presynaptic GABAergic receptors modulate inhibitory synaptic feedback in the avian cochlear nucleus angularis. *BioRxiv*, 619783. <https://doi.org/10.1101/619783>
- Erulkar, S. D. (1972). Comparative aspects of spatial localization of sound. *Physiological Reviews*, 52(1), 237–360. <https://doi.org/10.1152/physrev.1972.52.1.237>
- Escabi, C. D., Frye, M. D., Trevino, M., & Lobarinas, E. (2019). The rat animal model for noise-induced hearing loss. *The Journal of the Acoustical Society of America*, 146(5), 3692–3709.  
<https://doi.org/10.1121/1.5132553>
- Feldman, M. L., & Harrison, J. M. (1969). The projection of the acoustic nerve to the ventral cochlear nucleus of the rat. A Golgi study. *Journal of Comparative Neurology*, 137(3), 267–293. <https://doi.org/10.1002/cne.901370303>
- Feng, Y., Zhang, Q., Lu, X., Li, X., & Liu, W. (2023). Development of Neuronal Excitability of the Bushy Cells in Anteroventral Cochlear Nucleus of Rats. *Developmental Neuroscience*, 44(6), 566–575. <https://doi.org/10.1159/000526078>
- Ferragamo, M. J., Golding, N. L., & Oertel, D. (1998). Synaptic Inputs to Stellate Cells in the Ventral Cochlear Nucleus. *Journal of Neurophysiology*, 79(1), 51–63.  
<https://doi.org/10.1152/jn.1998.79.1.51>
- Fischer, F. P., Köppl, C., & Manley, G. A. (1988). The basilar papilla of the barn owl *Tyto alba*: A quantitative morphological SEM analysis. *Hearing Research*, 34(1), 87–101.  
[https://doi.org/10.1016/0378-5955\(88\)90053-6](https://doi.org/10.1016/0378-5955(88)90053-6)

- Fischl, M. J., Combs, T. D., Klug, A., Grothe, B., & Burger, R. M. (2012). Modulation of synaptic input by GABAB receptors improves coincidence detection for computation of sound location. *The Journal of Physiology*, *590*(13), 3047–3066. <https://doi.org/10.1113/jphysiol.2011.226233>
- Fischl, M. J., Weimann, S. R., Kears, M. G., & Burger, R. M. (2014). Slowly emerging glycinergic transmission enhances inhibition in the sound localization pathway of the avian auditory system. *Journal of Neurophysiology*, *111*(3), 565–572. <https://doi.org/10.1152/jn.00640.2013>
- Fontaine, B., MacLeod, K. M., Lubejko, S. T., Steinberg, L. J., Köppl, C., & Peña, J. L. (2014). Emergence of band-pass filtering through adaptive spiking in the owl's cochlear nucleus. *Journal of Neurophysiology*, *112*(2), 430–445. <https://doi.org/10.1152/jn.00132.2014>
- Franken, T. P., Roberts, M. T., Wei, L., Golding, N. L., & Joris, P. X. (2015). In vivo coincidence detection in mammalian sound localization generates phase delays. *Nature Neuroscience*, *18*(3), 444–452. <https://doi.org/10.1038/nn.3948>
- Frisina, R. D., Smith, R. L., & Chamberlain, S. C. (1990). Encoding of amplitude modulation in the gerbil cochlear nucleus: II. Possible neural mechanisms. *Hearing Research*, *44*(2–3), 123–141. [https://doi.org/10.1016/0378-5955\(90\)90075-z](https://doi.org/10.1016/0378-5955(90)90075-z)
- Fu, M., Zhang, L., Xie, X., Wang, N., & Xiao, Z. (2021). Differential contributions of voltage-gated potassium channel subunits in enhancing temporal coding in the bushy cells of the ventral cochlear nucleus. *Journal of Neurophysiology*, *125*(5), 1954–1972. <https://doi.org/10.1152/jn.00435.2020>
- Fuchs, P., Nagai, T., & Evans, M. (1988). Electrical tuning in hair cells isolated from the chick cochlea. *The Journal of Neuroscience*, *8*(7), 2460–2467. <https://doi.org/10.1523/jneurosci.08-07-02460.1988>
- Fukui, I., Burger, R. M., Ohmori, H., & Rubel, E. W. (2010). GABAergic inhibition sharpens the frequency tuning and enhances phase locking in chicken nucleus magnocellularis neurons. *The Journal of Neuroscience : The Official Journal of the Society for Neuroscience*, *30*(36), 12075–12083. <https://doi.org/10.1523/jneurosci.1484-10.2010>
- Fukui, I., & Ohmori, H. (2003). Developmental changes in membrane excitability and morphology of neurons in the nucleus angularis of the chicken. *The Journal of Physiology*, *548*(1), 219–232. <https://doi.org/10.1111/j.2003.t01-1-00219.x>
- Fukui, I., & Ohmori, H. (2004). Tonotopic gradients of membrane and synaptic properties for neurons of the chicken nucleus magnocellularis. *The Journal of Neuroscience : The Official Journal of the Society for Neuroscience*, *24*(34), 7514–7523. <https://doi.org/10.1523/jneurosci.0566-04.2004>

- Fukui, I., Sato, T., & Ohmori, H. (2006). Improvement of Phase Information at Low Sound Frequency in Nucleus Magnocellularis of the Chicken. *Journal of Neurophysiology*, *96*(2), 633–641. <https://doi.org/10.1152/jn.00916.2005>
- Funabiki, K., Ashida, G., & Konishi, M. (2011). Computation of Interaural Time Difference in the Owl's Coincidence Detector Neurons. *The Journal of Neuroscience*, *31*(43), 15245–15256. <https://doi.org/10.1523/jneurosci.2127-11.2011>
- Gabel, L. A., & Nisenbaum, E. S. (1998). Biophysical Characterization and Functional Consequences of a Slowly Inactivating Potassium Current in Neostriatal Neurons. *Journal of Neurophysiology*, *79*(4), 1989–2002. <https://doi.org/10.1152/jn.1998.79.4.1989>
- Gai, Y., & Carney, L. H. (2008). Influence of Inhibitory Inputs on Rate and Timing of Responses in the Anteroventral Cochlear Nucleus. *Journal of Neurophysiology*, *99*(3), 1077–1095. <https://doi.org/10.1152/jn.00708.2007>
- Garcia, M., & Favaro, L. (2017). Animal vocal communication: function, structures, and production mechanisms. *Current Zoology*, *63*(4), 417–419. <https://doi.org/10.1093/cz/zox040>
- Gazula, V., Strumbos, J. G., Mei, X., Chen, H., Rahner, C., & Kaczmarek, L. K. (2010). Localization of Kv1.3 channels in presynaptic terminals of brainstem auditory neurons. *Journal of Comparative Neurology*, *518*(16), 3205–3220. <https://doi.org/10.1002/cne.22393>
- Gittelman, J. X., & Tempel, B. L. (2006). Kv1.1-Containing Channels Are Critical for Temporal Precision During Spike Initiation. *Journal of Neurophysiology*, *96*(3), 1203–1214. <https://doi.org/10.1152/jn.00092.2005>
- Glazebrook, P. A., Ramirez, A. N., Schild, J. H., Shieh, C., Doan, T., Wible, B. A., & Kunze, D. L. (2002). Potassium channels Kv1.1, Kv1.2 and Kv1.6 influence excitability of rat visceral sensory neurons. *The Journal of Physiology*, *541*(2), 467–482. <https://doi.org/10.1113/jphysiol.2001.018333>
- Goldberg, E. M., Clark, B. D., Zagha, E., Nahmani, M., Erisir, A., & Rudy, B. (2008). K<sup>+</sup> Channels at the Axon Initial Segment Dampen Near-Threshold Excitability of Neocortical Fast-Spiking GABAergic Interneurons. *Neuron*, *58*(3), 387–400. <https://doi.org/10.1016/j.neuron.2008.03.003>
- Golding, N. L., & Oertel, D. (2012). Synaptic integration in dendrites: exceptional need for speed. *The Journal of Physiology*, *590*(22), 5563–5569. <https://doi.org/10.1113/jphysiol.2012.229328>
- Grigg, J. J., Brew, H. M., & Tempel, B. L. (2000). Differential expression of voltage-gated potassium channel genes in auditory nuclei of the mouse brainstem. *Hearing Research*, *140*(1–2), 77–90. [https://doi.org/10.1016/s0378-5955\(99\)00187-2](https://doi.org/10.1016/s0378-5955(99)00187-2)

- Grothe, B., & Pecka, M. (2014). The natural history of sound localization in mammals – a story of neuronal inhibition. *Frontiers in Neural Circuits*, 8, 116. <https://doi.org/10.3389/fncir.2014.00116>
- Grothe, B., & Sanes, D. (1994). Synaptic inhibition influences the temporal coding properties of medial superior olivary neurons: an in vitro study. *The Journal of Neuroscience*, 14(3), 1701–1709. <https://doi.org/10.1523/jneurosci.14-03-01701.1994>
- Hackett, J. T., Jackson, H., & Rubel, E. W. (1982). Synaptic excitation of the second and third order auditory neurons in the avian brain stem. *Neuroscience*, 7(6), 1455–1469. [https://doi.org/10.1016/0306-4522\(82\)90257-3](https://doi.org/10.1016/0306-4522(82)90257-3)
- Hamlet, W. R., Liu, Y.-W., Tang, Z.-Q., & Lu, Y. (2014). Interplay between low threshold voltage-gated K<sup>+</sup> channels and synaptic inhibition in neurons of the chicken nucleus laminaris along its frequency axis. *Frontiers in Neural Circuits*, 8, 51. <https://doi.org/10.3389/fncir.2014.00051>
- Hansen, H. H., Waroux, O., Seutin, V., Jentsch, T. J., Aznar, S., & Mikkelsen, J. D. (2008). Kv7 channels: interaction with dopaminergic and serotonergic neurotransmission in the CNS. *The Journal of Physiology*, 586(7), 1823–1832. <https://doi.org/10.1113/jphysiol.2007.149450>
- Heller, S., Bell, A. M., Denis, C. S., Choe, Y., & Hudspeth, A. J. (2002). Parvalbumin 3 is an Abundant Ca<sup>2+</sup> Buffer in Hair Cells. *Journal of the Association for Research in Otolaryngology*, 3(4), 488–498. <https://doi.org/10.1007/s10162-002-2050-x>
- Higgs, M. H., Slee, S. J., & Spain, W. J. (2006). Diversity of Gain Modulation by Noise in Neocortical Neurons: Regulation by the Slow Afterhyperpolarization Conductance. *The Journal of Neuroscience*, 26(34), 8787–8799. <https://doi.org/10.1523/jneurosci.1792-06.2006>
- Higgs, M. H., & Spain, W. J. (2011). Kv1 channels control spike threshold dynamics and spike timing in cortical pyramidal neurones. *The Journal of Physiology*, 589(21), 5125–5142. <https://doi.org/10.1113/jphysiol.2011.216721>
- Hill, K. G., Mo, J., & Stange, G. (1989). Excitation and suppression of primary auditory fibres in the pigeon. *Hearing Research*, 39(1–2), 37–48. [https://doi.org/10.1016/0378-5955\(89\)90080-4](https://doi.org/10.1016/0378-5955(89)90080-4)
- Hirsch, J. A., & Oertel, D. (1988). Synaptic connections in the dorsal cochlear nucleus of mice, in vitro. *The Journal of Physiology*, 396(1), 549–562. <https://doi.org/10.1113/jphysiol.1988.sp016977>
- Hodgkin, A. L. (1948). The local electric changes associated with repetitive action in a non-medullated axon. *The Journal of Physiology*, 107(2), 165–181. <https://doi.org/10.1113/jphysiol.1948.sp004260>

- Hodgkin, A. L., & Huxley, A. F. (1952a). A quantitative description of membrane current and its application to conduction and excitation in nerve. *The Journal of Physiology*, *117*(4), 500–544. <https://doi.org/10.1113/jphysiol.1952.sp004764>
- Hodgkin, A. L., & Huxley, A. F. (1952b). The dual effect of membrane potential on sodium conductance in the giant axon of Loligo. *The Journal of Physiology*, *116*(4), 497–506. <https://doi.org/10.1113/jphysiol.1952.sp004719>
- Hong, H., Rollman, L., Feinstein, B., & Sanchez, J. T. (2016). Developmental Profile of Ion Channel Specializations in the Avian Nucleus Magnocellularis. *Frontiers in Cellular Neuroscience*, *10*, 80. <https://doi.org/10.3389/fncel.2016.00080>
- Hong, H., & Sanchez, J. T. (2018). Need for Speed and Precision: Structural and Functional Specialization in the Cochlear Nucleus of the Avian Auditory System. *Journal of Experimental Neuroscience*, *12*, 1179069518815628. <https://doi.org/10.1177/1179069518815628>
- Hong, H., Wang, X., Lu, T., Zorio, D. A. R., Wang, Y., & Sanchez, J. T. (2018). Diverse Intrinsic Properties Shape Functional Phenotype of Low-Frequency Neurons in the Auditory Brainstem. *Frontiers in Cellular Neuroscience*, *12*, 175. <https://doi.org/10.3389/fncel.2018.00175>
- Houtsma, A. J., Durlach, N. I., & Braida, L. D. (1980). Intensity perception XI. Experimental results on the relation of intensity resolution to loudness matching. *The Journal of the Acoustical Society of America*, *68*(3), 807–813. <https://doi.org/10.1121/1.384819>
- Howard, M. A., Burger, R. M., & Rubel, E. W. (2007). A developmental switch to GABAergic inhibition dependent on increases in Kv1-type K<sup>+</sup> currents. *The Journal of Neuroscience : The Official Journal of the Society for Neuroscience*, *27*(8), 2112–2123. <https://doi.org/10.1523/jneurosci.5266-06.2007>
- Howard, M. A., & Rubel, E. W. (2010). Dynamic Spike Thresholds during Synaptic Integration Preserve and Enhance Temporal Response Properties in the Avian Cochlear Nucleus. *The Journal of Neuroscience*, *30*(36), 12063–12074. <https://doi.org/10.1523/jneurosci.1840-10.2010>
- Huang, C., Resnik, A., Celikel, T., & Englitz, B. (2016). Adaptive Spike Threshold Enables Robust and Temporally Precise Neuronal Encoding. *PLoS Computational Biology*, *12*(6), e1004984. <https://doi.org/10.1371/journal.pcbi.1004984>
- Hudspeth, A. J. (1983). The Hair Cells of the Inner Ear. *Scientific American*, *248*(1), 54–64. <https://doi.org/10.1038/scientificamerican0183-54>
- II, R. A. F., Gourévitch, B., Gómez-Álvarez, M., Leijon, S. C. M., Saldaña, E., & Magnusson, A. K. (2017). Octopus Cells in the Posteroventral Cochlear Nucleus Provide the Main Excitatory

- Input to the Superior Paraolivary Nucleus. *Frontiers in Neural Circuits*, 11, 37. <https://doi.org/10.3389/fncir.2017.00037>
- Irie, T. (2021). Essential Role of Somatic Kv2 Channels in High-Frequency Firing in Cartwheel Cells of the Dorsal Cochlear Nucleus. *ENeuro*, 8(3), ENEURO.0515-20.2021. <https://doi.org/10.1523/eneuro.0515-20.2021>
- Jackson, H., & Parks, T. (1982). Functional synapse elimination in the developing avian cochlear nucleus with simultaneous reduction in cochlear nerve axon branching. *The Journal of Neuroscience*, 2(12), 1736–1743. <https://doi.org/10.1523/jneurosci.02-12-01736.1982>
- Jadi, M., Polsky, A., Schiller, J., & Mel, B. W. (2012). Location-Dependent Effects of Inhibition on Local Spiking in Pyramidal Neuron Dendrites. *PLoS Computational Biology*, 8(6), e1002550. <https://doi.org/10.1371/journal.pcbi.1002550>
- Jan, L. Y., & Jan, Y. N. (2012). Voltage-gated potassium channels and the diversity of electrical signalling. *The Journal of Physiology*, 590(11), 2591–2599. <https://doi.org/10.1113/jphysiol.2011.224212>
- Jeffress, L. A. (1948). A place theory of sound localization. *Journal of Comparative and Physiological Psychology*, 41(1), 35–39. <https://doi.org/10.1037/h0061495>
- Jentsch, T. J. (2000). Neuronal KCNQ potassium channels: physiology and role in disease. *Nature Reviews. Neuroscience*, 1(1), 21–30. <https://doi.org/10.1038/35036198>
- Jhaveri, S., & Morest, D. K. (1982). Sequential alterations of neuronal architecture in nucleus magnocellularis of the developing chicken: A golgi study. *Neuroscience*, 7(4), 837–853. [https://doi.org/10.1016/0306-4522\(82\)90046-x](https://doi.org/10.1016/0306-4522(82)90046-x)
- Johnson, B., Leek, A. N., & Tamkun, M. M. (2019). Kv2 channels create endoplasmic reticulum / plasma membrane junctions: a brief history of Kv2 channel subcellular localization. *Channels*, 13(1), 88–101. <https://doi.org/10.1080/19336950.2019.1568824>
- Johnston, J. (2021). Pharmacology of A-Type K<sup>+</sup> Channels. *Handbook of Experimental Pharmacology*, 267, 167–183. [https://doi.org/10.1007/164\\_2021\\_456](https://doi.org/10.1007/164_2021_456)
- Johnston, J., Forsythe, I. D., & Kopp-Scheinflug, C. (2010). Going native: voltage-gated potassium channels controlling neuronal excitability. *The Journal of Physiology*, 588(Pt 17), 3187–3200. <https://doi.org/10.1113/jphysiol.2010.191973>
- Johnston, J., Griffin, S. J., Baker, C., & Forsythe, I. D. (2008). Kv4 (A-type) potassium currents in the mouse medial nucleus of the trapezoid body. *European Journal of Neuroscience*, 27(6), 1391–1399. <https://doi.org/10.1111/j.1460-9568.2008.06116.x>
- Johnston, J., Griffin, S. J., Baker, C., Skrzypiec, A., Chernova, T., & Forsythe, I. D. (2008). Initial segment Kv2.2 channels mediate a slow delayed rectifier and maintain high frequency

- action potential firing in medial nucleus of the trapezoid body neurons. *The Journal of Physiology*, 586(14), 3493–3509. <https://doi.org/10.1113/jphysiol.2008.153734>
- Joris, P. X., Carney, L. H., Smith, P. H., & Yin, T. C. (1994). Enhancement of neural synchronization in the anteroventral cochlear nucleus. I. Responses to tones at the characteristic frequency. *Journal of Neurophysiology*, 71(3), 1022–1036. <https://doi.org/10.1152/jn.1994.71.3.1022>
- Joris, P. X., Louage, D. H., Cardoen, L., & Heijden, M. van der. (2006). Correlation Index: A new metric to quantify temporal coding. *Hearing Research*, 216, 19–30. <https://doi.org/10.1016/j.heares.2006.03.010>
- Kale, S., & Heinz, M. G. (2010). Envelope Coding in Auditory Nerve Fibers Following Noise-Induced Hearing Loss. *Journal of the Association for Research in Otolaryngology*, 11(4), 657–673. <https://doi.org/10.1007/s10162-010-0223-6>
- Kalluri, S., & Delgutte, B. (2003). Mathematical Models of Cochlear Nucleus Onset Neurons: I. Point Neuron with Many Weak Synaptic Inputs. *Journal of Computational Neuroscience*, 14(1), 71–90. <https://doi.org/10.1023/a:1021128418615>
- Karcz, A., Hennig, M. H., Robbins, C. A., Tempel, B. L., Rübsamen, R., & Kopp-Scheinpflug, C. (2011). Low-voltage activated Kv1.1 subunits are crucial for the processing of sound source location in the lateral superior olive in mice. *The Journal of Physiology*, 589(5), 1143–1157. <https://doi.org/10.1113/jphysiol.2010.203331>
- Karten, H. J. (1967). The organization of the ascending auditory pathway in the pigeon (*Columba livia*) I. Diencephalic projections of the inferior colliculus (nucleus mesencephali lateralis, pars dorsalis). *Brain Research*, 6(3), 409–427. [https://doi.org/10.1016/0006-8993\(67\)90055-8](https://doi.org/10.1016/0006-8993(67)90055-8)
- Keine, C., & Rübsamen, R. (2015). Inhibition Shapes Acoustic Responsiveness in Spherical Bushy Cells. *The Journal of Neuroscience*, 35(22), 8579–8592. <https://doi.org/10.1523/jneurosci.0133-15.2015>
- Keine, C., Rübsamen, R., & Englitz, B. (2016). Inhibition in the auditory brainstem enhances signal representation and regulates gain in complex acoustic environments. *ELife*, 5, e19295. <https://doi.org/10.7554/elife.19295>
- Kharkovets, T., Dedek, K., Maier, H., Schweizer, M., Khimich, D., Nouvian, R., Vardanyan, V., Leuwer, R., Moser, T., & Jentsch, T. J. (2006). Mice with altered KCNQ4 K<sup>+</sup> channels implicate sensory outer hair cells in human progressive deafness. *The EMBO Journal*, 25(3), 642–652. <https://doi.org/10.1038/sj.emboj.7600951>
- Khubieh, A., Ratté, S., Lankarany, M., & Prescott, S. A. (2016). Regulation of Cortical Dynamic Range by Background Synaptic Noise and Feedforward Inhibition. *Cerebral Cortex*, 26(8), 3357–3369. <https://doi.org/10.1093/cercor/bhv157>

- Khurana, S., Liu, Z., Lewis, A. S., Rosa, K., Chetkovich, D., & Golding, N. L. (2012). An Essential Role for Modulation of Hyperpolarization-Activated Current in the Development of Binaural Temporal Precision. *The Journal of Neuroscience*, *32*(8), 2814–2823. <https://doi.org/10.1523/jneurosci.3882-11.2012>
- Khurana, S., Remme, M. W. H., Rinzel, J., & Golding, N. L. (2011). Dynamic Interaction of Ih and IK-LVA during Trains of Synaptic Potentials in Principal Neurons of the Medial Superior Olive. *The Journal of Neuroscience*, *31*(24), 8936–8947. <https://doi.org/10.1523/jneurosci.1079-11.2011>
- Kim, Y., & Trussell, L. O. (2007). Ion Channels Generating Complex Spikes in Cartwheel Cells of the Dorsal Cochlear Nucleus. *Journal of Neurophysiology*, *97*(2), 1705–1725. <https://doi.org/10.1152/jn.00536.2006>
- Kirk, E. C., & Smith, D. W. (2003). Protection from Acoustic Trauma Is Not a Primary Function of the Medial Olivocochlear Efferent System. *Journal of the Association for Research in Otolaryngology*, *4*(4), 445–465. <https://doi.org/10.1007/s10162-002-3013-y>
- Klug, A., & Trussell, L. O. (2006). Activation and Deactivation of Voltage-Dependent K<sup>+</sup> Channels During Synaptically Driven Action Potentials in the MNTB. *Journal of Neurophysiology*, *96*(3), 1547–1555. <https://doi.org/10.1152/jn.01381.2005>
- Kobayashi, R., & Kitano, K. (2016). Impact of slow K<sup>+</sup> currents on spike generation can be described by an adaptive threshold model. *Journal of Computational Neuroscience*, *40*(3), 347–362. <https://doi.org/10.1007/s10827-016-0601-0>
- Kolston, J., Osen, K. K., Hackney, C. M., Ottersen, O. P., & Storm-Mathisen, J. (1992). An atlas of glycine- and GABA-like immunoreactivity and colocalization in the cochlear nuclear complex of the guinea pig. *Anatomy and Embryology*, *186*(5), 443–465. <https://doi.org/10.1007/bf00185459>
- König, P., Engel, A. K., & Singer, W. (1996). Integrator or coincidence detector? The role of the cortical neuron revisited. *Trends in Neurosciences*, *19*(4), 130–137. [https://doi.org/10.1016/s0166-2236\(96\)80019-1](https://doi.org/10.1016/s0166-2236(96)80019-1)
- Konishi, M., Sullivan, W. E., & Takahashi, T. (1985). The owl's cochlear nuclei process different sound localization cues. *The Journal of the Acoustical Society of America*, *78*(1 Pt 2), 360–364. <https://doi.org/10.1121/1.392499>
- Köppl, C. (1997a). Frequency Tuning and Spontaneous Activity in the Auditory Nerve and Cochlear Nucleus Magnocellularis of the Barn Owl *Tyto alba*. *Journal of Neurophysiology*, *77*(1), 364–377. <https://doi.org/10.1152/jn.1997.77.1.364>
- Köppl, C. (1997b). Phase Locking to High Frequencies in the Auditory Nerve and Cochlear Nucleus Magnocellularis of the Barn Owl, *Tyto alba*. *The Journal of Neuroscience*, *17*(9), 3312–3321. <https://doi.org/10.1523/jneurosci.17-09-03312.1997>

- Köppl, C. (2001). Tonotopic projections of the auditory nerve to the cochlear nucleus angularis in the barn owl. *Journal of the Association for Research in Otolaryngology : JARO*, 2(1), 41–53. <https://doi.org/10.1007/s101620010027>
- Köppl, C., & Carr, C. E. (2003). Computational Diversity in the Cochlear Nucleus Angularis of the Barn Owl. *Journal of Neurophysiology*, 89(4), 2313–2329. <https://doi.org/10.1152/jn.00635.2002>
- Kopp-Scheinflug, C., Dehmel, S., Dörrscheidt, G. J., & Rübsamen, R. (2002). Interaction of Excitation and Inhibition in Anteroventral Cochlear Nucleus Neurons That Receive Large Endbulb Synaptic Endings. *The Journal of Neuroscience*, 22(24), 11004–11018. <https://doi.org/10.1523/jneurosci.22-24-11004.2002>
- Kopp-Scheinflug, C., Fuchs, K., Lippe, W. R., Tempel, B. L., & Rübsamen, R. (2003). Decreased temporal precision of auditory signaling in Kcna1-null mice: an electrophysiological study in vivo. *The Journal of Neuroscience : The Official Journal of the Society for Neuroscience*, 23(27), 9199–9207.
- Koyama, S., & Appel, S. B. (2006). Characterization of M-Current in Ventral Tegmental Area Dopamine Neurons. *Journal of Neurophysiology*, 96(2), 535–543. <https://doi.org/10.1152/jn.00574.2005>
- Koyano, K., Funabiki, K., & Ohmori, H. (1996). Voltage-gated ionic currents and their roles in timing coding in auditory neurons of the nucleus magnocellularis of the chick. *Neuroscience Research*, 26(1), 29–45. [https://doi.org/10.1016/0168-0102\(96\)01071-1](https://doi.org/10.1016/0168-0102(96)01071-1)
- Kreeger, L. J., Arshed, A., & MacLeod, K. M. (2012). Intrinsic firing properties in the avian auditory brain stem allow both integration and encoding of temporally modulated noisy inputs in vitro. *Journal of Neurophysiology*, 108(10), 2794–2809. <https://doi.org/10.1152/jn.00092.2012>
- Kros, C. J., Ruppersberg, J. P., & Rüsç, A. (1998). Expression of a potassium current in inner hair cells during development of hearing in mice. *Nature*, 394(6690), 281–284. <https://doi.org/10.1038/28401>
- Kuba, H. (2007). Cellular and molecular mechanisms of avian auditory coincidence detection. *Neuroscience Research*, 59(4), 370–376. <https://doi.org/10.1016/j.neures.2007.08.003>
- Kuba, H., Koyano, K., & Ohmori, H. (2002a). Development of membrane conductance improves coincidence detection in the nucleus laminaris of the chicken. *The Journal of Physiology*, 540(2), 529–542. <https://doi.org/10.1113/jphysiol.2001.013365>
- Kuba, H., Koyano, K., & Ohmori, H. (2002b). Synaptic depression improves coincidence detection in the nucleus laminaris in brainstem slices of the chick embryo. *European Journal of Neuroscience*, 15(6), 984–990. <https://doi.org/10.1046/j.1460-9568.2002.01933.x>

- Kuba, H., Yamada, R., Fukui, I., & Ohmori, H. (2005). Tonotopic Specialization of Auditory Coincidence Detection in Nucleus Laminaris of the Chick. *The Journal of Neuroscience*, 25(8), 1924–1934. <https://doi.org/10.1523/jneurosci.4428-04.2005>
- Kuba, H., Yamada, R., Ishiguro, G., & Adachi, R. (2015). Redistribution of Kv1 and Kv7 enhances neuronal excitability during structural axon initial segment plasticity. *Nature Communications*, 6(1), 8815. <https://doi.org/10.1038/ncomms9815>
- Kubisch, C., Schroeder, B. C., Friedrich, T., Lütjohann, B., El-Amraoui, A., Marlin, S., Petit, C., & Jentsch, T. J. (1999). KCNQ4, a Novel Potassium Channel Expressed in Sensory Outer Hair Cells, Is Mutated in Dominant Deafness. *Cell*, 96(3), 437–446. [https://doi.org/10.1016/s0092-8674\(00\)80556-5](https://doi.org/10.1016/s0092-8674(00)80556-5)
- Kubke, M. F., & Carr, C. E. (1998). Development of AMPA-selective glutamate receptors in the auditory brainstem of the barn owl. *Microscopy Research and Technique*, 41(3), 176–186. [https://doi.org/10.1002/\(sici\)1097-0029\(19980501\)41:3<176::aid-jemt2>3.0.co;2-s](https://doi.org/10.1002/(sici)1097-0029(19980501)41:3<176::aid-jemt2>3.0.co;2-s)
- Kuenzel, T., Borst, J. G. G., & Heijden, M. van der. (2011). Factors controlling the input-output relationship of spherical bushy cells in the gerbil cochlear nucleus. *The Journal of Neuroscience : The Official Journal of the Society for Neuroscience*, 31(11), 4260–4273. <https://doi.org/10.1523/jneurosci.5433-10.2011>
- Kuo, S. P., Bradley, L. A., & Trussell, L. O. (2009). Heterogeneous kinetics and pharmacology of synaptic inhibition in the chick auditory brainstem. *The Journal of Neuroscience : The Official Journal of the Society for Neuroscience*, 29(30), 9625–9634. <https://doi.org/10.1523/jneurosci.0103-09.2009>
- Kuo, S. P., Lu, H.-W., & Trussell, L. O. (2012). Intrinsic and synaptic properties of vertical cells of the mouse dorsal cochlear nucleus. *Journal of Neurophysiology*, 108(4), 1186–1198. <https://doi.org/10.1152/jn.00778.2011>
- Kuwabara, N., & Zook, J. M. (1992). Projections to the medial superior olive from the medial and lateral nuclei of the trapezoid body in rodents and bats. *The Journal of Comparative Neurology*, 324(4), 522–538. <https://doi.org/10.1002/cne.903240406>
- Kuznetsova, M. S., Higgs, M. H., & Spain, W. J. (2008). Adaptation of Firing Rate and Spike-Timing Precision in the Avian Cochlear Nucleus. *The Journal of Neuroscience*, 28(46), 11906–11915. <https://doi.org/10.1523/jneurosci.3827-08.2008>
- Kyweriga, M., Stewart, W., Cahill, C., & Wehr, M. (2014). Synaptic mechanisms underlying interaural level difference selectivity in rat auditory cortex. *Journal of Neurophysiology*, 112(10), 2561–2571. <https://doi.org/10.1152/jn.00389.2014>
- Lachica, E. A., Rübsamen, R., & Rubel, E. W. (1994). GABAergic terminals in nucleus magnocellularis and laminaris originate from the superior olivary nucleus. *The Journal of Comparative Neurology*, 348(3), 403–418. <https://doi.org/10.1002/cne.903480307>

- Levin, M. D., Kubke, M. F., Schneider, M., Wenthold, R., & Carr, C. E. (1997). Localization of AMPA-selective glutamate receptors in the auditory brainstem of the barn owl. *Journal of Comparative Neurology*, 378(2), 239–253. [https://doi.org/10.1002/\(sici\)1096-9861\(19970210\)378:2<239::aid-cne7>3.0.co;2-4](https://doi.org/10.1002/(sici)1096-9861(19970210)378:2<239::aid-cne7>3.0.co;2-4)
- Lieberman, M. C. (1982). Single-Neuron Labeling in the Cat Auditory Nerve. *Science*, 216(4551), 1239–1241. <https://doi.org/10.1126/science.7079757>
- Lu, Y., Burger, R. M., & Rubel, E. W. (2005). GABAB Receptor Activation Modulates GABAA Receptor-Mediated Inhibition in Chicken Nucleus Magnocellularis Neurons. *Journal of Neurophysiology*, 93(3), 1429–1438. <https://doi.org/10.1152/jn.00786.2004>
- Lu, Y., Monsivais, P., Tempel, B. L., & Rubel, E. W. (2004). Activity-dependent regulation of the potassium channel subunits Kv1.1 and Kv3.1. *Journal of Comparative Neurology*, 470(1), 93–106. <https://doi.org/10.1002/cne.11037>
- Lubejko, S. T., Fontaine, B., Soueidan, S. E., & MacLeod, K. M. (2019). Spike threshold adaptation diversifies neuronal operating modes in the auditory brain stem. *Journal of Neurophysiology*, 122(6), 2576–2590. <https://doi.org/10.1152/jn.00234.2019>
- Lundstrom, B. N., Famulare, M., Sorensen, L. B., Spain, W. J., & Fairhall, A. L. (2009). Sensitivity of firing rate to input fluctuations depends on time scale separation between fast and slow variables in single neurons. *Journal of Computational Neuroscience*, 27(2), 277–290. <https://doi.org/10.1007/s10827-009-0142-x>
- MacLeod, K. M., & Carr, C. E. (2005). Synaptic Physiology in the Cochlear Nucleus Angularis of the Chick. *Journal of Neurophysiology*, 93(5), 2520–2529. <https://doi.org/10.1152/jn.00898.2004>
- MacLeod, K. M., & Carr, C. E. (2007). Beyond timing in the auditory brainstem: intensity coding in the avian cochlear nucleus angularis. *Progress in Brain Research*, 165, 123–133. [https://doi.org/10.1016/s0079-6123\(06\)65008-5](https://doi.org/10.1016/s0079-6123(06)65008-5)
- MacLeod, K. M., & Pandya, S. (2022). Expression and Neurotransmitter Association of the Synaptic Calcium Sensor Synaptotagmin in the Avian Auditory Brain Stem. *Journal of the Association for Research in Otolaryngology*, 23(6), 701–720. <https://doi.org/10.1007/s10162-022-00863-1>
- Mainen, Z. F., & Sejnowski, T. J. (1995). Reliability of Spike Timing in Neocortical Neurons. *Science*, 268(5216), 1503–1506. <https://doi.org/10.1126/science.7770778>
- Mancilla, J. G., & Manis, P. B. (2009). Two Distinct Types of Inhibition Mediated by Cartwheel Cells in the Dorsal Cochlear Nucleus. *Journal of Neurophysiology*, 102(2), 1287–1295. <https://doi.org/10.1152/jn.91272.2008>

- Manis, P. B., Kasten, M. R., & Xie, R. (2019). Classification of neurons in the adult mouse cochlear nucleus: Linear discriminant analysis. *PLoS ONE*, *14*(10), e0223137. <https://doi.org/10.1371/journal.pone.0223137>
- Manis, P. B., Spirou, G. A., Wright, D. D., Paydar, S., & Ryvgo, D. K. (1994). Physiology and morphology of complex spiking neurons in the guinea pig dorsal cochlear nucleus. *Journal of Comparative Neurology*, *348*(2), 261–276. <https://doi.org/10.1002/cne.903480208>
- Manis, P., & Marx, S. (1991). Outward currents in isolated ventral cochlear nucleus neurons. *The Journal of Neuroscience*, *11*(9), 2865–2880. <https://doi.org/10.1523/jneurosci.11-09-02865.1991>
- Manley, G. A. (2017). Comparative Auditory Neuroscience: Understanding the Evolution and Function of Ears. *Journal of the Association for Research in Otolaryngology*, *18*(1), 1–24. <https://doi.org/10.1007/s10162-016-0579-3>
- Manley, G. A., Kaiser, A., Brix, J., & Gleich, O. (1991). Activity patterns of primary auditory-nerve fibres in chickens: Development of fundamental properties. *Hearing Research*, *57*(1), 1–15. [https://doi.org/10.1016/0378-5955\(91\)90068-k](https://doi.org/10.1016/0378-5955(91)90068-k)
- Manley, G., Koppl, C., & Konishi, M. (1988). A neural map of interaural intensity differences in the brain stem of the barn owl. *The Journal of Neuroscience*, *8*(8), 2665–2676. <https://doi.org/10.1523/jneurosci.08-08-02665.1988>
- Matthews, G., & Fuchs, P. (2010). The diverse roles of ribbon synapses in sensory neurotransmission. *Nature Reviews Neuroscience*, *11*(12), 812–822. <https://doi.org/10.1038/nrn2924>
- McGinley, M. J., & Oertel, D. (2006). Rate thresholds determine the precision of temporal integration in principal cells of the ventral cochlear nucleus. *Hearing Research*, *216*, 52–63. <https://doi.org/10.1016/j.heares.2006.02.006>
- Mensi, S., Hagens, O., Gerstner, W., & Pozzorini, C. (2016). Enhanced Sensitivity to Rapid Input Fluctuations by Nonlinear Threshold Dynamics in Neocortical Pyramidal Neurons. *PLoS Computational Biology*, *12*(2), e1004761. <https://doi.org/10.1371/journal.pcbi.1004761>
- Middleton, J. W., Kiritani, T., Pedersen, C., Turner, J. G., Shepherd, G. M. G., & Tzounopoulos, T. (2011). Mice with behavioral evidence of tinnitus exhibit dorsal cochlear nucleus hyperactivity because of decreased GABAergic inhibition. *Proceedings of the National Academy of Sciences*, *108*(18), 7601–7606. <https://doi.org/10.1073/pnas.1100223108>
- Miller, C. T., Hale, M. E., Okano, H., Okabe, S., & Mitra, P. (2018). Comparative Principles for Next-Generation Neuroscience. *Frontiers in Behavioral Neuroscience*, *13*, 12. <https://doi.org/10.3389/fnbeh.2019.00012>

- Mogdans, J., & Knudsen, E. I. (1994). Site of auditory plasticity in the brain stem (VLVp) of the owl revealed by early monaural occlusion. *Journal of Neurophysiology*, 72(6), 2875–2891. <https://doi.org/10.1152/jn.1994.72.6.2875>
- Moiseff, A., & Konishi, M. (1983). Binaural characteristics of units in the owl's brainstem auditory pathway: precursors of restricted spatial receptive fields. *The Journal of Neuroscience*, 3(12), 2553–2562. <https://doi.org/10.1523/jneurosci.03-12-02553.1983>
- Monsivais, P., & Rubel, E. W. (2001). Accommodation Enhances Depolarizing Inhibition in Central Neurons. *The Journal of Neuroscience*, 21(19), 7823–7830. <https://doi.org/10.1523/jneurosci.21-19-07823.2001>
- Monsivais, P., Yang, L., & Rubel, E. W. (2000). GABAergic Inhibition in Nucleus Magnocellularis: Implications for Phase Locking in the Avian Auditory Brainstem. *The Journal of Neuroscience*, 20(8), 2954–2963. <https://doi.org/10.1523/jneurosci.20-08-02954.2000>
- Moran, O., & Conti, F. (1995). Properties of the Kv1.1 Rat Brain Potassium Channels Expressed in Mammalian Cells: Temperature Effects. *Biochemical and Biophysical Research Communications*, 215(3), 915–920. <https://doi.org/10.1006/bbrc.1995.2551>
- Müller, M., Smolders, J. W. T., Ding-Pfennigdorff, D., & Klünke, R. (1997). Discharge properties of pigeon single auditory nerve fibers after recovery from severe acoustic trauma. *International Journal of Developmental Neuroscience*, 15(4–5), 401–416. [https://doi.org/10.1016/s0736-5748\(96\)00100-1](https://doi.org/10.1016/s0736-5748(96)00100-1)
- Myoga, M. H., Lehnert, S., Leibold, C., Felmy, F., & Grothe, B. (2014). Glycinergic inhibition tunes coincidence detection in the auditory brainstem. *Nature Communications*, 5(1), 3790. <https://doi.org/10.1038/ncomms4790>
- Nakajo, K., & Kasuya, G. (2024). Modulation of potassium channels by transmembrane auxiliary subunits via voltage-sensing domains. *Physiological Reports*, 12(6), e15980. <https://doi.org/10.14814/phy2.15980>
- Needham, K., & Paolini, A. G. (2003). Fast Inhibition Underlies the Transmission of Auditory Information between Cochlear Nuclei. *The Journal of Neuroscience*, 23(15), 6357–6361. <https://doi.org/10.1523/jneurosci.23-15-06357.2003>
- Nelson, B. S., & Takahashi, T. T. (2010). Spatial Hearing in Echoic Environments: The Role of the Envelope in Owls. *Neuron*, 67(4), 643–655. <https://doi.org/10.1016/j.neuron.2010.07.014>
- Ngodup, T., Romero, G. E., & Trussell, L. O. (2020). Identification of an inhibitory neuron subtype, the L-stellate cell of the cochlear nucleus. *ELife*, 9, e54350. <https://doi.org/10.7554/elife.54350>

- Nishino, E., Yamada, R., Kuba, H., Hioki, H., Furuta, T., Kaneko, T., & Ohmori, H. (2008). Sound-intensity-dependent compensation for the small interaural time difference cue for sound source localization. *The Journal of Neuroscience : The Official Journal of the Society for Neuroscience*, 28(28), 7153–7164. <https://doi.org/10.1523/jneurosci.4398-07.2008>
- Noble, D., & Stein, R. B. (1966). The threshold conditions for initiation of action potentials by excitable cells. *The Journal of Physiology*, 187(1), 129–162. <https://doi.org/10.1113/jphysiol.1966.sp008079>
- Oertel, D. (1983). Synaptic responses and electrical properties of cells in brain slices of the mouse anteroventral cochlear nucleus. *The Journal of Neuroscience*, 3(10), 2043–2053. <https://doi.org/10.1523/jneurosci.03-10-02043.1983>
- Oertel, D. (1997). Encoding of Timing in the Brain Stem Auditory Nuclei of Vertebrates. *Neuron*, 19(5), 959–962. [https://doi.org/10.1016/s0896-6273\(00\)80388-8](https://doi.org/10.1016/s0896-6273(00)80388-8)
- Oertel, D., Bal, R., Gardner, S. M., Smith, P. H., & Joris, P. X. (2000). Detection of synchrony in the activity of auditory nerve fibers by octopus cells of the mammalian cochlear nucleus. *Proceedings of the National Academy of Sciences*, 97(22), 11773–11779. <https://doi.org/10.1073/pnas.97.22.11773>
- Oertel, D., Shatadal, S., & Cao, X.-J. (2008). In the ventral cochlear nucleus Kv1.1 and subunits of HCN1 are colocalized at surfaces of neurons that have low-voltage-activated and hyperpolarization-activated conductances. *Neuroscience*, 154(1), 77–86. <https://doi.org/10.1016/j.neuroscience.2008.01.085>
- Oertel, D., Wright, S., Cao, X.-J., Ferragamo, M., & Bal, R. (2011). The multiple functions of T stellate/multipolar/chopper cells in the ventral cochlear nucleus. *Hearing Research*, 276(1–2), 61–69. <https://doi.org/10.1016/j.heares.2010.10.018>
- Oertel, D., Wu, S. H., Garb, M. W., & Dizack, C. (1990). Morphology and physiology of cells in slice preparations of the posteroventral cochlear nucleus of mice. *Journal of Comparative Neurology*, 295(1), 136–154. <https://doi.org/10.1002/cne.902950112>
- Ohmori, H. (1984). Mechano-electrical transducer has discrete conductances in the chick vestibular hair cell. *Proceedings of the National Academy of Sciences*, 81(6), 1888–1891. <https://doi.org/10.1073/pnas.81.6.1888>
- Ohmori, H. (2014). Neuronal specializations for the processing of interaural difference cues in the chick. *Frontiers in Neural Circuits*, 8, 47. <https://doi.org/10.3389/fncir.2014.00047>
- Oline, S. N., Ashida, G., & Burger, R. M. (2016). Tonotopic Optimization for Temporal Processing in the Cochlear Nucleus. *The Journal of Neuroscience*, 36(32), 8500–8515. <https://doi.org/10.1523/jneurosci.4449-15.2016>

- Ollo, C., & Schwartz, I. R. (1979). The superior olivary complex in C57BL/6 mice. *American Journal of Anatomy*, 155(3), 349–373. <https://doi.org/10.1002/aja.1001550306>
- Palmer, A. R., Wallace, M. N., Arnott, R. H., & Shackleton, T. M. (2003). Morphology of physiologically characterised ventral cochlear nucleus stellate cells. *Experimental Brain Research*, 153(4), 418–426. <https://doi.org/10.1007/s00221-003-1602-6>
- Paolini, A. G., FitzGerald, J. V., Burkitt, A. N., & Clark, G. M. (2001). Temporal processing from the auditory nerve to the medial nucleus of the trapezoid body in the rat. *Hearing Research*, 159(1–2), 101–116. [https://doi.org/10.1016/s0378-5955\(01\)00327-6](https://doi.org/10.1016/s0378-5955(01)00327-6)
- Parameshwaran, S., Carr, C. E., & Perney, T. M. (2001). Expression of the Kv3.1 Potassium Channel in the Avian Auditory Brainstem. *The Journal of Neuroscience*, 21(2), 485–494. <https://doi.org/10.1523/jneurosci.21-02-00485.2001>
- Parameshwaran-Iyer, S., Carr, C. E., & Perney, T. M. (2003). Localization of KCNC1 (Kv3.1) potassium channel subunits in the avian auditory nucleus magnocellularis and nucleus laminaris during development. *Journal of Neurobiology*, 55(2), 165–178. <https://doi.org/10.1002/neu.10198>
- Parks, T. N., & Jackson, H. (1984). A developmental gradient of dendritic loss in the avian cochlear nucleus occurring independently of primary afferents. *Journal of Comparative Neurology*, 227(3), 459–466. <https://doi.org/10.1002/cne.902270315>
- Parks, T. N., & Rubel, E. W. (1975). Organization and development of brain stem auditory nuclei of the chicken: Organization of projections from N. magnocellularis to N. laminaris. *Journal of Comparative Neurology*, 164(4), 435–448. <https://doi.org/10.1002/cne.901640404>
- Parks, T. N., & Rubel, E. W. (1978). Organization and development of the brain stem auditory nuclei of the chicken: Primary afferent projections. *Journal of Comparative Neurology*, 180(3), 439–448. <https://doi.org/10.1002/cne.901800303>
- Payne, R. S. (1971). Acoustic Location of Prey by Barn Owls (*Tyto Alba*). *Journal of Experimental Biology*, 54(3), 535–573. <https://doi.org/10.1242/jeb.54.3.535>
- Pecka, M., Brand, A., Behrend, O., & Grothe, B. (2008). Interaural Time Difference Processing in the Mammalian Medial Superior Olive: The Role of Glycinergic Inhibition. *Journal of Neuroscience*, 28(27), 6914–6925. <https://doi.org/10.1523/jneurosci.1660-08.2008>
- Petitpré, C., Wu, H., Sharma, A., Tokarska, A., Fontanet, P., Wang, Y., Helmbacher, F., Yackle, K., Silberberg, G., Hadjab, S., & Lallemand, F. (2018). Neuronal heterogeneity and stereotyped connectivity in the auditory afferent system. *Nature Communications*, 9(1), 3691. <https://doi.org/10.1038/s41467-018-06033-3>

- Pfeiffer, R. R. (1966). Classification of response patterns of spike discharges for units in the cochlear nucleus: Tone-burst stimulation. *Experimental Brain Research*, 1(3), 220–235. <https://doi.org/10.1007/bf00234343>
- Pinheiro, B. P., Müller, M., Bös, M., Guezguez, J., Burnet, M., Tornincasa, M., Rizzetto, R., Rolland, J.-F., Liberati, C., Lohmer, S., Adel, Y., & Löwenheim, H. (2022). A potassium channel agonist protects hearing function and promotes outer hair cell survival in a mouse model for age-related hearing loss. *Cell Death & Disease*, 13(7), 595. <https://doi.org/10.1038/s41419-022-04915-5>
- Platkiewicz, J., & Brette, R. (2010). A Threshold Equation for Action Potential Initiation. *PLoS Computational Biology*, 6(7), e1000850. <https://doi.org/10.1371/journal.pcbi.1000850>
- Platkiewicz, J., & Brette, R. (2011). Impact of Fast Sodium Channel Inactivation on Spike Threshold Dynamics and Synaptic Integration. *PLoS Computational Biology*, 7(5), e1001129. <https://doi.org/10.1371/journal.pcbi.1001129>
- Pliego, J. A. F., & Pedroarena, C. M. (2020). Kv1 potassium channels control action potential firing of putative GABAergic deep cerebellar nuclear neurons. *Scientific Reports*, 10(1), 6954. <https://doi.org/10.1038/s41598-020-63583-7>
- Prescott, S. A., Koninck, Y. D., & Sejnowski, T. J. (2008). Biophysical Basis for Three Distinct Dynamical Mechanisms of Action Potential Initiation. *PLoS Computational Biology*, 4(10), e1000198. <https://doi.org/10.1371/journal.pcbi.1000198>
- Prescott, S. A., Ratté, S., Koninck, Y. D., & Sejnowski, T. J. (2006). Nonlinear Interaction between Shunting and Adaptation Controls a Switch between Integration and Coincidence Detection in Pyramidal Neurons. *The Journal of Neuroscience*, 26(36), 9084–9097. <https://doi.org/10.1523/jneurosci.1388-06.2006>
- Prescott, S. A., Ratté, S., Koninck, Y. D., & Sejnowski, T. J. (2008). Pyramidal Neurons Switch From Integrators In Vitro to Resonators Under In Vivo-Like Conditions. *Journal of Neurophysiology*, 100(6), 3030–3042. <https://doi.org/10.1152/jn.90634.2008>
- Prinz, A. A., Abbott, L. F., & Marder, E. (2004). The dynamic clamp comes of age. *Trends in Neurosciences*, 27(4), 218–224. <https://doi.org/10.1016/j.tins.2004.02.004>
- Puelles, L., & Martinez, S. (2013). Patterning and Cell Type Specification in the Developing Cns and Pns. *I: Induction and Patterning of the CNS and PNS*, 151–172. <https://doi.org/10.1016/b978-0-12-397265-1.00048-4>
- Pyott, S. J., & Duncan, R. K. (2016). BK Channels in the Vertebrate Inner Ear. *International Review of Neurobiology*, 128, 369–399. <https://doi.org/10.1016/bs.irn.2016.03.016>

- Raman, I., Zhang, S., & Trussell, L. (1994). Pathway-specific variants of AMPA receptors and their contribution to neuronal signaling. *The Journal of Neuroscience*, *14*(8), 4998–5010. <https://doi.org/10.1523/jneurosci.14-08-04998.1994>
- Ranjan, R., Logette, E., Marani, M., Herzog, M., Tâche, V., Scantamburlo, E., Buchillier, V., & Markram, H. (2019). A Kinetic Map of the Homomeric Voltage-Gated Potassium Channel (Kv) Family. *Frontiers in Cellular Neuroscience*, *13*, 358. <https://doi.org/10.3389/fncel.2019.00358>
- Rathouz, M., & Trussell, L. (1998). Characterization of Outward Currents in Neurons of the Avian Nucleus Magnocellularis. *Journal of Neurophysiology*, *80*(6), 2824–2835. <https://doi.org/10.1152/jn.1998.80.6.2824>
- Ratté, S., Hong, S., De Schutter, E., & Prescott, S. A. (2013). Impact of Neuronal Properties on Network Coding: Roles of Spike Initiation Dynamics and Robust Synchrony Transfer. *Neuron*, *78*(5), 758–772. <https://doi.org/10.1016/j.neuron.2013.05.030>
- Ratté, S., Lankarany, M., Rho, Y.-A., Patterson, A., & Prescott, S. A. (2015). Subthreshold membrane currents confer distinct tuning properties that enable neurons to encode the integral or derivative of their input. *Frontiers in Cellular Neuroscience*, *8*, 452. <https://doi.org/10.3389/fncel.2014.00452>
- Rautenberg, P. L., Grothe, B., & Felmy, F. (2009). Quantification of the three-dimensional morphology of coincidence detector neurons in the medial superior olive of gerbils during late postnatal development. *Journal of Comparative Neurology*, *517*(3), 385–396. <https://doi.org/10.1002/cne.22166>
- Reyes, A. D., Rubel, E. W., & Spain, W. J. (1994). Membrane properties underlying the firing of neurons in the avian cochlear nucleus. *The Journal of Neuroscience : The Official Journal of the Society for Neuroscience*, *14*(9), 5352–5364.
- Reyes, A., Rubel, E., & Spain, W. (1996). In vitro analysis of optimal stimuli for phase-locking and time-delayed modulation of firing in avian nucleus laminaris neurons. *The Journal of Neuroscience*, *16*(3), 993–1007. <https://doi.org/10.1523/jneurosci.16-03-00993.1996>
- Rhode, W. S., & Greenberg, S. (1994). Encoding of amplitude modulation in the cochlear nucleus of the cat. *Journal of Neurophysiology*, *71*(5), 1797–1825. <https://doi.org/10.1152/jn.1994.71.5.1797>
- Rhode, W. S., Oertel, D., & Smith, P. H. (1983). Physiological response properties of cells labeled intracellularly with horseradish peroxidase in cat ventral cochlear nucleus. *Journal of Comparative Neurology*, *213*(4), 448–463. <https://doi.org/10.1002/cne.902130408>
- Rhode, W. S., Smith, P. H., & Oertel, D. (1983). Physiological response properties of cells labeled intracellularly with horseradish peroxidase in cat dorsal cochlear nucleus. *Journal of Comparative Neurology*, *213*(4), 426–447. <https://doi.org/10.1002/cne.902130407>

- Robbins, J. (2001). KCNQ potassium channels: physiology, pathophysiology, and pharmacology. *Pharmacology & Therapeutics*, 90(1), 1–19. [https://doi.org/10.1016/s0163-7258\(01\)00116-4](https://doi.org/10.1016/s0163-7258(01)00116-4)
- Rothman, J. S., & Manis, P. B. (2003a). Differential Expression of Three Distinct Potassium Currents in the Ventral Cochlear Nucleus. *Journal of Neurophysiology*, 89(6), 3070–3082. <https://doi.org/10.1152/jn.00125.2002>
- Rothman, J. S., & Manis, P. B. (2003b). Kinetic Analyses of Three Distinct Potassium Conductances in Ventral Cochlear Nucleus Neurons. *Journal of Neurophysiology*, 89(6), 3083–3096. <https://doi.org/10.1152/jn.00126.2002>
- Rothman, J. S., & Manis, P. B. (2003c). The Roles Potassium Currents Play in Regulating the Electrical Activity of Ventral Cochlear Nucleus Neurons. *Journal of Neurophysiology*, 89(6), 3097–3113. <https://doi.org/10.1152/jn.00127.2002>
- Rothman, J. S., Young, E. D., & Manis, P. B. (1993). Convergence of auditory nerve fibers onto bushy cells in the ventral cochlear nucleus: implications of a computational model. *Journal of Neurophysiology*, 70(6), 2562–2583. <https://doi.org/10.1152/jn.1993.70.6.2562>
- Rubio, M. E., & Juiz, J. M. (2004). Differential distribution of synaptic endings containing glutamate, glycine, and GABA in the rat dorsal cochlear nucleus. *Journal of Comparative Neurology*, 477(3), 253–272. <https://doi.org/10.1002/cne.20248>
- Rudy, B., Chow, A., Lau, D., Amarillo, Y., Ozaita, A., Saganich, M., Moreno, H., Nadal, M. S., Hernandez-Pineda, R., Hernandez-Cruz, A., Erisir, A., Leonard, C., & Miera, E. V.-S. de. (1999). Contributions of Kv3 channels to neuronal excitability. *Annals of the New York Academy of Sciences*, 868(1), 304–343. <https://doi.org/10.1111/j.1749-6632.1999.tb11295.x>
- Ryugo, D. K., & Parks, T. N. (2003). Primary innervation of the avian and mammalian cochlear nucleus. *Brain Research Bulletin*, 60(5–6), 435–456. [https://doi.org/10.1016/s0361-9230\(03\)00049-2](https://doi.org/10.1016/s0361-9230(03)00049-2)
- Ryugo, D. K., & Sento, S. (1991). Synaptic connections of the auditory nerve in cats: Relationship between endbulbs of held and spherical bushy cells. *Journal of Comparative Neurology*, 305(1), 35–48. <https://doi.org/10.1002/cne.903050105>
- Sachs, M. B., & Abbas, P. J. (1974). Rate versus level functions for auditory-nerve fibers in cats: tone-burst stimuli. *The Journal of the Acoustical Society of America*, 56(6), 1835–1847. <https://doi.org/10.1121/1.1903521>
- Sachs, M. B., & Sinnott, J. M. (1978). Responses to tones of single cells in nucleus magnocellularis and nucleus angularis of the redwing blackbird (*Agelaius phoeniceus*). *Journal of Comparative Physiology*, 126(4), 347–361. <https://doi.org/10.1007/bf00667105>

- Sachs, M. B., Sinnott, J. M., & Hienz, R. D. (1978). Behavioral and physiological studies of hearing in birds. *Federation Proceedings*, 37(10), 2329–2335.
- Sachs, M. B., Young, E. D., & Lewis, R. H. (1974). Discharge patterns of single fibers in the pigeon auditory nerve. *Brain Research*, 70(3), 431–447. [https://doi.org/10.1016/0006-8993\(74\)90253-4](https://doi.org/10.1016/0006-8993(74)90253-4)
- Salvi, R. J., Saunders, S. S., Powers, N. L., & Boettcher, F. A. (1992). Discharge patterns of cochlear ganglion neurons in the chicken. *Journal of Comparative Physiology A*, 170(2), 227–241. <https://doi.org/10.1007/bf00196905>
- Sanchez, J. T., Quinones, K., & Otto-Meyer, S. (2015). Factors Influencing Short-term Synaptic Plasticity in the Avian Cochlear Nucleus Magnocellularis. *Journal of Experimental Neuroscience*, 9(Suppl 2), 11–24. <https://doi.org/10.4137/jen.s25472>
- Sanes, D., & Rubel, E. (1988). The ontogeny of inhibition and excitation in the gerbil lateral superior olive. *The Journal of Neuroscience*, 8(2), 682–700. <https://doi.org/10.1523/jneurosci.08-02-00682.1988>
- Sato, T., Fukui, I., & Ohmori, H. (2010). Interaural phase difference modulates the neural activity in the nucleus angularis and improves the processing of level difference cue in the lateral lemniscal nucleus in the chicken. *Neuroscience Research*, 66(2), 198–212. <https://doi.org/10.1016/j.neures.2009.11.001>
- Saunders, J. C., Dear, S. P., & Schneider, M. E. (1985). The anatomical consequences of acoustic injury: A review and tutorial. *The Journal of the Acoustical Society of America*, 78(3), 833–860. <https://doi.org/10.1121/1.392915>
- Schneider, D. M., & Woolley, S. M. N. (2010). Discrimination of communication vocalizations by single neurons and groups of neurons in the auditory midbrain. *Journal of Neurophysiology*, 103(6), 3248–3265. <https://doi.org/10.1152/jn.01131.2009>
- Scott, S. K. (2005). Auditory processing — speech, space and auditory objects. *Current Opinion in Neurobiology*, 15(2), 197–201. <https://doi.org/10.1016/j.conb.2005.03.009>
- Shannon, C. E. (2001). A mathematical theory of communication. *ACM SIGMOBILE Mobile Computing and Communications Review*, 5(1), 3–55. <https://doi.org/10.1145/584091.584093>
- Sharp, A. A., O’Neil, M. B., Abbott, L. F., & Marder, E. (1993). The dynamic clamp: artificial conductances in biological neurons. *Trends in Neurosciences*, 16(10), 389–394. [https://doi.org/10.1016/0166-2236\(93\)90004-6](https://doi.org/10.1016/0166-2236(93)90004-6)
- Shu, Y., Yu, Y., Yang, J., & McCormick, D. A. (2007). Selective control of cortical axonal spikes by a slowly inactivating K<sup>+</sup> current. *Proceedings of the National Academy of Sciences*, 104(27), 11453–11458. <https://doi.org/10.1073/pnas.0702041104>

- Simmons, J. A., Wever, E. G., & Pylka, J. M. (1971). Periodical Cicada: Sound Production and Hearing. *Science*, *171*(3967), 212–213. <https://doi.org/10.1126/science.171.3967.212>
- Singh, N. C., & Theunissen, F. E. (2003). Modulation spectra of natural sounds and ethological theories of auditory processing. *The Journal of the Acoustical Society of America*, *114*(6), 3394–3411. <https://doi.org/10.1121/1.1624067>
- Smith, D. J., & Rubel, E. W. (1979). Organization and development of brain stem auditory nuclei of the chicken: Dendritic gradients in nucleus laminaris. *Journal of Comparative Neurology*, *186*(2), 213–239. <https://doi.org/10.1002/cne.901860207>
- Smith, P. H. (1995). Structural and functional differences distinguish principal from nonprincipal cells in the guinea pig MSO slice. *Journal of Neurophysiology*, *73*(4), 1653–1667. <https://doi.org/10.1152/jn.1995.73.4.1653>
- Smith, P. H., Joris, P. X., & Yin, T. C. T. (1998). Anatomy and Physiology of Principal Cells of the Medial Nucleus of the Trapezoid Body (MNTB) of the Cat. *Journal of Neurophysiology*, *79*(6), 3127–3142. <https://doi.org/10.1152/jn.1998.79.6.3127>
- Soares, D., & Carr, C. E. (2001). The cytoarchitecture of the nucleus angularis of the barn owl (*Tyto alba*). *Journal of Comparative Neurology*, *429*(2), 192–205. [https://doi.org/10.1002/1096-9861\(20000108\)429:2<192::aid-cne2>3.0.co;2-5](https://doi.org/10.1002/1096-9861(20000108)429:2<192::aid-cne2>3.0.co;2-5)
- Soares, D., Chitwood, R. A., Hyson, R. L., & Carr, C. E. (2002). Intrinsic Neuronal Properties of the Chick Nucleus Angularis. *Journal of Neurophysiology*, *88*(1), 152–162. <https://doi.org/10.1152/jn.2002.88.1.152>
- Stange, A., Myoga, M. H., Lingner, A., Ford, M. C., Alexandrova, O., Felmy, F., Pecka, M., Siveke, I., & Grothe, B. (2013). Adaptation in sound localization: from GABAB receptor-mediated synaptic modulation to perception. *Nature Neuroscience*, *16*(12), 1840–1847. <https://doi.org/10.1038/nn.3548>
- Steinberg, L. J., & Peña, J. L. (2011). Difference in Response Reliability Predicted by Spectrotemporal Tuning in the Cochlear Nuclei of Barn Owls. *The Journal of Neuroscience*, *31*(9), 3234–3242. <https://doi.org/10.1523/jneurosci.5422-10.2011>
- Steveninck, R. R. de R. van, Lewen, G. D., Strong, S. P., Koberle, R., & Bialek, W. (1997). Reproducibility and Variability in Neural Spike Trains. *Science*, *275*(5307), 1805–1808. <https://doi.org/10.1126/science.275.5307.1805>
- Storm, J. F. (1987). Action potential repolarization and a fast after-hyperpolarization in rat hippocampal pyramidal cells. *The Journal of Physiology*, *385*(1), 733–759. <https://doi.org/10.1113/jphysiol.1987.sp016517>
- Storm, J. F. (1988). Temporal integration by a slowly inactivating K<sup>+</sup> current in hippocampal neurons. *Nature*, *336*(6200), 698–698. <https://doi.org/10.1038/336698b0>

- Street, S. E., & Manis, P. B. (2007). Action Potential Timing Precision in Dorsal Cochlear Nucleus Pyramidal Cells. *Journal of Neurophysiology*, 97(6), 4162–4172. <https://doi.org/10.1152/jn.00469.2006>
- Sullivan, W. E. (1985). Classification of response patterns in cochlear nucleus of barn owl: correlation with functional response properties. *Journal of Neurophysiology*, 53(1), 201–216. <https://doi.org/10.1152/jn.1985.53.1.201>
- Sullivan, W. E., & Konishi, M. (1984). Segregation of stimulus phase and intensity coding in the cochlear nucleus of the barn owl. *The Journal of Neuroscience : The Official Journal of the Society for Neuroscience*, 4(7), 1787–1799.
- Svirskis, G., Kotak, V., Sanes, D. H., & Rinzel, J. (2002). Enhancement of Signal-to-Noise Ratio and Phase Locking for Small Inputs by a Low-Threshold Outward Current in Auditory Neurons. *The Journal of Neuroscience*, 22(24), 11019–11025. <https://doi.org/10.1523/jneurosci.22-24-11019.2002>
- Svirskis, G., Kotak, V., Sanes, D. H., & Rinzel, J. (2004). Sodium Along With Low-Threshold Potassium Currents Enhance Coincidence Detection of Subthreshold Noisy Signals in MSO Neurons. *Journal of Neurophysiology*, 91(6), 2465–2473. <https://doi.org/10.1152/jn.00717.2003>
- Swensen, A. M., & Bean, B. P. (2003). Ionic Mechanisms of Burst Firing in Dissociated Purkinje Neurons. *The Journal of Neuroscience*, 23(29), 9650–9663. <https://doi.org/10.1523/jneurosci.23-29-09650.2003>
- Tabor, K. M., Coleman, W. L., Rubel, E. W., & Burger, R. M. (2012). Tonotopic organization of the superior olivary nucleus in the chicken auditory brainstem. *Journal of Comparative Neurology*, 520(7), 1493–1508. <https://doi.org/10.1002/cne.22807>
- Tabor, K. M., Wong, R. O. L., & Rubel, E. W. (2011). Topography and morphology of the inhibitory projection from superior olivary nucleus to nucleus laminaris in chickens (*Gallus gallus*). *Journal of Comparative Neurology*, 519(2), 358–375. <https://doi.org/10.1002/cne.22523>
- Takahashi, T., Moiseff, A., & Konishi, M. (1984). Time and intensity cues are processed independently in the auditory system of the owl. *The Journal of Neuroscience : The Official Journal of the Society for Neuroscience*, 4(7), 1781–1786.
- Takahashi, T. T., Barberini, C. L., & Keller, C. H. (1995). An anatomical substrate for the inhibitory gradient in the VLVp of the owl. *Journal of Comparative Neurology*, 358(2), 294–304. <https://doi.org/10.1002/cne.903580210>
- Takahashi, T. T., & Konishi, M. (1988a). Projections of nucleus angularis and nucleus laminaris to the lateral lemniscal nuclear complex of the barn owl. *Journal of Comparative Neurology*, 274(2), 212–238. <https://doi.org/10.1002/cne.902740207>

- Takahashi, T. T., & Konishi, M. (1988b). Projections of the cochlear nuclei and nucleus laminaris to the inferior colliculus of the barn owl. *Journal of Comparative Neurology*, 274(2), 190–211. <https://doi.org/10.1002/cne.902740206>
- Takahashi, Y., & Konishi, M. (2002). Manipulation of inhibition in the owl's nucleus laminaris and its effects on optic tectum neurons. *Neuroscience*, 111(2), 373–378. [https://doi.org/10.1016/s0306-4522\(02\)00010-6](https://doi.org/10.1016/s0306-4522(02)00010-6)
- Viemeister, N. F. (1974). Intensity discrimination of noise in the presence of band-reject noise. *The Journal of the Acoustical Society of America*, 56(5), 1594–1600. <https://doi.org/10.1121/1.1903483>
- Viemeister, N. F. (1983). Auditory Intensity Discrimination at High Frequencies in the Presence of Noise. *Science*, 221(4616), 1206–1208. <https://doi.org/10.1126/science.6612337>
- Viete, S., Peña, J. L., & Konishi, M. (1997). Effects of Interaural Intensity Difference on the Processing of Interaural Time Difference in the Owl's Nucleus Laminaris. *The Journal of Neuroscience*, 17(5), 1815–1824. <https://doi.org/10.1523/jneurosci.17-05-01815.1997>
- Wang, H., Kunkel, D., Schwartzkroin, P., & Tempel, B. (1994). Localization of Kv1.1 and Kv1.2, two K channel proteins, to synaptic terminals, somata, and dendrites in the mouse brain. *The Journal of Neuroscience*, 14(8), 4588–4599. <https://doi.org/10.1523/jneurosci.14-08-04588.1994>
- Wang, L., Gan, L., Forsythe, I. D., & Kaczmarek, L. K. (1998). Contribution of the Kv3.1 potassium channel to high-frequency firing in mouse auditory neurones. *The Journal of Physiology*, 509(1), 183–194. <https://doi.org/10.1111/j.1469-7793.1998.183bo.x>
- Wang, W., Zhang, Li. S., Zinsmaier, A. K., Patterson, G., Leptich, E. J., Shoemaker, S. L., Yatskievych, T. A., Gibboni, R., Pace, E., Luo, H., Zhang, J., Yang, S., & Bao, S. (2019). Neuroinflammation mediates noise-induced synaptic imbalance and tinnitus in rodent models. *PLoS Biology*, 17(6), e3000307. <https://doi.org/10.1371/journal.pbio.3000307>
- Wang, Y., & Manis, P. B. (2005). Synaptic Transmission at the Cochlear Nucleus Endbulb Synapse During Age-Related Hearing Loss in Mice. *Journal of Neurophysiology*, 94(3), 1814–1824. <https://doi.org/10.1152/jn.00374.2005>
- Warchol, M. E., & Dallos, P. (1990). Neural coding in the chick cochlear nucleus. *Journal of Comparative Physiology A*, 166(5), 721–734. <https://doi.org/10.1007/bf00240021>
- Westerberg, B. D., & Schwarz, D. W. (1995). Connections of the superior olive in the chicken. *The Journal of Otolaryngology*, 24(1), 20–30.
- Wickesberg, R. E., Whitlon, D., & Oertel, D. (1994). In vitro modulation of somatic glycine-like immunoreactivity in presumed glycinergic neurons. *Journal of Comparative Neurology*, 339(3), 311–327. <https://doi.org/10.1002/cne.903390302>

- Williamson, T. T., Zhu, X., Walton, J. P., & Frisina, R. D. (2015). Auditory brainstem gap responses start to decline in mice in middle age: a novel physiological biomarker for age-related hearing loss. *Cell and Tissue Research*, 361(1), 359–369.  
<https://doi.org/10.1007/s00441-014-2003-9>
- Winter, I. M. (2005). Pitch. *Springer Handbook of Auditory Research*, 99–146.  
[https://doi.org/10.1007/0-387-28958-5\\_4](https://doi.org/10.1007/0-387-28958-5_4)
- Wu, J., & Kaczmarek, L. K. (2021). Modulation of Neuronal Potassium Channels During Auditory Processing. *Frontiers in Neuroscience*, 15, 596478.  
<https://doi.org/10.3389/fnins.2021.596478>
- Wu, S., & Oertel, D. (1986). Inhibitory circuitry in the ventral cochlear nucleus is probably mediated by glycine. *The Journal of Neuroscience*, 6(9), 2691–2706.  
<https://doi.org/10.1523/jneurosci.06-09-02691.1986>
- Xie, R., & Manis, P. B. (2013). Target-Specific IPSC Kinetics Promote Temporal Processing in Auditory Parallel Pathways. *The Journal of Neuroscience*, 33(4), 1598–1614.  
<https://doi.org/10.1523/jneurosci.2541-12.2013>
- Xie, R., & Manis, P. B. (2014). GABAergic and glycinergic inhibitory synaptic transmission in the ventral cochlear nucleus studied in VGAT channelrhodopsin-2 mice. *Frontiers in Neural Circuits*, 8, 84. <https://doi.org/10.3389/fncir.2014.00084>
- Xie, R., & Manis, P. B. (2017). Synaptic transmission at the endbulb of Held deteriorates during age-related hearing loss. *The Journal of Physiology*, 595(3), 919–934.  
<https://doi.org/10.1113/jp272683>
- Yamada, R., & Kuba, H. (2021). Dendritic synapse geometry optimizes binaural computation in a sound localization circuit. *Science Advances*, 7(48), eabh0024.  
<https://doi.org/10.1126/sciadv.abh0024>
- Yamada, R., & Kuba, H. (2022). Cellular Strategies for Frequency-Dependent Computation of Interaural Time Difference. *Frontiers in Synaptic Neuroscience*, 14, 891740.  
<https://doi.org/10.3389/fnsyn.2022.891740>
- Yamada, R., Kuba, H., Ishii, T. M., & Ohmori, H. (2005). Hyperpolarization-Activated Cyclic Nucleotide-Gated Cation Channels Regulate Auditory Coincidence Detection in Nucleus Laminaris of the Chick. *The Journal of Neuroscience*, 25(39), 8867–8877.  
<https://doi.org/10.1523/jneurosci.2541-05.2005>
- Yamada, R., Okuda, H., Kuba, H., Nishino, E., Ishii, T. M., & Ohmori, H. (2013). The Cooperation of Sustained and Phasic Inhibitions Increases the Contrast of ITD-Tuning in Low-Frequency Neurons of the Chick Nucleus Laminaris. *The Journal of Neuroscience*, 33(9), 3927–3938. <https://doi.org/10.1523/jneurosci.2377-12.2013>

- Yang, L., Monsivais, P., & Rubel, E. W. (1999). The Superior Olivary Nucleus and Its Influence on Nucleus Laminaris: A Source of Inhibitory Feedback for Coincidence Detection in the Avian Auditory Brainstem. *The Journal of Neuroscience*, *19*(6), 2313–2325. <https://doi.org/10.1523/jneurosci.19-06-02313.1999>
- Yellen, G. (2002). The voltage-gated potassium channels and their relatives. *Nature*, *419*(6902), 35–42. <https://doi.org/10.1038/nature00978>
- Yin, T. C., & Chan, J. C. (1990). Interaural time sensitivity in medial superior olive of cat. *Journal of Neurophysiology*, *64*(2), 465–488. <https://doi.org/10.1152/jn.1990.64.2.465>
- Yin, T. C. T. (2002). Integrative Functions in the Mammalian Auditory Pathway. *Springer Handbook of Auditory Research*, 99–159. [https://doi.org/10.1007/978-1-4757-3654-0\\_4](https://doi.org/10.1007/978-1-4757-3654-0_4)
- Zhang, S., & Oertel, D. (1993). Tuberculoventral cells of the dorsal cochlear nucleus of mice: intracellular recordings in slices. *Journal of Neurophysiology*, *69*(5), 1409–1421. <https://doi.org/10.1152/jn.1993.69.5.1409>
- Zhang, S., & Trussell, L. O. (1994). A characterization of excitatory postsynaptic potentials in the avian nucleus magnocellularis. *Journal of Neurophysiology*, *72*(2), 705–718. <https://doi.org/10.1152/jn.1994.72.2.705>